NTNU

Norwegian University of
Science and Technology

DP Solutions with Rudder Force Feedback for Exposed Aquaculture

Johan Magne Haugland

Abstract

Aquaculture and especially exposed aquaculture is a business heading into a period of large growth and rapid change. Considerable amounts of resources are and will be put into research to insure safe and sustainable operations at exposed locations, and for the business in general. A key factor is precise manoeuvrability of vessels operating at fish farms, both to avoid collision and in insuring minimal disturbance on the fish environment.

Thrust and manoeuvring devices are obviously a critical part of this process. The rudder is known for its efficiency in transit, though has shortcomings in terms of flexibility and low speed manoeuvring. Though the rudder may never be as precise as e.g. azimuth thrusters at DP operations, it might be able to compete on overall operational performance such as fuel consumption. However to avoid that the expenses of DP operation absorbs the gains of effective transit, we need to utilize the potential of the rudder to its maximum.

Thrust allocation schemes for effective use of rudders in DP is already developed in e.g. Lindegaard and Fossen [2003]. When a rudder is exposed to incoming velocity it is able to produce sideways lift forces and longitudinal drag forces. With a twin propeller-rudder configuration one might utilize the lift forces to produce sum sideways forces. This can add to manoeuvrability, and in a best case scenario one might be able to comply with safety and performance standards with one less tunnel thruster.

An obstacle when utilizing rudders to produce sideways forces, is mathematical modelling. Precise modelling of rudder forces is challenging at steady state conditions, and to add further difficulties, rudder performance is known to change with varying external conditions. The main contribution of this thesis is the design and testing of a simple force feedback control system. The goal is to minimize the effect of deviations between the mathematical model of rudders in the control allocation, and the actual thruster output.

Through simulations we prove that the force feedback system is both power saving compared to not using rudders and has enhanced motion tracking compared to DP with rudders but without force feedback. Overall we conclude that it is absolutely possible that rudders are a part of the manoeuvring system which is most cost effective for well boats in aquaculture. Further work is however necessary. Relevant areas are e.g. control allocation, the effect of noisy force measurements on station keeping performance, time varying rudder dynamics, utilizing of force measurement in autopilots and life cycle cost analysis.

Sammendrag

Akvakultur og spesielt akvakultur i eksponerte farvann er en næring på tur inn i en periode med stor vekst og rask endring. Betydelige ressurser er og vil bli satt inn i forskning for å sikre trygg og bærekraftig virksomhet på eksponerte lokasjoner, og for virksomheten generelt. En viktig faktor på dette området er presis manøvrering av skip som opererer i og rundt anlegg, både for å hindre kollisjoner og unngå unødvendige forstyrrelser i fiskens miljø.

Trust- og manøvreringsutstyr er åpenbart en kritisk del av denne prosessen. Roret er kjent for sin effektivitet i transitt, men det har mangler med hensyn til fleksibilitet og manøvrering ved lave hastigheter. Selv om roret kanskje aldri kan komme på nivå med for eksempel azimuth trustere i DP-operasjoner, kan det konkurrere på generelle operasjonelle ytelser som drivstofforbruk. For å unngå at fordelene med effektiv transitt blir absorbert av lite effektiv eller upresis bruk i DP bør potensialet til roret utnyttes til sitt maksimum.

Kontrolallokerings-algoritmer for effektiv bruk av ror i DP er allerede utviklet i f.eks. Lindegaard [2003]. Når et ror er utsatt for innkommende hastighet, er det i stand til å produsere sideveis løft. Med en twin-propeller-ror-konfigurasjon kan man utnytte dette løftet til å produsere sidesideveis kraft. Dette kan forbedre skipets manøvrerbarhet, og i beste fall kan sikkerhetskrav overholdes med én tunneltruster mindre installert.

Et hinder ved bruk av ror til generering av sideveis krefter, er matematisk modellering. Presis modellering av rorkrefter er utfordrende ved stasjonære forhold, og det blir ytterligere komplisert ved at rorytelse endrer seg med varierende forhold. Denne masteravhandlingens viktigste kontribusjon er design og testing av et enkelt krafttilbakekoblings-system. Målet er å minimere effekten av avvik mellom den matematiske modellen av roret i kontrollallokasjonen, og den reelt produserte trusten.

Gjennom simuleringer viser vi at kontrollsystemet med krafttilbakekobling er både energibesparende sammenlignet med kontroll uten bruk av ror og har forbedret posisjonskontroll i forhold til DP med ror men uten bruk av krafttilbakkobling. Totalt sett konkluderer vi med at det er absolutt mulig at ror er en del av manøvreringssystemet som er mest kostnadseffektivt for brønnbåter i akvakultur. Videre forskning er imidlertid nødvendig. Relevante områder er f.eks. kontrollallokering, effekt av betydelig støy i kraftmålingene, tidsvariabel rordynamikk, bruk av kraftmåling i autopilotsystemer og livssyklusanalyser.

Preface

Writing a master thesis has been a challenge not easily compared to anything else. Whilst I have enjoyed working on a five moths long project of my own choosing, it has to be admitted that limitless freedom is a challenge of its own. That said, I can truly say I have appreciated the experience.

Producing the thesis could not have been possible without help from several key personalities. I would like to thank my supervisor, Ingrid Schjølberg for fruitful discussions, her positive attitude and valuable feedback, as well as for being the link between me and the industry. PhD candidates Svenn Are Værnø and Astrid Helene Brodtkorb has effectively acted as co supervisors through the pre project and master thesis. They did as well provide me with the basis of the simulink vessel model central to the work in this thesis, and has both certainly deserved my gratitude. The idea of force measurement feedback came from Andreas Lingner and the rest of the team at Becker Marine Systems. Without this idea, the contents of this master thesis would surely have been something else entirely. I would as well like to thank them for their assistance through the thesis and for hosting me for a week in Hamburg. A city I will surely return to.
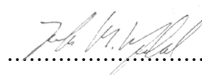
Karl-Petter Lindegaard has been an important contributor to this thesis. Not only where his article on thrust allocation with rudders vital to my understanding of the subject. His article did as well contribute on the field of thruster and rudder dynamics, and he has even provided code for implementation of his thrust allocation scheme. There can be no doubt that this has saved me days of work, and I can only hope that this thesis honours the basis on which it is laid.

A few courses and professors deserves to be mentioned. *Marine Control Systems* and *Guidance and Control of Vehicles*, have been of immense importance in connecting control theory with marine applications. I would like to thank professors Thor Inge Fossen and Asgeir Sørensen, for coordinating these great courses. I would as well like to give an honourable mention to UCSD professor Miroslav Krstic. Through my 17 years of study, no course have been more inspiring than his take on Nonlinear Systems Theory.

Last but not least, fellow students and comrades at office C1.084, has been vital throughout the master thesis process. The value of their humour, friendship and accumulated knowledge can not be overstated, and it is safe to say my time at NTNU would not have been the same without them.

Trondheim, 14/06/2017 ....

....

Place and time

Johan M. Haugland

Contents

List of Figures

List of Tables

Nomenclature

Note that symbols are given once in the text, when first utilized, and later used without reference.

Main nomenclature

L_{pp}	Length between perpendiculars
T	Vessel draught
B	Breadth
CG	Centre of gravity
GM_L	Longitudinal metacentric height
GM_T	Transverse metacentric height
C_B	Block coefficient
CB	Centre of buoyancy
S	Wet surface
M	Total mass
$M_r b$	Rigid body mass
M_a	Added mass
D	Total damping
D_v	Viscous damping
D_p	Potential damping
η	Position and orientation vector
$J(\eta)$	Rotation matrix from body to NED
ν_c	current velocity in body frame
$C(\nu_r)$	Corriolis-centripetal matrix
$g(\eta)$	Gravitational/buoyancy forces and moments
g_0	Pre trimming (ballast control) vector
τ	Control input - Commanded Thrust
τ_{wave}	Wind induced forces
τ_{wind}	Wave induced forces
w	Disturbance vector (Environmental forces)
μ	Fluid memory effects
ω_k	Wave frequency of wave k
β_i	Wave direction
ω_e	Wave encounter frequency
U	Total speed of ship
A_k	Wave amplitude of wave k
η_w	Wave frequency induced motion
η_{tot}	Total vessel motion

$S(w)$	Wave spectrum
ω_p	Peak frequency
H_s	Significant wave height
γ	Peakedness parameter
α	high frequency, shape parameter
σ	JONSWAP parameter
$\zeta(t)$	Time varying wave elevation
ϵ_n	Phase angle
$\Delta\omega$	Frequency interval
V_c	Surface current
ψ_c	Current direction
$V_{c,tide}$	Surface tidal current
$V_{c,wind}$	Surface wind current
h	Depth
$\bar{U}_{10}$	Mean wind at 10 metres.
$\bar{U}$	Mean wind velocity
κ	Sea surface drag coefficient (Wind models)
$\dot{U}_{SV}$	Slowly varying wind component
$S(f)$	Wind spectrum
f	Wind frequency in hertz
Δf	Frequency interval
T_i	Output thrust from thruster i
ρ	Fluid density
D_{pi}	Propeller diameter
K_{Ti}	Thrust coefficient
n_i	Revolution speed (rpm)
R_T	Total resistance
V	Vessels speed
C_T	Total resistance coefficient
C_f	Friction resistance coefficient
C_w	Wave resistance coefficient
K_Q	Torque Coefficient
Q	Torque (Thruster and Rudder Dynamics)
P	Power
L	Lift force
D	Drag force
C_L	Lift coefficient
C_D	Drag coefficient
G	Restoring terms matrix
b	Bias vector
$M3$	3DOF mass matrix
$D3$	3DOF damping matrix
$G3$	3DOF restoring matrix
ξ	Wave filter states

τ_η	Motion control
τ_F	Force control
τ_d	Desired control
$K_{P\tau}$	Proportional force feedback controller gain matrix
$K_{I\tau}$	Integral force feedback controller gain matrix
τ_m	Measured thrust

Nomenclature for Literature Study of Lindegaard and Fossen [2003]

Symbols in this list might as well be used with equal definition in other sections, though if otherwise defined in the main nomenclature, the main nomenclature denotes correct interpretation.

ω	Shaft speed
ω_d	Desired shaft speed
δ	Rudder angle
δ_d	Desired Rudder Angle
τ_c	Attainable thrust
p	Number of actuators
p_r	Number of rotatable devices
p_f	Number of fixed devices
n_r	Number of rotatable device controls
n_f	Number of fixed device controls
n	Total number of device controls
q	Number of controllable DOFs
r_k	Position of thruster k with regards to origin of device k
$l_{k,x}$	Longitudinal position with regards to origin of device k
$l_{k,y}$	Transverse position with regards to origin of device k
α_k	Angle of rotatable device k
ρ_k	Normalized thrust from device k
F_k	Thrust force from device k
F_k^{max}	Maximum thrust force from device k
$\mathbb{R}$	Set of real numbers
τ	Sum of generalized forces
$\bar{A}(\alpha)$	Configuration matrix
$\bar{F}$	Diagonal matrix of maximum thrust forces
u	Extended thrust
u_k	Extended thrust of device k
$u_{k,x}$	Extended thrust for device k in x direction
$u_{k,y}$	Extended thrust for device k in y direction
Π_k	Matrix for extraction of u_k from u
$\mathcal{D}_k$	Feasible domain of device k

B	Configuration matrix
A	Configuration matrix $B\bar{F}$
f	Linear constraint
$\mathcal{N}(A)$	Null-space of A
N	Orthonormal basis of the null-space of A
$\mathcal{R}(A)$	Row-space of A
$A^\dagger$	Normalized inverse of A
W	PDF design matrix
u_*	Optimal unconstrained solution
A^+	Pseudoinverse of A
δu	Optimal step to feasible region
δu_k	Optimal step to feasible region for device k
a	Region boundary
L	Lagrangian
λ	Lagrangian parameter
u^o	Constrained solution in O-frame
u^b	Constrained solution in B-frame
r^o	B-frame design parameter
e_l	Equicost line
J	Optimal cost

Nomenclature for Literature Study of Villani [2015]

Symbols in this list might as well be used with equal definition in other sections, though if otherwise defined in the main nomenclature, the main nomenclature denotes correct interpretation.

p_e	End-effector position
R_e	Rotation matrix
v_e	End-effector velocity
$\dot{p}_e$	Translational velocity
ω_e	Angular velocity
J	Jacobian
$\dot{q}$	Joint velocity vector
h_e	End-effector wrench
f_e	Force applied by end-effector
m_e	Moment applied by end effector
τ	Joint torque
Λ	Operational space inertia matrix
Γ	Wrench including Coriolis and centrifugal effects
$\dot{v}_e$	End-effector velocity
η	Gravitational wrench
h_c	Commanded end-effector wrench
τ_c	Input joint torques

S_v Velocity subspace matrix
S_f Force subspace matrix
ν Velocity vector corresponding to S_f
λ Forces vector corresponding to S_v
v_d Desired velocity
h_d Desired wrench
ν_d Desired velocity vector corresponding to S_f
λ_d Desired force vector corresponding to S_v
μ $\Gamma v_e + \eta$
Λ_v $S_v^T \Lambda S_v$
α_v Control input for velocity
f_λ Control input for force
$K_{P\lambda}$ Proportional force matrix gain
$K_{I\lambda}$ Integral force matrix gain
$K_{P\nu}$ Proportional velocity matrix gain
$K_{I\nu}$ Integral velocity matrix gain

Abreviations

CA	Control Allocation
D	Derivative
DP	Dynamic Positioning
EKF	Extended Kalman Filter
FFC	Force Feedback Control
I	Integral
LF	Low Frequecies
LQG	Linear Quadratic Gaussian Control
LQR	Linear Quadratic Regulator
NED	North east down
P	Proportional
PDF	Positive Definite
ROV	Remotely Operated Vehicle
R/V	Research vessel
rpm	Revolutions per minute
WF	Wave frequencies

Chapter 1

Introduction

1.1 Motivation

1.1.1 Dynamic Positioning in Aquaculture

Aquaculture and especially exposed aquaculture is a business heading into a period of large growth and rapid change. Considerable amounts of resources will be put into research to insure safe and sustainable operations at exposed locations and for the business in general. A key factor here is precise manoeuvrability of vessels operating at fish farms, both to avoid collision and in insuring minimal disturbance in the fish environment.

As the business grows, so does the vessels. This will impose even higher demands on their manoeuvrability. One way to meet this demand might be DP systems, but to insure the necessary manoeuvrability we should aim to develop the solutions of today even further. Measuring drag and lift forces on the rudder and using these directly in the feedback loop, might improve performance. Research is however needed. In this thesis, we therefore aim to provide more knowledge on the application of rudder force measurements in dynamic positioning (DP) solutions.

1.1.2 Force Measurements and Applications

In DP applications the rudder competes with systems which are both more flexible and provides better manoeuvrability in low speed operations. As an example Azimuth thrusters, such as ABB's *Azipod*, has been hugely popular and successfully applied in DP solutions. Yet another solution with high performance in low speed operations are the *Voith Sceneider Propeller*. The one area where they can not

compete with the traditional propeller-rudder setup, is fuel efficiency in transit. For a well boat which spends a significant part of its operation time in transit, this is obviously important. The question which arise is thus, "how may the rudder become more relevant in DP operations?" Using rudder force measurements to improve manoeuvrability might be a solution.

In order to utilize rudder force measurements in manoeuvring, we need to address two problems. Firstly a reliable and precise force measurement system is necessary. Becker Marine System has developed a system where sensors or strain gauges mounted to the rudder trunk and shaft is utilized to compute rudder forces. In this thesis force measurements is applied with the Becker system in mind.

When a measurement system is in place, it is necessary to consider how rudder forces could be utilized to promote effective manoeuvring, and how force measurements could improve the performance of such applications. With a twin propeller-rudder arrangement sum sideways force can be generated by running the propellers in opposite directions. This can add to manoeuvring capacity, and in a best case scenario one might be able to comply with safety and performance standards with one less tunnel thruster installed. An obstacle when utilizing rudders to produce sideways forces, is however mathematical modelling. Precise modelling of rudder forces is challenging at steady state conditions, and to add further difficulties, rudder performance is known to change with varying external conditions such as current velocity and direction. To counteract this we propose two possible approaches.

- *Force feedback control (ffc).* Through utilizing rudder force measurements in a feedback control loop, the gap between actual output forces and the mathematical models might be bridged. Direct force control is a well tested method in robotics, and in the literature study later in this chapter, we look to this field of study for inspiration.

- *Online model adjustment.* Through monitoring rudder forces the possibility of online model adjustment arises. Hespanha [2001] describes how supervisory control and hybrid systems might be utilized in order to choose the optimal controller amongst a bank of predefined systems. The basic idea is shown in Figure 1.1. The process plant, e.g. a surface vessel or remotely operated vehicle (ROV) yields output Y. This is fed to a family of controllers which simultaneously computes controller gains based on their specific parameters. The supervisor computes a switching signal based on process output, such as measurements of position and environmental conditions. This is in turn delivered as input to a switch, which picks the optimal control gains. This idea can easily be transferred from a hybrid system of controllers to supervisory control of rudder models. The single difference would be that process data such as environmental conditions and rudder force measurements could be used to choose between a family of rudder models instead of controllers.

Note that these approaches might as well be utilized in autopilot design to insure precise and energy efficient use of rudders during transit.

In this thesis focus is directed towards the first application, force feedback control. That said we believe that online model adjustment has significant potential, and strongly encourage others to investigate this further.
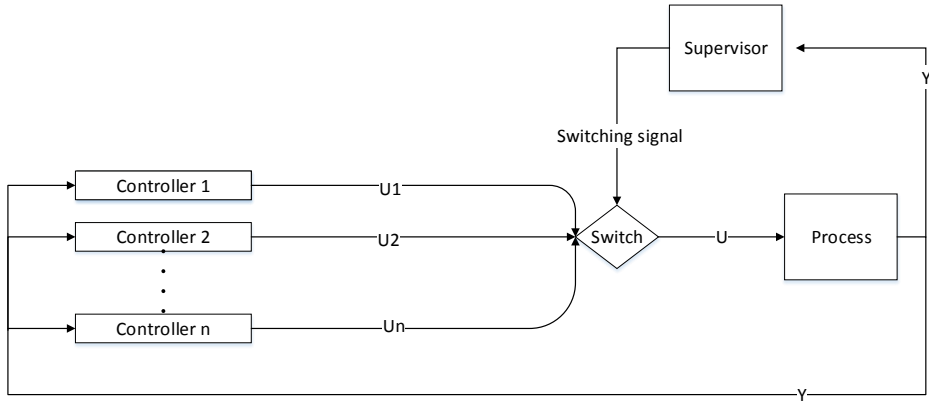
Figure 1.1: *General structure of hybrid control system with supervisory control*

1.2   Contributions

This thesis has two main contributions. Firstly a functioning DP simulator in Matlab and Simulink is implemented. The simulation model includes vessel dynamics based on R/V Gunnerus, sensors, thrust and rudder dynamics, observer, PID controller, and advanced control allocation. The control allocation algorithm is capable of utilizing a twin propeller-rudder configuration to produce sideways forces. We were unable to acquire a model which carries out this specific task at NTNU, and hope that the model implemented throughout this thesis could might be the basis for the work of other students. This will hopefully enable them to reach even further in developing and testing applications of rudders in DP.

Secondly a force feedback control scheme based on measurements of rudder forces is implemented and tested. The goal is to minimize the effect of deviation between the mathematical model of rudders in the control allocation, and the actual thruster output. In this thesis we use quadratic models for lift and drag in the rudder dynamics and linear models for inverse mapping in control allocation. Through simulations it is demonstrated that the force feedback system is both power saving compared to not using rudders and has enhanced position tracking compared to DP with rudders but without force feedback.

1.3 Scope

The scope of this thesis is as follows

1. Identify a test case and ship model with relevance for exposed aquaculture
2. Investigate rudder models and adapt to profiles of rudder force measurements
3. Implement and test control allocation with use of rudder in simulator
4. Implement and test force feedback in simulator
5. Testing and verification of solutions for rudder force feedback in DP
6. Write thesis

The problem description including scope, may be found in Appendix A.1.

1.4 Structure of Thesis

The motivation and contributions of the thesis have been introduced, and in the final section of this chapter a twofold literature study is presented. The first part on control allocation with use of rudders and the second on direct force control in robotics.

In Chapter 2, modelling of the marine vessel is described in detail. The system includes vessel dynamics, thrust allocation, actuator models and control system amongst others. Thereafter the design and implementation of the force feedback control system is described in Chapter 3 before results and discussion is presented in Chapter 4. In the final chapter conclusions on applicability of the force feedback in exposed aquaculture is drawn, before the thesis is closed with propositions for further work.

In the appendix, two notable documents is included. The problem description of this thesis and documentation of R/V Gunnerus anno 2006.

1.5 Literature Study

In this section a sample of previous work done in the field of dynamic positioning with rudders and in force feedback control is presented. In addition the documents which has been especially important in the development of this thesis is described in detail .

The first paper, written by Lindegaard and Fossens, describes a control allocation algorithm for efficient use of rudders in DP operations. Secondly we have a look at *Force Control in Robotics* written by Luigi Villani. Combining the principles presented in these two papers are the main goal of this thesis.

For an overview of previous research on dynamic positioning, see Sørensen [2011].

1.5.1   Previous Research on Rudder and Propeller Control Allocation in DP

The amount of research done in this specific area is limited. Lindegaard and Fossen [2003] and Johansen et al. [2008] suggests each their control allocation algorithm for use of rudders in DP. In Johansen et al. [2008] it is further stated that even though rudders are often used in low speed manoeuvring, it is "*not much studied in the literature, with the exception of the work of Lindegaard and Fossen [2003].*" In the following subsection of this thesis we therefore aim to present the approach suggested in the paper of Lindegaard and Fossen. Parts of the material in this paper will be covered highly detailed, as it introduces the basis for one of the most important parts of this thesis - the control allocation scheme. It should be strictly noted that all theory and every equation in the following subsection is based directly on Lindegaard and Fossen [2003], and may be found in its entirety there.

1.5.2   Fuel-Efficient Rudder and Propeller Control Allocation

Introduction

The main contribution from Lindegaard and Fossen [2003] is an algorithm for thrust and rudder control allocation for a twin propeller/rudder ship with one bow thruster. An outline of the thruster setup is shown in Figure 1.2. Simultaneous thrust and rudder control allocation for ships at zero speed is relatively challenging. This is due to the fact that rudders can only produces lift at positive propeller speed, and is limited by rudder angle. In Figure 1.2 the force domains of rudders are shown. Note that for negative thrust e.g. backwards running propeller, the rudder forces drag and lift, are both approximately zero.
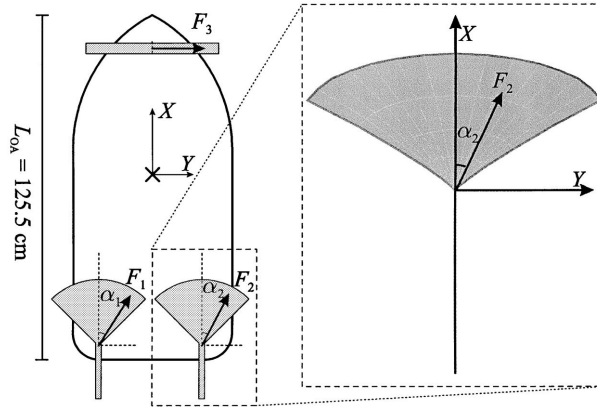
Figure 1.2: *Illustration of thruster setup on Cybership 2, with feasible thrust domains. Figure from Lindegaard and Fossen [2003]*

For ships with more actuators than controllable degrees of freedom, it is possible to find a so called optimal thrust allocation. This optimality is not optimal in the broader, or global sense of the expression. It is only optimal with regards to whichever constraints are applied to the model. When optimality is referred to later in this thesis, it is in this non-global sense. The commanded forces in each controllable degree of freedom, is given by a joystick or an automatic controller. The control allocation algorithm then transforms these to the optimal output from each individual actuator. Due to the sector limitations of the propeller-rudder pairs, control allocation is a dynamic nonlinear optimization problem, which might be solved with nonlinear optimizations techniques such as quadratic programming. Other applied methods are singular value decomposition and filtering.

The general goal of thrust allocation should for a marine vessel be low fuel consumption, by minimizing the total thrust forces. An effective control allocation (CA) algorithm will reduces fuel consumption and emission due to its higher efficiency, and a controller is therefore only as good as its CA. The fact that allocation has received significantly less attention in research than control design, might therefore be surprising.

As mentioned, the problem of control allocation arises when there are more actuators than controllable degrees of freedom. As seen in Figure 1.3, the problem can be divided into two subproblems. First one has to map the commanded forces into output from each actuator. This step decides the quality of the algorithm or the fuel efficiency. The next step is an inverse mapping from actuator output to the actual thruster setpoints, shaft speed ω_d, and rudder angle δ_d. It is called an inverse mapping, as one finds the setpoints from the inverse actuator models. The relative velocity, the vessels velocity relative to the fluid, must be accounted for, as the rudder forces are dependent on the incoming velocity. For low speed

applications such as DP, this effect might however be neglected.
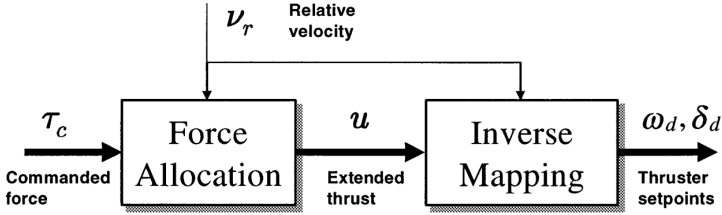
Figure 1.3: *Control allocation broken down into two subproblems. Figure from Lindegaard and Fossen [2003]*

The requirements for thrust allocation are many. Some which may or may not be included, depending on the thrust allocation's level of sophistication are

- Max capacity of each thrust device

- Feasible thrust domains

- Avoiding singular solutions which produce large thrust magnitudes

- Time constraints - The solution has to be available for real time applications with limited resources

- Support for preferred thruster direction

- Dynamic constraints, such as rudder angle rate

Notation and Definitions

In this subsection the notations used in this paper is presented.

The vessel has p actuators, such as fixed propellers or tunnel thrusters. A main propeller with rudder is considered as a rotatable device due to its thrust sector. There are p_r rotatable devices and p_f fixed devices, and the sum are $p = p_r + p_f$. As noted earlier rotatable devices has two controls n_r, rudder angle and shaft such that $n_r = 2p_r$. Nonrotatable such as fixed pitch tunnel thrusters, has only one and thus $n_f = p_f$. The vessel is overactuated if the total number of controls $n = n_r + n_f$ is greater than the controllable DOFs q, i.e. if $n > p$. In Lindegaard and Fossens paper, a 3DOF DP model in the horizontal plane is considered, i.e. surge sway and yaw.

The coordinate system of the ship is centered at the origin of the ship, with the x-axis pointing forwards and the y-axis towards starboard (right). Each thrust device k, is located at

$$r_k = \begin{bmatrix} l_{k,x} & l_{k,y} \end{bmatrix}^T \tag{1.1}$$

with regards to the origin, where $l_{k,x}$ and $l_{k,y}$ is the distance in x and y direction respectively. The rotatable thrusters, which has variable angle α_k, is numbered as $k \in [1, p_r]$ and the fixed is numbered as $k \in [p_r + 1, p]$

The normalized thrust ρ_k is defined such that

$$\rho_k = \frac{1}{F_k^{max}} F_k, \tag{1.2}$$

where F_k and $F_k^{max} > 0$ is the thrust force and maximum thrust force from thrust device k. Equation (1.2) must satisfy $|\rho_k| \leq 1$ for all k. $\mathcal{I}$ is defined as the subset of $\mathbb{R}$

$$\mathcal{I} = \{x \in \mathbb{R} | -1 \leq x \leq 1\}. \tag{1.3}$$

This gives $\rho_k \in \mathcal{I}$ and $\rho \in \mathcal{I}^\rho$.

The sum of generalized forces on the vessel τ, is defined as

$$\tau = \bar{A}(\alpha)\bar{F}\rho \tag{1.4}$$

where $\tau \in \mathbb{R}^3$, the configuration matrix $\bar{A}(\alpha)$ is

$$\bar{A}(\alpha) = \begin{bmatrix} \cos \alpha_1 & \cdots & \cos \alpha_p \\ \sin \alpha_1 & \cdots & \sin \alpha_p \\ -l_{1,y} \cos \alpha_1 + l_{1,x} \sin \alpha_1 & \cdots & -l_{1,y} \cos \alpha_1 + l_{1,x} \sin \alpha_1 \end{bmatrix} \tag{1.5}$$

and $\bar{F}$ is the diagonal matrix of maximum thrust forces

$$\bar{F} = diag\{F_1^{max}, \cdots, F_3^{max}\}. \tag{1.6}$$

Note that for certain values of α, $\bar{A}(\alpha)$ looses rank and becomes singular.

The normalized thrust ρ_k is decomposed in the horizontal plane as the extended thrust $u \in \mathcal{I}^n$, according to

$$u_{k,x} = \rho_k \cos \alpha_k, \qquad u_{k,y} = \rho_k \sin \alpha_k, \tag{1.7}$$

where $u_{k,x}$ and $u_{k,y}$ is extended thrust for device k in x and y direction respectively. For each thruster k, the extended thrust vector u_k is extracted from u through the projection Π_k, according to

$$u_k = \Pi_k u. \tag{1.8}$$

According to the previous definitions $u_k \in \mathcal{I}^2$ for rotable thrusters, and $u_k = \rho_k \in \mathcal{I}$ for fixed devices. Many thrust devices, such as the propeller-rudder pair, are however constrained to a domain within $\mathcal{I}^2$ or $\mathcal{I}$. This domain is for each u_k defined as $\mathcal{D}_k \subset \mathcal{I}^2$ for $k \in [1, p_r]$ and $\mathcal{D}_k \subset \mathcal{I}$ for $k \in [p_r + 1, p]$. The domain $\mathcal{D}_k$ of a propeller-rudder pair is shown in Figure 1.4
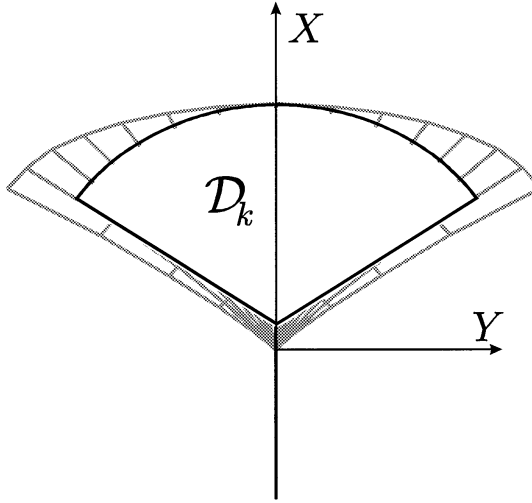
Figure 1.4: *Attainable thrust region $\mathcal{D}_k \subset \mathcal{I}^2$ for a propeller-rudder pair. The region includes the inscribed circular sector as well as the negative x axis. Figure from Lindegaard and Fossen [2003]*

Using extended thrust, the the generalized thrust vector can now be described as

$$\tau = B\bar{F}u, \tag{1.9}$$

where the configuration matrix $B \in \mathbb{R}^{3 \times n}$ is constructed from $B_r \in \mathbb{R}^{3 \times n_r}$ and $B_f \in \mathbb{R}^{3 \times n_f}$, defined as

$$B = \begin{bmatrix} B_r & B_f \end{bmatrix} \tag{1.10}$$

$$B_r = \begin{bmatrix} 1 & 0 & \cdots & 1 & 0 \\ 0 & 1 & \cdots & 0 & 1 \\ -l_{1,y} & l_{1,x} & \cdots & -l_{n_r,y} & l_{n_r,x} \end{bmatrix} \tag{1.11}$$

$$B_f = \begin{bmatrix} \cos \alpha_{p_r+1} & \cdots & \cos \alpha_p \\ \sin \alpha_{p_r+1} & \cdots & \sin \alpha_p \\ -l_{p_r+1,y} \cos \alpha_{p_r+1} + l_{p_r+1,x} \sin \alpha_{p_r+1} & \cdots & -l_{p,y} \cos \alpha_p + l_{p,x} \sin \alpha_p \end{bmatrix}, \tag{1.12}$$

Note that B has always rank of $q = 3$ for a 3DOF system as long as it is overactuated. For simplicity, define

$$A = BF_u. \tag{1.13}$$

If the constraint

$$f = Au - \tau_c = 0 \tag{1.14}$$

holds, and every u_k lies in its respective domain $\mathcal{D}_k$, the control vector of extended thrust u is feasible.

The columns of the matrix N is an orthonormal basis of $\mathcal{N}(A)$, the null-space of A. We then know that $AN = 0$. $\mathcal{R}(A)$ the row-space of A and $\mathcal{N}(A)$ are orthogonal subspaces of $\mathbb{R}$.

Finally the paper defines the generalized inverse of a matrix A as

$$A^\dagger = W^{-1} A^T \left(A W^{-1} A^T \right)^{-1}, \tag{1.15}$$

where $W = W^T > 0$. Now combining equation (1.14) and (1.15) we have an optimal, unconstrained solution

$$u_* = A^\dagger \tau_c \tag{1.16}$$

in a weighed 2-norm sense, i.e. in the sense that

$$u_*^T W u_* \leq u^T W u \quad \forall \left\{ u \in \mathbb{R}^n | Au - \tau_c = 0 \right\}, \tag{1.17}$$

and $u_* \in \mathcal{R} \left(W^{-1} A^T \right)$.

For $W = I$, the pseudoinverse simplifies to

$$A^+ = A^T (A A^T)^{-1} \tag{1.18}$$

and thus $u_* \in \mathcal{R}(A^T)$, which is used without loss of generality.

Problem Introduction

The main aim of the paper is to find a feasible control vector u, optimal with regards to a quadratic cost function. These can be solved in finite time, and is thus suitable when there is limited time and resources involved. Challenges does however arise due to nonconvexity of the thrust region. One of the challenges that arises is that of chattering, because of an introduced discontinuity in the mapping from $\tau_c \to u$ if the optimal solution is to be used at all times. In Figure 1.5 one can see that the optimal solution rapidly changes when $u_{*,k}$ crosses the dashed line. This would lead to sudden changes in the commanded thrust from each actuator. This phenomenon is called chattering, and must be avoided.
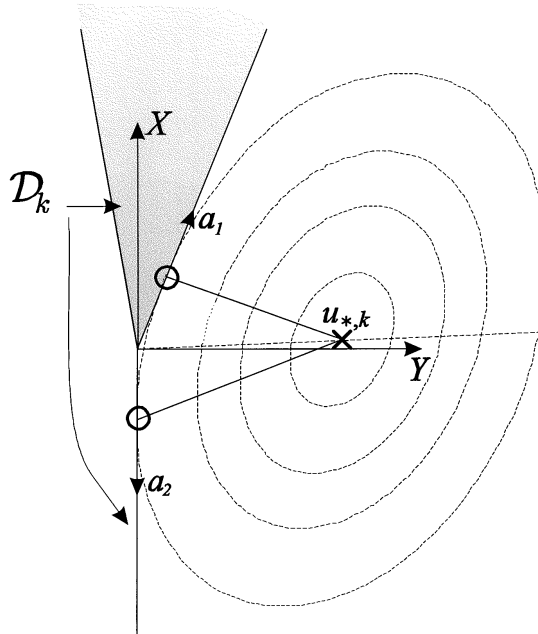
Figure 1.5: *Discontinous mapping from τ_c to u, due to nonconvex thrust domain. Figure from Lindegaard and Fossen [2003]*

Force Allocation

The paper proposes a analytical solutions, which requires no iterations. This is an obvious advantage when dealing with time constrained systems. For this to be possible, some assumptions has to be made. First one may only have one thruster with thruster constraints at any single time. This first assumption is the key to having an analytical solution. The downside being of course, that one may only utilize one out of two propeller-rudder pairs, whilst the other rudder is locked to zero angle. In DP operations, this will in most cases not be an important issue, as the thrusters will generally produce thrust in opposite directions. The second restriction, is that thrust force magnitude constraints is not considered. In iterative solvers, thrust saturation can be handled by distributing overshoot to other actuators, provided that the desired demanded thrust is attainable.

The process of finding a feasible solution u, whilst minimizing computational effort is divided into two steps. First an unconstrained, 2-norm optimal solution is found. Thereafter, if this extended thrust vector is not in the domain $\mathcal{D}$, an algorithm is used to find the minimum cost to take the unconstrained solution to the feasible domain.

Unconstrained Solution

First the unconstrained solution is calculated through the pseudoinverse as

$$u_* = A^+ \tau_c \qquad (1.19)$$

which minimizes the 2-norm of u_*. If $u_* \notin \mathcal{D}$, simply projecting the unconstrained solution on to the feasible region, will not guarantee a minimal cost solution. One has to calculate the cost of traversing the null space of A, $\mathcal{N}(A)$. The procedure is explained in the following subsection.

Sector Constraints

Assume that we have found the unconstrained solution u_* and that each thrust device k is restricted to a sector $\mathcal{D}_k$, as indicated in Figure 1.4. As the unconstrained solution satisfies the linear constraint (1.14), we may add any linear combination of the columns in N, and still satisfy the linear constraint. The linear combinations of N are denoted $\delta u = N\sigma$ where sigma is a vector of appropriate dimension. The constrained solution can be written as

$$u = u_* + \delta u = u_* + N\sigma \qquad (1.20)$$

and thus our goal is to find a σ which minimizes the two norm of u whilst at the same time rendering u feasible. δu represents the optimal step to the feasible sector.

The square two-norm may be rewritten as

$$||u||_2^2 = (u_* + N\sigma)^T (u_* + N\sigma) = ||u_*||_2^2 + ||\sigma||_2^2. \qquad (1.21)$$

Equation (1.21) is simplified by exploiting the fact that $N^T N = I$ as N is an orthonormal basis, and that $N^T u_* = 0$ since $u_* \in \mathcal{R}(A^T)$. Note that the simplified equation implies that the objective is to find a σ with minimum 2-norm.

It is necessary to find an increment δu_k such that u_k is in its feasible domain $\mathcal{D}_k$ for each actuator k.

$$u_k = u_{*,k} + \delta u_k, \quad \delta u_k = \Pi_k N\sigma. \qquad (1.22)$$

As the pseudo-inverse minimizes the 2-norm it might be applied, and we have

$$\sigma = (\Pi_k N)^+ \delta u_k, \qquad (1.23)$$

as the solution. δu_k has yet to be determined.

At the moment when the solution u_k enters the region spanned by a_1 and a_2, we know that it will be parallel to one of those. By choosing which boundary to

approach, and denoting this boundary as a, we may say that the minimum distance is traversed when $u_k \| a$, or stated as a linear constraint

$$f_s = a_\perp^T u_k = a_\perp^T \left(u_{*,k} + \delta u_k \right) = 0. \tag{1.24}$$

In equation (1.24) $a_\perp$ is perpendicular to a, and thus the inner product $a^T a_\perp = 0$. How to decide which boundary a_i to approach is discussed later on.

Next the Lagrangian L, with Lagrangian parameter λ, is defined as

$$L = \frac{1}{2} \sigma^T \sigma + \lambda f_s = \frac{1}{2} \left(\delta u_k \right)^T W_k \delta u_k + \lambda \left(a_\perp^T u_{*,k} + a_\perp^T \delta u_k \right) \tag{1.25}$$

where we may show that

$$W_k = \left(\Pi_k N N^T \Pi_k \right)^{-1} \tag{1.26}$$

is positive definite under the condition that $dim \left(\mathcal{N} \left(A \right) \right) > 1$. This is to insure that N has at least two columns. As only W_k^{-1} is utilized it is not necessary to know if equation (1.26) is invertible.

If $W_k > 0$, the problem at hands is a trivial quadratic programming problem, which may be solved using the generalized inverse. To find the minimum solution, L is minimized as

$$\frac{\partial L}{\partial \delta u_k} = W_k \delta u_k + a_\perp \lambda = 0 \tag{1.27}$$

$$\delta u_k = -W_k^{-1} a_\perp \lambda. \tag{1.28}$$

Solving for δu_k in equation (1.24), (1.28) is used to get

$$\lambda = \left(a_\perp^T W_k^{-1} a_\perp \right)^{-1} a_\perp^T u_{*,k} \tag{1.29}$$

and the optimal solution is

$$\delta u_k = -W_k^{-1} a_\perp \left(a_\perp^T W_k^{-1} a_\perp \right)^{-1} a_\perp^T u_{*,k}. \tag{1.30}$$

To get the optimal increment δu for every thrust device, equations (1.20), (1.23) and (1.28) is combined to yield

$$\delta u = N \left(\Pi_k N \right)^+ \delta u_k. \tag{1.31}$$

Assuming that $u \in \mathcal{D}$, we can finally conclude that the modified extended thrust may be given as

$$u = u_* - N \left(\Pi_k N \right)^+ W_k^{-1} a_\perp \left(a_\perp^T W_k^{-1} a_\perp \right)^{-1} a_\perp^T u_{*,k}$$
$$= \left(I - N N^T \Pi_k^T a_\perp \left(a_\perp^T W_k^{-1} a_\perp \right)^{-1} a_\perp^T \Pi_k \right) u_*. \tag{1.32}$$

An advantage of this approach is that no time consuming matrix operations has to be done, as W_k^{-1}, N and Π_k are constant matrices, and a_i are design parameters.

Sector Constraints with Rudder Anti-Chat

To avoid rudder chattering they propose to translate the coordinate system a small distance r^o along the x-axis, as shown in Figure 1.6. This insures that the rudder is not activated until the desired lift exceeds some threshold. It does as well insure a smooth transition from zero to maximum rudder angle. The new frame is denoted the B-frame, shifted r^o from the O-frame.
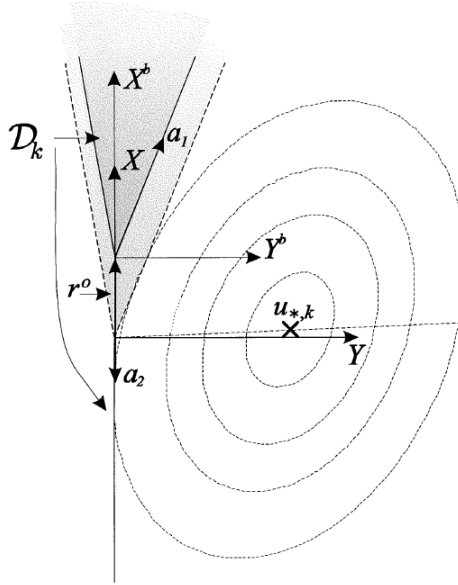
Figure 1.6: *Illustration of the B-frame, designed for rudder anti chattering. Figure from Lindegaard and Fossen [2003]*

A point c^b in the B-frame is thus given as $c^o = r^o + c^b$ in the O-frame, and $u_*^b = u_*^o - r^o$, where u_*^b is the optimal unconstrained solution decomposed in the body frame. As this is a linear translation without rotation, $\delta u_k^o = \delta u_k^b$. Due to this fact we may carry out the sector constraint adjustments in the B-frame. The previous results holds, and the Lagrangian with W_k as weighting is given as.

$$L = \frac{1}{2} \left(\delta u_k^b \right)^T W_k \delta u_k^b + \lambda \left(a_\perp^T u_{*,k}^b + a_\perp^T \delta u_k^b \right). \tag{1.33}$$

where $a_\perp$ is given in the O-frame. Minimum cost adjustment, is then written as

$$\delta u_k^b = -W_k^{-1} a_\perp \left(a_\perp^T W_k^{-1} a_\perp \right)^{-1} a_\perp^T u_{*,k}^b, \tag{1.34}$$

and the constrained solutions are given as

$$u^b = u^b_* + N \left(\Pi_k N\right)^+ \delta u^b_k \tag{1.35}$$

$$u^o = u^o_* + N \left(\Pi_k N\right)^+ \delta u^o_k \tag{1.36}$$

in O- (u^o) and B-frame (u^b). A detailed calculation gives

$$u = \left(I - N N^T \Pi_k^T a_\perp \left(a_\perp^T W_k^{-1} a_\perp\right)^{-1} a_\perp^T \Pi_k\right) u_*$$

$$+ N \left(\Pi_k N\right)^+ W_k^{-1} a_\perp \left(a_\perp^T W_k^{-1} a_\perp\right)^{-1} a_\perp^T r^o. \tag{1.37}$$

Note that the first term is identical to (1.32), whilst the second term is a linear contribution from the translation r^o.

The Equicost Line

If the solution $u_{*,k}$ is not in the feasible domain $\mathcal{D}_k$, it is necessary to decide whether to approach boundary a_1 or a_2. To do this the equicost line e_l, shown as a dotted line in Figure 1.6, is needed. On any point p on e_l, the cost of approaching each of the two boundaries are equal. From the previous subsections we have

$$\delta p_1 = W_k^{-1} \left(a_1\right)_\perp \left(\left(a_1\right)_\perp^T W^{-1} \left(a_1\right)_\perp\right)^{-1} \left(a_1\right)_\perp^T p \tag{1.38}$$

$$\delta p_2 = W_k^{-1} \left(a_2\right)_\perp \left(\left(a_2\right)_\perp^T W^{-1} \left(a_2\right)_\perp\right)^{-1} \left(a_2\right)_\perp^T p, \tag{1.39}$$

as the optimal step δp_i, approaching each boundary. The cost J is calculated as

$$J_i = \left(\delta p_i\right)^T W_k \delta p_i = p^T \left(\left(a_i\right)_\perp \left(\left(a_i\right)_\perp^T W^{-1} \left(a_i\right)_\perp\right)^{-1} \left(a_i\right)_\perp^T\right) p, \tag{1.40}$$

for each boundary $i \in (1, 2)$, and thus to find the equicost line $J_1 = J_2$, or $\Delta J = J_1 - J_2 = 0$ is required. We may write this as

$$\Delta J = p^T L p = 0 \Leftrightarrow e_l^T L e_l = 0, \tag{1.41}$$

where $L = L^T$ is given as

$$L = \begin{bmatrix} L_{11} & L_{12} \\ L_{12} & L_{22} \end{bmatrix} = \frac{\left(a_1\right)_\perp \left(a_1\right)_\perp^T}{\left(a_1\right)_\perp^T W_k^{-1} \left(a_1\right)_\perp} - \frac{\left(a_2\right)_\perp \left(a_2\right)_\perp^T}{\left(a_2\right)_\perp^T W_k^{-1} \left(a_2\right)_\perp}. \tag{1.42}$$

Defining the vector $e_l = [x, y]$ and expanding, one can see that equation (1.42) may be written as

$$L_{11} x^2 + 2 L_{12} x y + L_{22} y^2 = 0. \tag{1.43}$$

This equation may be solved using polar coordinates with $e_l = [\cos\theta, \sin\theta]$, yielding

$$\theta = \arctan\left(-\frac{L_{12}}{L_{22}} \pm \sqrt{\left(\frac{L_{12}}{L_{22}}\right)^2 - \frac{L_{11}}{L_{22}}}\right) + j\pi. \qquad (1.44)$$

Here $j = 1, 2$ and the solution spanned by a_1 and a_2 is selected among the different possibilities.

1.5.3 Previous Research on Force Control

We have been unable to locate previous research on force feedback control utilized in DP systems, and therefore conclude that there is probably little or no previous work in this field. Luckily this principle is widely used in robotics, where the goal is to control interactions between robot manipulator and environment. In the following subsection basics of force control is introduced including references to a small sample of previous work in the field. The literature study is finally concluded with 1.5.4 where research on direct force control as found in Villani [2015] is presented. Note that the term force feedback refers to control of both forces and moments as used in this thesis.

Introduction to Force Control

When a robot manipulator is interacting with the environment, it is in many cases crucial to control both motion and forces. Especially if the environment is stiff we might otherwise get large contact forces which could in turn ruin the equipment. Also when interacting with a dynamic or soft environment as is the case for medical robots with a human, large contact forces should be avoided for obvious reasons. To avoid unsafe values one might introduce passive measures, such as soft arms and elastic joints, or active compliances. Active compliances is further divided into two sub categories as seen in Siciliano and Villani [2012] - Indirect force control and direct force control. In indirect force control one does not necessarily have to close a force feedback loop. Instead forces are controlled through motion control. An example of indirect force control is impedance control as pressented in Hogan [1984]. In direct control one has the possibility to close the loop and guide the contact forces to desired values (Villani [2015]). Direct force control operates on force error, i.e. the difference between desired and measured force (Siciliano and Villani [2012]. One such control method is *hybrid force/motion control* as described in Raibert and Craig [1981]. The approach of direct force control seems promising for the purpose of this thesis and thus we will now delve deeper into it.

1.5.4   Force Control in Robotics

Modeling

In the following subsections parts of *Force Control In Robotics* (Villani [2015]) is presented. Interactions between a robot manipulator end-effector and environment is considered.

The end-effector pose can be described through its position $\mathbf{p}_e$ and the rotation matrix $\mathbf{R}_e$. The end-effector dynamics is described by its velocity $\mathbf{v}_e = \left(\dot{\mathbf{p}}_e^T \ \boldsymbol{\omega}_e^T\right)^T$ where $\dot{\mathbf{p}}_e$ and $\boldsymbol{\omega}_e$ is the translational and angular velocity, respectively. These can be calculated from the joint velocity vector $\dot{\mathbf{q}}$ through the end-effector Jacobian $\mathbf{J}$ as

$$\mathbf{v}_e = \mathbf{J}(\mathbf{q})\dot{\mathbf{q}}. \tag{1.45}$$

For simplicity a nonsingular, square matrix Jacobian is considered. The wrench of the end-effector is described by $\mathbf{h}_e = \left(\mathbf{f}_e^T, \ \mathbf{m}_e^T\right)^T$, where $\mathbf{f}_e$ is the force and $\mathbf{m}_e$ is the moment applied by the end-effector on the environment. The corresponding joint torque $\boldsymbol{\tau}$ is computed as

$$\boldsymbol{\tau} = \mathbf{J}^T(\mathbf{q})\mathbf{h}_e. \tag{1.46}$$

Finally the dynamic model of the manipulator is described as

$$\boldsymbol{\Lambda}\left(\mathbf{q}\right)\dot{\mathbf{v}}_e + \boldsymbol{\Gamma}\left(\mathbf{q}, \dot{\mathbf{q}}\right)\mathbf{v}_e + \boldsymbol{\eta}\left(\mathbf{q}\right) = \mathbf{h}_c - \mathbf{h}_e. \tag{1.47}$$

where $\mathbf{h}_c$ is the end-effector wrench corresponding to $\boldsymbol{\tau}_c$, $\mathbf{h}_c = \mathbf{J}^{-T}\boldsymbol{\tau}_c$, $\boldsymbol{\tau}_c$ is the input joint torques and $\dot{\mathbf{v}}_e$ is the end-effector acceleration. $\boldsymbol{\Lambda}\left(\mathbf{q}\right)$ is the operational space inertia matrix, $\boldsymbol{\Gamma}\left(\mathbf{q}, \dot{\mathbf{q}}\right)$ is the wrench including Coriolis and centrifugal effects, and $\boldsymbol{\eta}\left(\mathbf{q}\right)$ is the gravitational wrench. The equation (1.47) corresponds to Newton's second law of motion where forces on the joints work through the end-effector.

Direct Force Control

In direct force control a model of the interaction task is often necessary in order to compute desired forces. In this subsection the design of a task frame and task specifications is described and an example case is given. It is assumed that the environment is rigid, frictionless, and imposes kinematic constraints to the end-effector motion. Constraints in m independent degrees of freedom (DOFs) are imposed on the end-effector, yielding a velocity subspace of dimension $6 - m$, whilst the end-effector wrench lives in an m-dimensional subspace. They can be expressed as

$$\mathbf{v}_e = \mathbf{S}_v(\mathbf{q})\boldsymbol{\nu}, \quad \mathbf{h}_e = \mathbf{S}_f(\mathbf{q})\boldsymbol{\lambda} \tag{1.48}$$

where $\boldsymbol{\nu}$ and $\boldsymbol{\lambda}$ are suitable $(6 - m) \times 1$ and $m \times 1$ vectors describing velocities and forces respectively. $\mathbf{S}_v$ and $\mathbf{S}_f$ are matrices describing the subspaces of velocity

and force. Due to the assumption that the environment is rigid and frictionless, the subspaces of forces and velocities are reciprocal. I.e.

$$\mathbf{h}_e^T \mathbf{v}_e = 0, \quad \mathbf{S}_f(\mathbf{q})\mathbf{S}_v(\mathbf{q}) = 0. \tag{1.49}$$

Reciprocity implies that the wrench does not cause any work against the twist.

A task is specified through desired end-effector velocity $\mathbf{v_d}$, and wrench $\mathbf{h_d}$, calculated as

$$\mathbf{v}_d = \mathbf{S}_v \boldsymbol{\nu}_d, \quad \mathbf{h}_d = \mathbf{S}_f \mathbf{S}_v(\mathbf{q})\boldsymbol{\lambda}_d, \tag{1.50}$$

where $\boldsymbol{\nu}_d$ and $\boldsymbol{\lambda}_d$ are vectors describing desired velocities and forces respectively.

A "*peg-in-hole*" operation is given as an example task. The peg with axis system as given in 1.7, is allowed to have a non zero velocity along the z-axis and angular velocity around the z-axis. Desired forces and torques in and around the x and y axis is zero. The operation is over when a large positive force in z direction is detected - indicating that the peg has hit the bottom. This task description yields subspace matrices

$$\mathbf{S}_v = \begin{bmatrix} 1 & 0 & 0 & 0 \\ 0 & 1 & 0 & 0 \\ 0 & 0 & 0 & 0 \\ 0 & 0 & 1 & 0 \\ 0 & 0 & 0 & 1 \\ 0 & 0 & 0 & 0 \end{bmatrix}, \quad \mathbf{S}_f = \begin{bmatrix} 0 & 0 \\ 0 & 0 \\ 1 & 0 \\ 0 & 0 \\ 0 & 0 \\ 0 & 1 \end{bmatrix}. \tag{1.51}$$
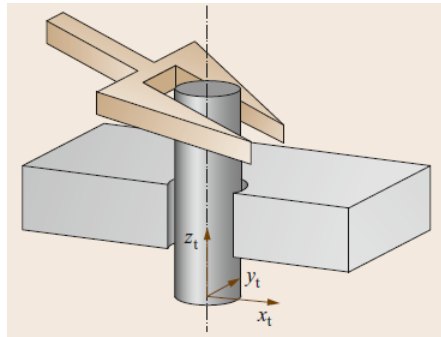

Figure 1.7: *Insertion of cylinder (peg) into hole. Figure from Villani [2015]*

Hybrid Force/Motion Control

Due to the reciprocity as mentioned in the previous subsection, an approach known as hybrid force/motion control is a naturally viable option. This method aims at

simultaneous control of end-effector force and motion in two reciprocal subspaces. Reduced order dynamics are described as

$$\mathbf{\Lambda}_v(\mathbf{q})\dot{\mathbf{\nu}} = \mathbf{S}_v^T\left[\mathbf{h}_c - \mathbf{\mu}\left(\mathbf{q}, \dot{\mathbf{q}}\right)\right], \tag{1.52}$$

where $\mathbf{\mu}\left(\mathbf{q}, \dot{\mathbf{q}}\right) = \mathbf{\Gamma}\left(\mathbf{q}, \dot{\mathbf{q}}\right)\mathbf{v}_e + \mathbf{\eta}\left(\mathbf{q}\right)$ and $\mathbf{\Lambda}_v = \mathbf{S}_v^T\mathbf{\Lambda}\mathbf{S}_v$ assumed constant subspace matrices. $\mathbf{\lambda}$ is computed as

$$\mathbf{\lambda} = \mathbf{S}_f^\dagger\left(\mathbf{q}\right)\left[\mathbf{h}_c - \mathbf{\mu}\left(\mathbf{q}, \dot{\mathbf{q}}\right)\right] \tag{1.53}$$

where we note that the contact forces $\mathbf{\lambda}$ instantly depends on applied input wrench $\mathbf{h}_c$. Further an inverse-dynamics inner control loop is designed through choosing $\mathbf{h_c}$ as

$$\mathbf{h}_c = \mathbf{\Lambda}\left(\mathbf{q}\right)\mathbf{S}_v\mathbf{\alpha}_\nu + \mathbf{S}_f\mathbf{f}_\lambda + \mathbf{\mu}\left(\mathbf{q}, \dot{\mathbf{q}}\right), \tag{1.54}$$

Proper choice of control inputs for velocity and force, $\mathbf{\alpha}_\nu$ and $\mathbf{f}_\lambda$ respectively, then yields

$$\dot{\mathbf{\nu}} = \mathbf{\alpha}_v, \quad \mathbf{\lambda} = \mathbf{f}_\lambda, \tag{1.55}$$

indicating decoupled motion and force control. Forces can now be driven to the desired forces $\mathbf{\lambda}_d$ through

$$\mathbf{f}_\lambda = \mathbf{\lambda}_d\left(t\right). \tag{1.56}$$

To account for disturbance forces and model errors, force feedback is introduced in the form of proportional (P)

$$\mathbf{f}_\lambda = \mathbf{\lambda}_d\left(t\right) + \mathbf{K}_{P\lambda}\left[\mathbf{\lambda}_d\left(t\right) - \mathbf{\lambda}\left(t\right)\right] \tag{1.57}$$

or integral (I) action

$$\mathbf{f}_\lambda = \mathbf{\lambda}_d\left(t\right) + \mathbf{K}_{I\lambda}\int_0^t\left[\mathbf{\lambda}_d\left(\tau\right) - \mathbf{\lambda}\left(\tau\right)\right]d\tau. \tag{1.58}$$

$\mathbf{K}_{P\lambda}$ and $\mathbf{K}_{I\lambda}$ are positive-definite (PDF) matrix gains. Proportional feedback reduces instantaneous force error whilst integral feedback compensates for constant or slowly varying force bias.

Velocity control is similarly achieved through the PI control scheme

$$\mathbf{\alpha}_\nu = \dot{\mathbf{\nu}}_d\left(t\right) + \mathbf{K}_{P\nu}\left[\mathbf{\nu}_d\left(t\right) - \mathbf{\nu}\left(t\right)\right] + \mathbf{K}_{I\nu}\int_0^t\left[\mathbf{\nu}_d\left(\tau\right) - \mathbf{\nu}\left(\tau\right)\right]d\tau \tag{1.59}$$

with suitable matrix gains $\mathbf{K}_{P\nu}$ and $\mathbf{K}_{I\nu}$. This control scheme insures exponential stability of $\mathbf{\nu}_d\left(t\right)$ and $\dot{\mathbf{\nu}}_d\left(t\right)$.

Note that the assumption of rigid contact might be loosened, indicating that both force and motion might be allowed in some or all DOFs.

Chapter 2

Modelling of Marine Vessel

2.1 Introduction

Prior to introducing each component in the simulation model, a few preliminary statements have to be made. Parts of the model were set up by PhD candidates Svenn Are Værnø and Astrid H. Brodtkorb, using the Marine Systems Simulator (MSS) toolbox [Fossen and Perez [2004]]. This includes the vessel dynamics, environmental models and measurement module. During the work with the thesis some minor changes and bug fixes have been made to these parts of the model, though the overall structure is not altered. Every other system including observer, guidance system, motion controller, control allocation and thruster/rudder dynamics were implemented by the author through the pre project and master thesis. The force feedback control system were designed and implemented during the work with the master thesis.

2.1.1 System Overview

The general idea behind a DP system is based on a few basic components, as shown in Figure 2.1. The vessel dynamics constitutes, together with sensor module, environmental model and thruster and rudder dynamics what is commonly referred to as the physical system or process. The process is in this case the research vessel Gunnerus along with the environment in which it operates. R/V Gunnerus is presented in 2.1.2, whilst the vessel dynamics, rudder and thruster models, sensors and environmental model is presented in sections through this chapter.

To implement the observer and controller for the position feedback loop, we have used Linear Quadratic Gaussian (LQG) control design as described in Sørensen [2013] and Fossen [2011]. Its two parts, the linear quadratic estimator (LQE) and

the linear quadratic regulator (LQR) can be computed and designed separately
and is guaranteed to be stable as long as each component is stable. The design
of position observer and controller is described in Section 2.6 and 2.7 respectively.
In this thesis an Extended Kalman filter (EKF) is used as observer in place of the
traditional Kalman filter. The EKF is a nonlinear system, and thus we do not
strictly speaking implement an LQE. This LQG setup has however been shown to
perform well compared to the regular LQG in e.g. Yang and Marjanovic [2011].

The simplest form of guidance is implemented and the system is described in short
terms in 2.8 whilst the final block in Figure 2.1, the control allocation is presented
in Section 2.9. The purpose of the control allocation algorithm is to map the
commanded thrust in body frame, to thruster commands applicable to the physical
system.
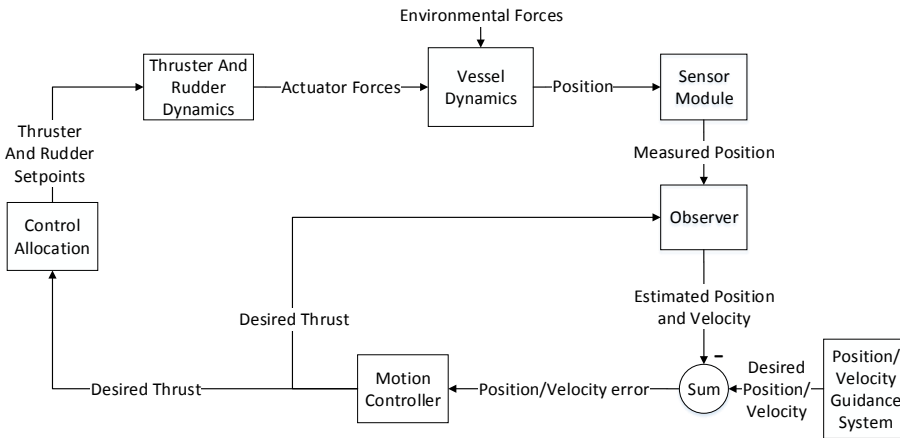
Figure 2.1: *System overview*

2.1.2   Vessel - R/V Gunnerus

R/V Gunnerus has the dimensions of a medium to small well boat, compared to
today's standards. The largest well boats today are up to around 80 m length.
As the aquaculture industry grows, and moves further into less sheltered waters,
the vessels are likely to grow even larger. R/V Gunnerus does however have a
thruster system which resembles what one might have on a well boat. The general
conclusions should thus hold, also for larger vessels. In this subsection the most
important data of the vessel will be provided in a short and concise manner. The
data where provided by Svenn Are Værnø and Astrid Brodtkorb.

The main dimensions of Gunnerus is given in Table 2.1, and other miscellaneous
data regarding center of gravity, metacentric height etc. is found in Table 2.2.
Symbols and abbreviations is described in the nomenclature and list of abbrevia-
tions.

Table 2.1: *Main dimensions of Gunnerus*

L_{pp} [m]	T [m]	B [m]
28.9	3.971	9.6

Table 2.2: *Miscellaneous Vessel Data*

$CG[m]$	$GM_L[m]$	$GM_T[m]$	$C_B[-]$	$CB[m]$	$S[m^2]$
[-1.947, 0, 3.971]	17.454	0.700	0.659	[-1.947, 0, 2.343]	353.683

The rigid body and added mass (at infinite frequency) is given respectively as

$$M_{rb} = 10^7 \times \begin{bmatrix} 0.0744 & 0 & 0 & 0 & 0 & 0 \\ 0 & 0.0744 & 0 & 0 & 0 & 0 \\ 0 & 0 & 0.0744 & 0 & 0 & 0 \\ 0 & 0 & 0 & 0.8398 & 0 & 0 \\ 0 & 0 & 0 & 0 & 3.8831 & 0 \\ 0 & 0 & 0 & 0 & 0 & 3.883 \end{bmatrix}$$

$$M_a = 10^7 \times \begin{bmatrix} 0.0083 & 0 & 0 & 0 & 0 & 0 \\ 0 & 0.0331 & 0 & -0.0126 & 0 & 0.0032 \\ 0 & 0 & 0.1066 & 0 & 0.1974 & 0 \\ 0 & -0.0110 & 0 & 0.1639 & 0 & -0.0023 \\ 0 & 0 & 0.1856 & 0 & 5.5226 & 0 \\ 0 & -0.0069 & 0 & 0.0431 & 0 & 1.9288 \end{bmatrix},$$

with the resulting total mass

$$M = M_{rb} + M_a. \tag{2.1}$$

Viscous damping and potential wave radiation damping is

$$D_v = 10^7 \times \begin{bmatrix} 0.0044 & 0 & 0 & 0 & 0 & 0 \\ 0 & 0.0177 & 0 & 0 & 0 & 0 \\ 0 & 0 & 0 & 0 & 0 & 0 \\ 0 & 0 & 0 & 0.0686 & 0 & 0 \\ 0 & 0 & 0 & 0 & 0 & 0 \\ 0 & 0 & 0 & 0 & 0 & 1.0259 \end{bmatrix}$$

$$D_p = 10^7 \times \begin{bmatrix} 0.0005 & 0 & 0 & 0 & 0 & 0 \\ 0 & 0.0021 & 0 & -0.0020 & 0 & 0.0294 \\ 0 & 0 & 0.0002 & 0 & -0.0068 & 0 \\ 0 & -0.0020 & 0 & 0.0008 & 0 & -0.0201 \\ 0 & 0 & -0.0068 & 0 & 0.0820 & 0 \\ 0 & 0.0294 & 0 & -0.0201 & 0 & 0.1894 \end{bmatrix}$$

with the resulting total damping

$$D = D_v + D_p. \tag{2.2}$$

For further information on R/V Gunnerus, consult NTNU's webpages at NTNU [2017a]. Data on thrusters are given in Section 2.5 and a data sheet on the vessel, as found in NTNU [2017b], is given in appendix A.2.

2.2 Vessel Dynamics

The vessel motion is a superposition of the wave frequency (WF) and low frequency (LF) motion. WF motion is calculated using the motion response amplitude operators(RAO), WF loads are calculated using the force RAOs and LF motion is calculated using the linearized 6DOF equation of motion for low-speed applications, included fluid memory effects. These concepts are thoroughly described in Fossen [2011]. In the following subsections the general concepts, and most important equations will be given.

2.2.1 Low Frequency Motion

For LF motion, we start with the equation of motion for irrotational and constant ocean currents, given as

$$\dot{\boldsymbol{\eta}} = \mathbf{J}(\boldsymbol{\eta})\boldsymbol{\nu} \tag{2.3}$$

$$\mathbf{M}\dot{\boldsymbol{\nu}}_r + \mathbf{C}(\boldsymbol{\nu}_r)\boldsymbol{\nu}_r + \mathbf{D}(\boldsymbol{\nu}_r)\boldsymbol{\nu}_r + \mathbf{g}(\boldsymbol{\eta}) + \mathbf{g}_0 = \boldsymbol{\tau}_{wind} + \boldsymbol{\tau}_{wave} + \boldsymbol{\tau},$$

in Fossen [2011]. $\mathbf{J}(\boldsymbol{\eta})$ is the rotation matrix from body to NED in euler angles, $\mathbf{M}$ is the sum of added and rigid body mass, $\mathbf{C}(\boldsymbol{\nu}_r)$ is the Corriolis-centripetal matrix and $\mathbf{D}(\boldsymbol{\nu}_r)$ is the damping matrix. $\mathbf{g}(\boldsymbol{\eta})$ is a vector of gravitational/buoyancy forces and moments and $\mathbf{g}_0$ is a vector used for pre trimming (ballast control). Finally $\boldsymbol{\tau}$, $\boldsymbol{\tau}_{wave}$ and $\boldsymbol{\tau}_{wind}$ are the vectors of control input, wind and wave induced forces. The environmental forces may be seen as a disturbance $\mathbf{w}$. Note that wind and waves are included in the model as forces, calculated from e.g. the force RAOs, whilst current is implemented as relative velocity

$$\boldsymbol{\nu}_r = \boldsymbol{\nu} - \boldsymbol{\nu}_c, \tag{2.4}$$

where $\boldsymbol{\nu}_c$ is the current velocity and $\boldsymbol{\nu}$ is the vessel velocity, both presented in body frame.

When assuming low velocities, small pitch and roll angles and $\mathbf{g}_0 = 0$ the model (2.3) may be linearised around zero, and simplified to

$$\dot{\boldsymbol{\eta}}_p = \boldsymbol{\nu} \tag{2.5}$$

$$\mathbf{M}\dot{\boldsymbol{\nu}} + \mathbf{D}\boldsymbol{\nu} + \mathbf{G}\boldsymbol{\eta}_p = \boldsymbol{\tau} + \mathbf{w}.$$

When including fluid memory effects $\boldsymbol{\mu}$, we get the implemented model

$$\dot{\boldsymbol{\eta}}_p = \boldsymbol{\nu} \tag{2.6}$$
$$\mathbf{M}\dot{\boldsymbol{\nu}} + \mathbf{D}\boldsymbol{\nu} + \mathbf{G}\boldsymbol{\eta}_p + \boldsymbol{\mu} = \boldsymbol{\tau} + \mathbf{w}$$

2.2.2 Wave frequency motion and force

The force and motion RAOs is the transfer functions from wave amplitude to 1st and 2nd order force and 1st order motion respectively. When given a sea state represented by the significant wave height and peak frequency, one uses the desired wave spectrum to acquire the time varying wave amplitude. At this stage one simply multiplies with the corresponding RAO, to acquire motion and force.

The first and second order forces for the six DOFs, are given in Fossen [2011] as

$$\tau_{wave1}^{\{DOF\}} = \sum_{k=1}^{N}\sum_{i=1}^{M} \rho g \left| F_{wave1}^{\{DOF\}}(\omega_k, \beta_i) \right| A_k \cos\left(\omega_e(U, \omega_k, \beta_i)t + \angle F_{wave1}^{\{DOF\}}(\omega_k, \beta_i) + \epsilon_k\right)$$
$$\tag{2.7}$$

$$\tau_{wave2}^{\{DOF\}} = \sum_{k=1}^{N}\sum_{i=1}^{M} \rho g \left| F_{wave2}^{\{DOF\}}(\omega_k, \beta_i) \right| A_k \cos\left(\omega_e(U, \omega_k, \beta_i)t + \epsilon_k\right) \tag{2.8}$$

where

$$\left| F_{wave1/2}^{\{DOF\}}(\omega_k, \beta_i) \right| \tag{2.9}$$

is the first or second order wave force amplitude, for varying wave frequencies ω_k and direction β_i, and

$$\angle F_{wave1/2}^{\{DOF\}}(\omega_k, \beta_i) \tag{2.10}$$

is the phase. The encounter frequency, ω_e is calculated as

$$\omega_e = \omega_k - \frac{\omega_k^2}{g} U \cos(\beta). \tag{2.11}$$

U is the vessel speed, and A_k is the wave amplitude.

In the same manner, the wave induced motions (WF motions) are defined as

$$\eta_w^{\{DOF\}} = \sum_{k=1}^{N}\sum_{i=1}^{M} \rho g \left| \eta_w^{\{DOF\}}(\omega_k, \beta_i) \right| A_k \cos\left(\omega_e(U, \omega_k, \beta_i)t + \angle\eta_w^{\{DOF\}}(\omega_k, \beta_i) + \epsilon_k\right),$$
$$\tag{2.12}$$

where $\left| \eta_w^{\{DOF\}}(\omega_k, \beta_i) \right|$ and $\angle\eta_w^{\{DOF\}}(\omega_k, \beta_i)$ is the amplitude and phase of of the motion RAO. The total motion $\boldsymbol{\eta}_{tot}$ is calculated as

$$\boldsymbol{\eta}_{tot} = \boldsymbol{\eta} + \boldsymbol{\eta}_w, \tag{2.13}$$

where $\boldsymbol{\eta}$ and $\boldsymbol{\eta}_w$ is the LF and WF motion respectively.

2.3 Sensor module

In this section we shortly introduce the concept of a sensor module and describe how measurement noise and bias is introduced to the states. In the case of a real vessel the sensor system gathers information on states such as position and acceleration. Measurement noise and system errors is unavoidable and signals should therefore be checked and bad signals should be rejected. A bad signal could e.g. be frozen, or have to large variance. This is done in a signal processing module. For a simulator, the situation is however quite different. As position output from the vessel dynamics is "perfect", we need to introduce measurement noise, failure states and realistic sampling time according to need. This is done in what is described as the sensor module in Figure 2.1. Tests regarding measurement errors and failure is not in the scope of this thesis, and thus no type of failure mode is implemented. For simplicity the sampling rate is set equal to the time step of the equation solver. The purpose of the sensor module is thus reduced to introduction of noise, and the process is described in the following subsection. Note that the sensor model were, as mentioned earlier, designed by Svenn Are Værnø and Astrid H. Brodtkorb.

2.3.1 Measurement noise

The position sensor is modelled as a Global Navigation Satellite System (GNSS). Noise is described by Gaussian white noise with zero mean and a given variance. In addition a constant bias attributed to atmosphere and a band limited white noise attributed to thermal effects is added. The GNSS signal is delayed as it propagates through the atmosphere, which yields a constant bias. Thermal noise is cause by *"the finite GNSS signal strength and the receiver amplifier noise"*(Jin et al. [2014]). There are several other potential sources of GNSS noise. Consult Jin et al. [2014] for further reading on the subject. Heading sensors is simply modelled as a compass with Gaussian white noise and a constant bias.

To create noisy signals the Gaussian white noise and bias signal is added to the original perfect one from the vessel dynamics. Noise parameters are given in Table 2.3. For the sake of simplicity bias terms and thermal noise where set to zero, as signal quality is not a vital part of this thesis. Do as well note that with the parameters given in Table 2.3 measurement noise is negligible compared to wave frequency motion. (See Section 2.6)

Table 2.3: *Sensor noise parameters*

Parameter	Value
Gaussian GNSS noise variance	0.01 [m]
Gaussian compass noise variance	$(0.01\pi/180)^2$ [rad]
Thermal noise, atmospheric bias, compas bias	0

2.4   Modelling of Environmental Forces

In this section environmental models for waves, current and wind are presented.

2.4.1   Wave Model

The wave model is based on the JONSWAP spectrum with constant direction. Wave direction is defined with zero degrees as incident waves from the south, and positive rotation is defined clockwise. The JONSWAP spectrum is given as

$$S(w) = \alpha \frac{g^2}{\omega^5} \exp\left[-\frac{5}{4}\left(\frac{\omega_p}{\omega}\right)^4\right] \gamma^{\exp\left[-\frac{1}{2}\left(\frac{\omega-\omega_p}{\sigma\omega_p}\right)^2\right]}, \qquad (2.14)$$

according to Sørensen [2013]. In the model implemented in this thesis, peak frequency is given as $\omega_p = 0.6$ and significant wave height is set to $H_s = 2$. The values for γ, a peakedness parameter, α, a parameter determining the shape of the spectrum at high frequencies, and σ has to be chosen. Faltinsen [1993] proposes the following JONSWAP parameters:

$$\gamma = 3.3; \quad \sigma = \begin{cases} 0.07\omega \leq \omega_p \\ 0.09\omega \geq \omega_p \end{cases} \quad ; \quad \alpha = 0.2\frac{H_s^2\omega_p^4}{g^2} \qquad (2.15)$$

The time varying wave elevation $\zeta(t)$, is then calculated as

$$\zeta(t) = \sum_{n=1}^{N} \sqrt{2S(\omega_n)\Delta\omega}\cos(\omega_n t + \epsilon_n), \qquad (2.16)$$

where the phase angle ϵ_n is a stochastic variable, statistically independent and uniformly distributed and $\Delta\omega$ is the frequency interval. In the simulation cases of this thesis a random selection of 50 different wave frequencies are used as input for the wave model.

2.4.2   Current Model

Current is modelled as constant surface current with velocity $V_c = 0.2\frac{m}{s}$, and incident direction ψ_c directly from north. In addition a current profile is modelled, though the effect of this is small, as R/V Gunnerus is a surface vessel. The current velocity vector in NED is calculated as

$$\mathbf{v}_c = [V_c\cos(\psi_c), V_c\sin(\psi_c), 0].$$

To model a time varying current velocity or direction, a Gauss-Markov process may be applied, as proposed by Fossen [2011]

$$\dot{V}_c + \mu V_c = w, \tag{2.17}$$

where w is a Gaussian white noise and the constant $\mu \geq 0$. For $\mu = 0$ The process is a random walk.

The current profile is implemented as proposed by Sørensen [2013] as

$$V_c = V_{c,tide}(z) + V_{c,wind}(z) \tag{2.18}$$

$$V_{c,tide}(z) = V_{c,tide} \left(\frac{h-z}{h} \right)^{\frac{1}{7}} \quad for \ z \geq 0 \tag{2.19}$$

$$V_{c,wind}(z) = V_{c,wind} \left(\frac{h_0-z}{h_0} \right)^{\frac{1}{7}} \quad for \ 0 \leq z \leq h_0 \tag{2.20}$$

$$V_{c,wind}(z) = 0 \quad for \ z \geq h_0. \tag{2.21}$$

Here $V_{c,tide}$ is the surface tidal current, and $V_{c,wind}$ is the surface wind current. h is the depth, and h_0 is the reference depth, set to for example 50 metres. The wind generated current is calculated based on the mean wind at 10 metres, $\bar{U}_{10}$. $V_{c,wind} = 0.015\bar{U}_{10}$.

2.4.3   Wind Model

Although it has been decided not to implement a wind model, we choose to go through a possible method here, for future reference. As described in Sørensen [2013], wind is commonly divided into three components. A mean wind component, a slowly varying component and a wind gust component. Constant direction is assumed in the following description.

Mean velocity $\bar{U}$, at elevation z, may be described as

$$\frac{\bar{U}(z)}{\bar{U}_{10}} = \frac{5}{2}\sqrt{\kappa}\ln\frac{z}{z_0}; \quad z_0 = 10\exp\left(-\frac{2}{5\sqrt{\kappa}}\right), \tag{2.22}$$

where $\bar{U}_{10}$ is the mean wind speed at 10 metres over one hour, and κ is the sea surface drag coefficient[Sørensen [2011]].

The slowly varying component $\dot{U}_{SV}(z)$ can be described as

$$\dot{U}_{SV}(z) + \mu U_{SV} = w, \tag{2.23}$$

where w is a zero mean white noise, and $\mu \geq 0$ is a constant.

The wind gust may be modelled by a wind spectrum, such as the following wind spectra, recommended by the NORSOK standard

$$S(f) = 320 \frac{\left(\frac{\bar{U}_{10}}{10}\right)^2 \left(\frac{z}{10}\right)^{0.45}}{\left(1 + x^n\right)^{\frac{5}{3n}}}, \quad n = 0.468 \tag{2.24}$$

$$x = 172 f \left(\frac{z}{10}\right)^{\frac{2}{3}} \left(\frac{\bar{U}_{10}}{10}\right)^{-\frac{3}{4}}, \tag{2.25}$$

where f is the frequency in hertz and n is a design parameter. Each harmonic component $U_{gi}(t)$ is than defined as

$$U_{gi}(t) = \sqrt{2 S(f_i) \Delta f_i} \cos(2\pi f_i t + \phi_i). \tag{2.26}$$

Here f_i is the i'th frequency, Δf is the frequency interval and ϕ_i is a evenly distributed phase angle (Sørensen [2013]).

With N gust components the total wind realization can be described as

$$\bar{U}(z) + U_{SV}(z) + \sum_{i=1}^{N} U_{gi}(t). \tag{2.27}$$

2.5   Thruster and Rudder Dynamics

With this thesis' focus on use of rudders in DP systems, realistic modelling of thruster and rudder dynamics is crucial. To create design parameters vessel data from R/V Gunnerus including available power and shaft speed and propeller/rudder position and diameter has been utilized. Data on position and diameter were measured from drawings of the general arrangement, and it is assumed that the position of the rudder and propeller in a pair is equal.

Upon delivery in 2006, the vessel were equipped with two 500 kW main engines producing power for each their 1 meter radius propeller (Appendix A.2). Each propeller were a part of a propeller rudder pair. This arangement is now substituted with azimuth thruster from Rolls-Royce, and we have not been able to obtain data for the rudders. The rudder area has therefore been estimated through DNV regulations as given in DNV [2000]. The ship were as well equipped with a 200 kW bow thruster delivered by Brunvoll.

In the following subsections the procedure for modelling of rudders and thrusters is presented. Propeller and rudder theory are both based on foil theory. We suggest consulting Steen [2007] for an introduction and further reading on the topic. Most of the theory in the following subsections is based on this compendium and Lindegaard [2003].

2.5.1   Thruster Dynamics

The thrust model is based on the formula

$$T_i = K_{Ti}\rho D_{pi}^4 n_i^2 \tag{2.28}$$

where T_i is output thrust, ρ is the fluid density, D_{pi} is the propeller diameter, K_{Ti} is the thrust coefficient and n_i is the revolution speed for each propeller i. The first three terms on the right hand side may for the sake of simplicity be combined to one parameter k_{iT} as done in Lindegaard [2003] to yield

$$T_i = k_{iT}n^2. \tag{2.29}$$

To implement thrust in both positive and negative direction, we have to take into account that thrust devices is often less effective when producing negative thrust. With this in mind the final thrust model becomes

$$T_i = \begin{cases} k_{iTp}n_i^2 & n \geq 0 \\ k_{iTn}\left|n_i\right|n_i & n < 0 \end{cases} \tag{2.30}$$

where p and n represents positive and negative thrust.

As thrust curves for the R/V Gunnerus propulsion system were unavailable, these had to be estimated to get reasonable thrust performance. Different approaches were used to find k_{iTp} and k_{iTn} for the main propulsion and bow thruster.

The main propulsion were dimensioned with regards to the ships total resistance. Resistance coefficients as described in Steen [2007] were calculated using Veres (SINTEF [2017]), which yielded total resistance by the equation

$$R_T = \frac{1}{2}\rho V^2 S C_T, \tag{2.31}$$

where R_T is the total resistance, V is the vessels speed, S wet surface and C_T is the total resistance coefficient. To insure sufficient thrust the thrust deduction factor were set to 1.12, and the total needed thrust per thrust devices were calculated. Total resistance where calculated at a sample of velocities. The data for vessel speed of 11.13 knots is found in Table 2.4. The procedure is thoroughly described in Steen [2007].

Table 2.4: *Resistance Data for R/V Gunnerus*

$V[knots]$	$C_w[-]$	$C_f[-]$	$C_T[-]$	$R_T[N]$	$T[N]$ (per propeller)
11.13	0.0047	0.0020	0.0067	39 811	22 294

Using a propeller with 19A nozzle, the main propeller coefficients as described in Table 2.5 were found using propeller efficiency curves at advance number $J = 0$ as described in Steen [2007].

Table 2.5: *Resistance Data for R/V Gunnerus*

	K_T	$10K_Q$	P/D_p
Ahead	0.85	0.9	1.4
Astern	0.55	1.0	1.4

Thrust parameters as given in equation (2.30) may now be calculated using the values in Table 2.5. They are provided in Table 2.7.

We may use K_Q to estimate the maximum shaft speed and thus thrust saturation for each propeller. The formula for torque is

$$Q_i = K_{Qi}\rho D_{pi}^5 n_i^2 \tag{2.32}$$

where Q_i is a function of power and rpm as

$$Q_i = \frac{P_i}{2\pi n_i/60}$$

.

which yields

$$\frac{P_i}{2\pi n_i/60} = K_{Qi}\rho D_{pi}^5 n_i^2$$

and maximum shaft may finally be calculated as

$$n_{i_{max}} = \sqrt[3]{\frac{P_{i_{max}}}{\frac{2\pi}{60}K_{Qi}D_{pi}^5}}. \tag{2.33}$$

Maximum and minimum thrust is calculated using equation (2.28).

There are two main engines with capacity 500 kW power each, and the propeller diameter is 2 [m]. The maximum positive and negative shaft speed is calculated using this data, which again provides the maximum thrust from each propeller. Saturation data is presented in Table 2.8.

To estimate thrust characteristics for the bow thruster a different approach where applied. We were able to obtain a limited amount of propeller data from the manufacturer Brunvoll, provided in Table 2.6. The thruster has a fixed pitch propeller.

Table 2.6: *Bow thruster data*

Power	200 [kW]
Propeller speed	502 [rpm]
Propeller Diameter	1 [m]

Assuming that the bow thruster provides the same thrust in both direction and that the propeller speed is the maximum rpm, eq (2.29) may be utilized to calculate the thrust parameters as

$$k_{3T} = \frac{T_{3max}}{n_{3max}^2}.$$ (2.34)

An estimate of maximum thrust might be obtained through

$$T_{3max} = \eta \left[D_p^2 P_{3max}^2 \right]^{1/3}$$ (2.35)

where η is the "goodness" number. Equation (2.35) is found in Steen [2007] where a "goodness" number of 843 is suggested for tunnel thrusters, with power given in [kW] and thrust in [N]. Calculated thrust limits are given in Table 2.8 and associated propulsion parameters in 2.7. Note that saturation limits for all three propulsion devices seems to be within what one might reasonably expect.

Table 2.7: *Propulsion Parameters*

Parameter	Value $[Ns^2]$
k_{1Tp}, k_{2Tp}	13940
k_{1Tn}, k_{2Tn}	9020
k_{3Tp}, k_{3Tn}	412

Table 2.8: *Rpm and thrust saturation in positive and negative direction*

	Port Propeller	Starboard Propeller	Bow Thruster
RPM	-114, 118	-114, 118	-502, 502
Thrust [kN]	-32.7, 54.5	-32.7, 54.5	-28.8, 28.8

2.5.2 Rudder Dynamics

In this subsection modelling of the implemented rudder dynamics is described.

In Lindegaard [2003] the following lift and drag models are proposed

$$L_i = \begin{cases} T_i \left(1 + k_{iLn} n_i\right) \left(k_{iL\delta_1} \delta_i + k_{iL\delta_2} |\delta_i| \delta_i\right) & n \geq 0 \\ 0 & n < 0 \end{cases}$$ (2.36)

$$D_i = \begin{cases} T_i \left(1 + k_{iDn} n_i\right) \left(k_{iD\delta_1} |\delta_i| + k_{iD\delta_2} \delta_i^2\right) & n \geq 0 \\ 0 & n < 0 \end{cases}$$ (2.37)

where L and D represents lift and drag forces δ_i is the rudder angle for rudder i, and k are constants describing the rudder characteristics. The first term in the equation for both lift and drag is designed to take into account laminar flow.

These are however aimed at model scale tests. For full scale vessels there are high Reynolds numbers giving turbulent flow, and thus the equations simplifies with $(1 + k_{iLn}n_i) \approx (1 + k_{iDn}n_i) \approx 1$. The model for rudder lift is thus

$$L_i = \begin{cases} T_i \left(k_{iL\delta_1} \delta_i + k_{iL\delta_2} |\delta_i| \delta_i \right) & n \geq 0 \\ 0 & n < 0 \end{cases} \tag{2.38}$$

and

$$D_i = \begin{cases} T_i \left(k_{iD\delta_1} |\delta_i| + k_{iD\delta_2} \delta_i^2 \right) & n \geq 0 \\ 0 & n < 0 \end{cases} \tag{2.39}$$

for rudder induced drag forces.

As explained in 1.5.2, the rudder is unable to produce lift (and drag) for negative propeller speed at bollard pull conditions. This can be attributed to the fact that rudders need to see a incoming fluid velocity to produce lift and drag forces. This fact is reflected in the equations above as we have zero lift and drag at negative shaft speed n. The constant $k_{iL\delta_1}$ connected to rudder angle will be positive, whilst $k_{iL\delta_2}$ connected to square rudder angle is in general negative. This creates the characteristic lift curve as shown in Figure 2.2. For drag both constants are in general positive, resulting in a drag curve as shown in Figure 2.3.
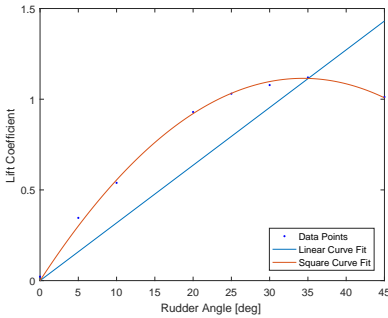

Figure 2.2: *Lift curve found using linear and square curve fitting of lift data for NACA 0020 rudder*
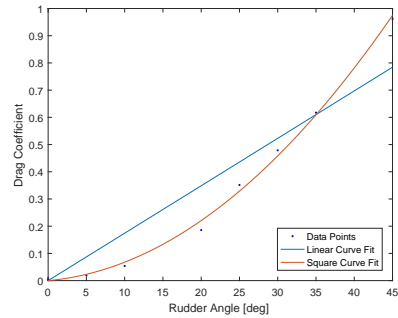

Figure 2.3: *Drag curve found using linear and square curve fitting of drag data for NACA 0020 rudder*

Coefficients were calculated through curve fitting of lift and drag data, found using 3D CFD simulations at bollard pull conditions. These simulations where carried out by Becker Marine Systems. Rudder data used for these simulations may be found in Table 2.9. Necessary rudder area were estimated according to DNV [2000].

Table 2.9: *Rudder Data*

Type	NACA 0020
Area	2.58 [m]
Aspect ratio	1.71

The lift and drag coefficients C_L and C_D are defined as

$$C_{L(D)}\left(\delta\right) = \frac{L\left(D\right)}{\frac{1}{2}\rho A_r K_T D_p^2 n^2} \tag{2.40}$$

where A_r is the rudder surface area and $K_T D_p^2 n^2$ represents square velocity, V^2. From equation (2.28), we know that

$$K_T \rho D_p^2 n^2 = \frac{T}{D^2}.$$

which combined with (2.40) yields

$$L\left(D\right) = C_{L(D)}\left(\delta\right)\frac{A_r}{2D_p^2}T. \tag{2.41}$$

The curve fit of $C_L\left(\delta\right)$ and $C_D\left(\delta\right)$ is on the form

$$C_L\left(\delta\right) = \left(p_{L1}\delta_i + p_{L2}\left|\delta_i\right|\delta_i\right) \tag{2.42}$$
$$C_D\left(\delta\right) = \left(p_{D1}\delta_i + p_{D2}\left|\delta_i\right|\delta_i\right). \tag{2.43}$$

Combining this with (2.41), we may finally conclude that

$$k_{iL\delta_1} = \left(A_r/2D_p^2\right)p_{L1} \tag{2.44}$$
$$k_{iL\delta_2} = \left(A_r/2D_p^2\right)p_{L2} \tag{2.45}$$
$$k_{iD\delta_1} = \left(A_r/2D_p^2\right)p_{D1} \tag{2.46}$$
$$k_{iD\delta_2} = \left(A_r/2D_p^2\right)p_{D2}. \tag{2.47}$$

Parameter values are gives in Table 2.10.

Table 2.10: *Rudder Lift and Drag Parameters*

Parameter	Value	Unit
$k_{1L\delta_1}, k_{2L\delta_1}$	1.1999	rad^{-1}
$k_{1L\delta_2}, k_{2L\delta_2}$	-1.0010	rad^{-2}
$k_{1D\delta_1}, k_{2D\delta_1}$	0.0465	rad^{-1}
$k_{1D\delta_2}, k_{2D\delta_2}$	0.4505	rad^{-2}

As described in Lindegaard [2003] the forces in surge and sway from each propeller-rudder pair is calculated as

$$u_i = \begin{bmatrix} T_i - D_i \\ L_i \end{bmatrix}.$$

Moments from each actuator is calculated using the simple formula

$$Moment = Force \times arm.$$

The moment arm, i.e. position of each actuator relative to centre of mass is found in Table 2.11.

Table 2.11: *Position of actuators relative to center of gravity in x and y direction [m]*

Port Propeller-Rudder	Starboard Propeller-Rudder	Bow Thruster
-11.6, -2.7	-11.6, 2.7	14.0, 0.0

2.6   Observer Design

The observer has three main purposes, as stated in Sørensen [2013].

- *Filtering of noise and wave frequencies* . In DP we desire to filter out two components. Measurement noise and wave frequency (WF) motion. Wave induced vessel motion can in general be divided into two categories. Slow low-frequency (LF) motion or wave drift, and faster WF motion. WF motion can in most cases not be compensated for by the control system as the motion is to rapid and enough power and thrust capacity is not available. Introducing WF motion to the controller does therefore only cause unnecessary wear, tear and fuel consumption. In extreme seas where incident waves have large periods, one might consider not implementing a wave filter. This is however not the case through the simulations in this thesis (see wave models in Section 2.4.1).

- *Reconstruction of non-measured data.* In many cases not every important state can be measured. The reason could be that sensor systems are either nonexistent, imprecise or simply to expensive. In this model, velocity is reconstructed from position measurements and desired thrust. Estimated position and velocity is then used as input control system, as seen in Figure 2.1.

- *Dead reckoning.* In critical DP operations a system failure might have massive consequences. One of the most frequent failure modes in control systems is errors in sensor equipment. Through the application of model based filters, predictions of states such as position and velocity might be used in place of measurements for short periods, thus avoiding complete DP shut down. System failure is not a part of the scope of this thesis, and it follows that no case of dead reckoning will occur

As mentioned in 2.1 the observer is designed as an Extended Kalman Filter (EKF), and the process is described in the following subsections.

2.6.1   Control plant model

A simplified nonlinear low frequency (LF) control plant model in heave and yaw can be formulated as

$$\dot{\boldsymbol{\eta}} = \mathbf{R}(\psi)\boldsymbol{\nu} \tag{2.48}$$

$$\mathbf{M}\dot{\boldsymbol{\nu}} + \mathbf{D}\boldsymbol{\nu} + \mathbf{R}^T(\psi)\mathbf{G}\boldsymbol{\eta} = \boldsymbol{\tau} + \mathbf{R}^T(\psi)\mathbf{b}. \tag{2.49}$$

Here $\boldsymbol{\eta} = [x, y, \psi]$, $\boldsymbol{\nu} = [u, v, r]$ and the bias vector $\mathbf{b} \in \mathbb{R}^3$ are the states of the LF model and $\boldsymbol{\tau} = [\tau_x, \tau_y, \tau_\psi]$ is the control input. The model is nonlinear due to the rotation matrix

$$\mathbf{R}(\psi) = \begin{bmatrix} cos(\psi) & -\sin(\psi) & 0 \\ sin(\psi) & cos(\psi) & 0 \\ 0 & 0 & 1 \end{bmatrix} \tag{2.50}$$

The mass and damping matrices is defined in 6 DOF as

$$\mathbf{M} = \mathbf{M}_{RB} + \mathbf{M}_A \tag{2.51}$$

$$\mathbf{D} = \mathbf{D}_v + \mathbf{D}_p \tag{2.52}$$

where $\mathbf{D}_v$ and $\mathbf{D}_p$ are viscous and potential damping and $\mathbf{M}_{RB}$ and $\mathbf{M}_A$ is rigid body and added mass.

The reduced order form model can be written as

$$\begin{aligned} \mathbf{M}_3 &= \mathbf{H}_{3\times6}\mathbf{M}\mathbf{H}_{3\times6}^T \\ \mathbf{D}_3 &= \mathbf{H}_{3\times6}\mathbf{D}\mathbf{H}_{3\times6}^T \\ \mathbf{G}_3 &= \mathbf{0}, \end{aligned} \tag{2.53}$$

where

$$\mathbf{H}_{3\times6} = \begin{bmatrix} 1 & 0 & 0 & 0 & 0 & 0 \\ 0 & 1 & 0 & 0 & 0 & 0 \\ 0 & 0 & 0 & 0 & 0 & 1 \end{bmatrix}. \tag{2.54}$$

The restoring term is $\mathbf{G} = \mathbf{0}_{3\times3}$, as there is no mooring.

A wave frequency (WF) model can be designed to filter out the high frequent WF motion, which one does not wish to feed in to the control plant. The model can be written in state space as

$$\dot{\boldsymbol{\xi}} = \mathbf{A}_w \boldsymbol{\xi}_w + \mathbf{E}_w \mathbf{w}_w \tag{2.55}$$
$$\boldsymbol{\eta}_w = \mathbf{C}_w \boldsymbol{\xi}_w.$$

$\mathbf{A}_w$ is the wave filter system matrix, $\mathbf{E}_w$ is the wave filter disturbance matrix and $\mathbf{C}_w$ is the wave filter output matrix. $\boldsymbol{\xi} \in \mathbb{R}^6$ is the wave filter states, $\boldsymbol{w}_e \in \mathbb{R}^3$ is the zero-mean Gaussian white noise and $\boldsymbol{\eta}_w \in \mathbb{R}^3$ is the measurement vector of position and heading. The wave filter can be based on the second order wave model

$$\frac{\eta_{w_i}}{\omega_{w_i}}(s) = \frac{K_{w_i} s}{s^2 + 2\zeta_i \omega_i s + \omega_i^2}, \tag{2.56}$$

where i represents the i 'th state, here north, east and yaw. $\omega_i = \frac{2\pi}{T_i}$ corresponds to the dominating wave frequency in the sea state, and the relative damping ζ_i is usually in the the range 0.05 - 0.10.

In state space this corresponds to

$$\mathbf{A}_w = \begin{bmatrix} \mathbf{0}_{3\times 3} & \mathbf{I}_{3\times 3} \\ -\boldsymbol{\Omega}^2 & -2\boldsymbol{\Lambda}\boldsymbol{\Omega} \end{bmatrix} \tag{2.57}$$

$$\mathbf{C}_w = \begin{bmatrix} \mathbf{0}_{3\times 3} & \mathbf{I}_{3\times 3} \end{bmatrix} \tag{2.58}$$

$$\mathbf{E}_w = \begin{bmatrix} \mathbf{0}_{3\times 3} \\ \mathbf{K}_w \end{bmatrix}, \tag{2.59}$$

where $\boldsymbol{\Omega}$, $\boldsymbol{\Lambda}$ and $\mathbf{K}_w$ are diagonal matrices of respectively wave frequencies, damping ratios and wave filter gains.

The bias model accounting for model errors, and slowly varying wave, current and wind loads can be designed as a Wiener process

$$\dot{\mathbf{b}} = \mathbf{E}_b \mathbf{w}_b, \tag{2.60}$$

where $\mathbf{E}_b \in \mathbb{R}^{3\times 3}$ is a diagonal scaling matrix and $\mathbf{w}_b$ is a zero-mean white noise.

Finally the measurement is defined as

$$\mathbf{y} = \boldsymbol{\eta} + \boldsymbol{\eta}_w + \mathbf{v}, \tag{2.61}$$

where $\mathbf{v}$ is the measurement noise. This yields the final control plant model

$$\dot{\boldsymbol{\xi}} = \mathbf{A}_w\boldsymbol{\xi}_w + \mathbf{E}_w\mathbf{w}_w \tag{2.62}$$

$$\dot{\boldsymbol{\eta}} = \mathbf{R}(\psi)\boldsymbol{\nu} \tag{2.63}$$

$$\dot{\mathbf{b}} = \mathbf{E}_b\mathbf{w}_b \tag{2.64}$$

$$\mathbf{M}\dot{\boldsymbol{\nu}} = -\mathbf{D}\boldsymbol{\nu} + \mathbf{R}^T(\psi)\mathbf{b} + \boldsymbol{\tau} \tag{2.65}$$

$$\mathbf{y} = \boldsymbol{\eta} + \boldsymbol{\eta}_w + \mathbf{v}. \tag{2.66}$$

2.6.2 Extended Kalman Filter

The nonlinear model used to design the extended Kalman filter (EKF), is written as

$$\dot{\mathbf{x}} = \mathbf{f}(\mathbf{x}) + \mathbf{B}\boldsymbol{\tau} + \mathbf{E}\mathbf{w} \tag{2.67}$$

$$\mathbf{y} = \mathbf{H}\mathbf{x} + \mathbf{v} \tag{2.68}$$

based directly on (2.62) to (2.66). $\mathbf{f}(\mathbf{x})$ is the nonlinear system equations, $\mathbf{B}$ the input matrix, $\mathbf{E}$ the disturbance matrix and $\mathbf{H}$ is the output matrix. Thus for a heading-position system one has 15 states. The discrete EKF algorithm, is implemented as described in Sørensen [2013]. To tune the EKF, the position and heading measurement noise covariance matrix $\mathbf{R} = E\left[\mathbf{v}^T\mathbf{v}\right] \in \mathbb{R}^{3\times3}$ may be set to a diagonal matrix, consisting of the noise on the measurement. The process noice covariance matrix $\mathbf{Q} = E\left[\mathbf{w}^T\mathbf{w}\right] \in \mathbb{R}^{15\times15}$ is usually tuned as a diagonal matrix.

To simplify the tuning process, some simple observations may be made. The process noise effects the predictor in the EKF algorithm as

$$\bar{\mathbf{P}}_{k+1} = \boldsymbol{\Phi}_k\hat{\mathbf{P}}_k\boldsymbol{\Phi}_k^T + \boldsymbol{\Gamma}_k\mathbf{Q}\boldsymbol{\Gamma}_k^T. \tag{2.69}$$

Here, the process noise is multiplied with the square of $\boldsymbol{\Gamma}_k$, which is given as

$$\boldsymbol{\Gamma}_k = T\mathbf{E} \tag{2.70}$$

where T is the time step. The second part of the right hand side of eq (2.69), then may be simplified into tuning one diagonal matrix

$$\mathbf{Q}_p = \boldsymbol{\Gamma}_k\mathbf{Q}\boldsymbol{\Gamma}_k^T = diag[n \times n], \tag{2.71}$$

where n is the number of states.

2.7 Controller Design

In surface vessel DP systems it is in most cases sufficient to control the three horizontal degrees of freedom, surge, sway and yaw. In some applications other methods such as roll and pitch damping (Sørensen [2013]) may be of interest, though this is outside the scope of this thesis. In the following subsections we present the horizontal plane linear quadratic regulator (LQR) control scheme based on Sørensen [2013], which is implemented in this thesis.

LQR control is based on minimizing some cost function J, to achieve optimal controller gains for what is in the simplest sense a proportional, derivative and integral (PID) controller given as

$$u(t) = K_p e(t) + K_d \dot{e}(t) + K_i \int_0^t e(\tau) d\tau. \tag{2.72}$$

For the purpose of this thesis, $u(t)$ is the control input, $e(t)$ is the error in position at a given time t, $\dot{e}(t)$ is the velocity error and K_p, K_d and K_i are suitable control matrix gains. For further introduction to PID control, consult Astrom [1995].

In this thesis we apply PID control on position and velocity error, though the scheme might be further extended with e.g. accelearation feedback (Lindegaard [2003]) and wind feed forward (Sørensen [2013]).

2.7.1 Linear Control Plant Model

For the controller design it is convenient to derive a linear LF control plant model, for the 3DOF controller in surge sway and yaw. The reduced order model can be written as in (2.53) with $\mathbf{H}_{3 \times 6}$ as in (2.54).

The linearized control plant model in reference parallel frame is then written as

$$\mathbf{M}_3 \dot{\boldsymbol{\nu}}_3 + \mathbf{D}_3 \boldsymbol{\nu}_3 = \boldsymbol{\tau}_{3c} + \boldsymbol{w}_3, \tag{2.73}$$

where $\mathbf{M}_3$ and $\mathbf{D}_3$ is 3DOF mass and damping and $\dot{\boldsymbol{\nu}}_3$, $\boldsymbol{\nu}_3$, $\boldsymbol{\tau}_{3c}$ and $\boldsymbol{w}_3$ is 3DOF acceleration, velocity, control input and noise. The corresponding state space model is

$$\dot{\mathbf{x}}_3 = \mathbf{A}_3 \mathbf{x}_3 + \mathbf{B}_3 \boldsymbol{\tau}_{3c} + \mathbf{E}_3 \boldsymbol{w}_3 \tag{2.74}$$

$$\mathbf{y}_3 = \mathbf{C}_3 \mathbf{x}_3 + \mathbf{v}_3. \tag{2.75}$$

The states are defined as $\mathbf{x}_3 = [u, v, r, x, y, \psi] \in \mathbb{R}^6$ and the control vector is $\boldsymbol{\tau}_{3c} \in \mathbb{R}^3$. $\mathbf{w}_3$ is disturbance, $\mathbf{v}_3$ noise, and $\mathbf{y}_3$ represents the measurements.

This results in the system matrix

$$\mathbf{A}_3 = \begin{bmatrix} -\mathbf{M}_3^{-1} \mathbf{D}_3 & \mathbf{0}_{3 \times 3} \\ \mathbf{I}_{3 \times 3} & \mathbf{0}_{3 \times 3} \end{bmatrix}, \tag{2.76}$$

the control input matrix

$$\mathbf{B}_3 = \begin{bmatrix} \mathbf{M}_3^{-1} \\ \mathbf{0}_{3\times3} \end{bmatrix} \tag{2.77}$$

and the measurement matrix

$$\mathbf{C}_3 = \begin{bmatrix} \mathbf{0}_{3\times3} & \mathbf{I}_{3\times3} \end{bmatrix}. \tag{2.78}$$

The disturbance matrix $\mathbf{E}_3$ is not necessary for the LQR (Linear quadratic controller) design without disturbance feed forward.

2.7.2   PD control law

The conventional PD (Proportional and Derivative) state feedback controller is written as

$$\boldsymbol{\tau}_{pd} = -\mathbf{G}\mathbf{e} = -\mathbf{G}_p\mathbf{e}_2 - \mathbf{G}_d\mathbf{e}_1, \tag{2.79}$$

where $\mathbf{G}$ is the matrix controller gain defined as $\mathbf{G} = [\mathbf{G}_d \; \mathbf{G}_p]$ with matrix proportional gain $\mathbf{G}_p \geq 0 \in \mathbb{R}^{3\times3}$ and matrix derivative gain $\mathbf{G}_d \geq 0 \in \mathbb{R}^{3\times3}$. The error vector $\mathbf{e}$ is defined as

$$\mathbf{e} = \begin{bmatrix} \mathbf{e}_1 \\ \mathbf{e}_2 \end{bmatrix} \tag{2.80}$$

$$\mathbf{e}_1 = \dot{\mathbf{e}}_2 \tag{2.81}$$

$$\mathbf{e}_2 = \mathbf{R}^T(\psi_d)\left[\hat{\boldsymbol{\eta}} - \boldsymbol{\eta}_d\right]^T \tag{2.82}$$

where $\hat{\boldsymbol{\eta}} = \left[\hat{x}, \hat{y}, \hat{\psi}\right]^T$ is estimated position and $\boldsymbol{\eta}_d = [x_d, y_d, \psi_d]^T$ is desired positions. Assumed that the pair $(\mathbf{A}_3, \mathbf{B}_3)$ is reachable, we can compute the LQR gain through the linear quadratic performance index

$$J = E\left\{\lim_{T\to\infty} \frac{1}{T} \int_0^T \mathbf{e}^T\mathbf{Q}\mathbf{e} + \boldsymbol{\tau}_{pd}^T\mathbf{R}\boldsymbol{\tau}_{pd}dt\right\}. \tag{2.83}$$

The tunable error weighting matrix and control weighting matrix is defined respectively with constraints as $\mathbf{Q} = \mathbf{Q}^T > 0 \in \mathbb{R}^{3\times3}$ and $\mathbf{R} = \mathbf{R}^T \geq 0 \in \mathbb{R}^{3\times3}$.

The LQR method gives the gain $\mathbf{G}$ by minimising J. For a linear time invariant (LTI) system, this corresponds to solving the algebraic Ricatti equation

$$0 = -\mathbf{P}\mathbf{A}_3 - \mathbf{A}_3^T\mathbf{P} + \mathbf{P}\mathbf{B}_3\mathbf{R}^{-1}\mathbf{B}_3^T\mathbf{P} - \mathbf{Q}, \tag{2.84}$$

where $\mathbf{P} = \mathbf{P}^T > 0 \in \mathbb{R}^{6\times6}$. The LQG gain is then computed as

$$\mathbf{G} = \mathbf{R}^{-1}\mathbf{B}_3\mathbf{P}. \tag{2.85}$$

2.7.3   Integral Action

We define a property space, containing the states to be controlled towards certain set points as

$$\mathbf{z} = e_2. \tag{2.86}$$

An approximation of the integral loop controlling $\mathbf{z}$ is found to be

$$\dot{\mathbf{z}} = \mathbf{G}_i \mathbf{G}_z \left(\mathbf{A}_3 - \mathbf{B}_3 \mathbf{G} \right)^{-1} \mathbf{B}_3 \mathbf{z} = \mathbf{\Lambda}_G \mathbf{z}, \tag{2.87}$$

where $\mathbf{\Lambda}_G$ is the diagonal eigenvalue matrix, specifying desired eigenvalues, and the property matrix $\mathbf{G}_z$ is defined as $\mathbf{G}_z = \frac{dz}{de} = [\mathbf{0}_{3\times3} \ \mathbf{I}_{3\times3}]$. By solving for $\mathbf{G}_i$ we get the integrator gain defined as

$$\mathbf{G}_i = \mathbf{\Lambda}_G \left(\mathbf{G}_z \left(\mathbf{A}_3 - \mathbf{B}_3 \mathbf{G} \right)^{-1} \mathbf{B}_3 \right)^{-1}. \tag{2.88}$$

This gives us the final integral control law

$$\dot{\boldsymbol{\tau}}_i = \mathbf{G}_i \mathbf{z}. \tag{2.89}$$

One should as well implement some anti-windup measures, e.g. saturation on the integrator.

2.8   Guidance System

Guidance were not a priority in the work of this thesis, and it is therefore only superficially touched upon in this section. The applied guidance system is in any case easily explained in only a few sentences. For those seeking further knowledge on the topic, we refer to [Fossen, 2011].

The guidance system continuously calculates the desired position, velocity and acceleration for the vessel, and the overall goal is to drive the vessel towards a desired positon. The three forms of guidance is as defined in Fossen [2011], setpoint regulation, such as station keeping for DP, trajectory tracking, where the goal is to track a time varying position and velocity signal, and path following, where the vessel is set to follow a predefined path independent of time. The computation is based on input from e.g. a user, as constant station keeping coordinates or as a path from a path planner.

In this thesis the simplest form of guidance is chosen. Constant position coordinates and heading as well as surge, sway and yaw rates, are given directly to the control system as desired position, heading, velocity and angle rate.

2.9 Control Allocation

The aim of control allocation is to map desired forces and moments from the controller to feasible setpoints for the systems actuators. For the 3DOF DP model, the control forces and moments in body frame are

$$\boldsymbol{\tau_c} = \begin{bmatrix} F_x^b \\ F_y^b \\ M_z^b \end{bmatrix} \tag{2.90}$$

where F_x^b and F_y^b represents body frame force in surge and sway direction, and M_z^b is body frame moment about the z-axis. Note that considerations of thrust and forces are done in body frame throughout the thesis as this is by far most convenient.

As described in Section 1.5.2 control allocation (CA) can be broken down into two subproblems; *Force allocation* and *Inverse mapping*. The force allocation algorithm maps commanded thrust in surge sway and yaw to desired force for each actuator, whilst the inverse mapping maps actuator forces to actuator setpoints such as rudder angle and shaft speed. In this section the implemented control allocation scheme is presented. Background and theory are found in 1.5.2. The implemented force allocation scheme is based on python code provided by Karl-Petter Lindegaard. This is a simplified version of what is presented in Lindegaard and Fossen [2003]. Implementation and design of the inverse mapping are however results of work done in this master thesis.

2.9.1 Force Allocation

The implemented force allocation is based on three main assumption

1. Only one rudder may be active at any moment in time
2. Port rudder produces only negative lift, whilst starboard rudder produces only positive lift
3. Thrust saturation is not accounted for

The third assumption, or rather limitation implies that the system is not able to redistribute forces if a single or several thrusters or rudders reach their force saturation limit. The test cases in Chapter 4 is therefore designed to avoid such events.

The first and second assumption has larger implications as the algorithm is built around them. The steps of the force allocation can in short terms be summarized as

- Define configuration matrices for use of either port or starboard rudder

- Calculate unconstrained and constrained solution for each configuration

- Compare cost of using each configuration

- Choose configuration with lowest cost

The procedure is explained in more detail in the following subsections with notation
and theory from Section 1.5.2

Configuration

The configuration matrices A_1 and A_2 for use of port and starboard rudder respectively are defined as

$$A_1 = \begin{bmatrix} 1 & 0 & 1 & 0 \\ 0 & 1 & 0 & 1 \\ -l_{p,y} & l_{p,x} & -l_{s,y} & l_{b,x}]; \end{bmatrix} \tag{2.91}$$

$$A_2 = \begin{bmatrix} 1 & 1 & 0 & 0 \\ 0 & 0 & 1 & 1 \\ -l_{p,y} & -l_{s,y} & l_{s,x} & l_{b,x}]; \end{bmatrix} \tag{2.92}$$

where $l_{p,y}$, $l_{p,x}$, $l_{s,y}$, $l_{s,x}$ and $l_{b,x}$ are length in x and y direction to port (p),
starboard (s) and bow (b) thruster-rudder or tunnel thruster. Note that only one
of two rudders produce lift for each case and that the bow thruster produces pure
sideways force.

Unconstrained Solution

The unconstrained solution is calculated using the pseudoinverse A^+ through

$$u_* = A^+ \tau_c. \tag{2.93}$$

As discussed in Section 1.5.2 this yields an optimal solution u_* in terms of the
2-norm of u.

Sector Constraints With Rudder Anti-Chat

Sector boundaries a_{Aj} for A_1 and A_2 are defined as

$$a_{Aj} = a_{1,Aj} + a_{2,Aj} \tag{2.94}$$

where

$$a_{1,A1} = \cos\left(\delta_{max}\right) \tag{2.95}$$

$$a_{2,A1} = -\sin\left(\delta_{max}\right) \tag{2.96}$$

and

$$a_{1,A2} = \cos\left(\delta_{max}\right) \tag{2.97}$$
$$a_{2,A2} = \sin\left(\delta_{max}\right). \tag{2.98}$$

δ_{max} is the maximum allowed rudder angle, set to 34° as discussed in Section 2.5. These boundaries allocate the left force sector to the port rudder and the right force sector to the starboard rudder with regards to the x-axis (Figure 2.4). Note that the boundary is defined only for the rudder intended to produce sideways force. The bow tunnel thruster and propeller-rudder pair used only for thrust needs no boundary as thrust saturation is not included.

To avoid rudder chattering the constrained solution is mapped into the B-frame (not to be confused with body frame) through

$$u_*^b = u_* - r^o \tag{2.99}$$

where r^o is a design parameter set to 100 N in this implementation.

If the unconstrained solution in B-frame u_*^b is not in the feasible subset $\mathcal{D}$ as defined by $a_{i,Aj}$, the solution has to transverse the nullspace $\mathcal{N}\left(A_j\right)$ of A_j until it reaches the boundary. The optimal increment δu is calculated as

$$\delta u = N_j \kappa \tag{2.100}$$

where N_j is a null vector of corresponding configuration matrix A_j, and the magnitude κ, is calculated as

$$\kappa = -\frac{det\left(\left[F_{Rj}|a_j\right]^T\right)}{det\left(\left[N_{Rj}|a_j\right]^T\right)}. \tag{2.101}$$

where $F_{R}j$ is a vector containing the unconstrained forces from the active rudder whilst $N_{R}j$ contains the corresponding elements of the null vector. For configuration A_1, $F_{R}j = \left[u_*^b(1),\ u_*^b(2)\right]^T$ and $N_{R}j = [N(1),\ N(2)]$, and for configuration A_2, $F_{R}j = \left[u_*^b(2),\ u_*^b(3)\right]^T$ and $N_{R}j = [N(2),\ N(3)]$. $det\left([a|b]\right)$ is the determinant of a matrix built of two column vectors a and b.

The constrained solution in B-frame for each configuration can now be computed as

$$u_j^b = u_*^b + \delta u, \tag{2.102}$$

and finally the cost J_j of each configuration A_j is found through

$$J_j = u_j^T Q u_j, \tag{2.103}$$

where Q is a weighting matrix, given as I_4. I_4 is the four by four identity matrix. The configuration A_j with lowest cost is then utilized in control.
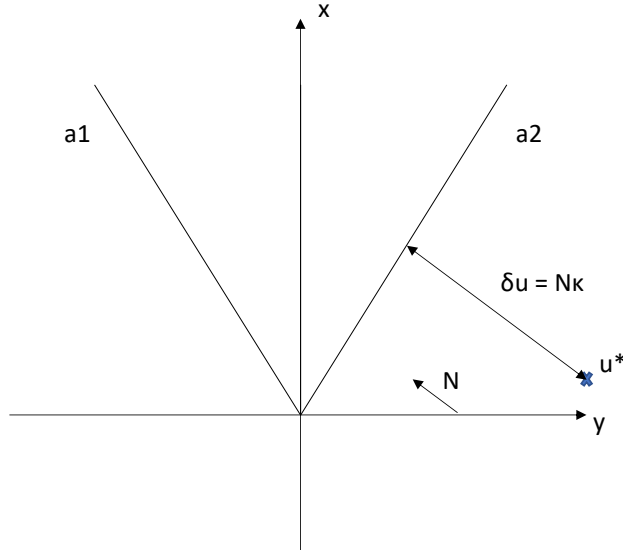
Figure 2.4: *Application of sector constraints on unconstrained solution u_**

2.9.2   Inverse Mapping

In the inverse mapping the optimal constrained forces u is mapped to corresponding actuator setpoints through the inverse thrust and rudder models. For the purpose of inverse mapping we have used the linear approximation of lift and drag curves. As a result there will be a gap between the commanded forces from the control allocation, and the actual lift and drag from actuator models. In Chapter 3 we propose a force feedback control method to bridge this gap.

The linear coefficients, found as described in 2.5.2, may be seen in Table 2.12. These values were problematic for one key reason. The resulting maximum rudder angle were way to large, which resulted in large rudder induced drag forces and little to no lift force. This did in turn yield an unstable control system. To compensate, the linear lift term were set equal to the linear lift term from the square lift model. This yielded $\delta_{max} \approx 34°$, and removed the unstable performance. The final model parameters are given in Table 2.13.

Table 2.12: *Linear rudder parameters from curve fitting*

Parameter	Value $[rad^{-1}]$
$k_{1L,lin}, k_{2L,lin}$	0.5877
$k_{1D,lin}, k_{2D,lin}$	0.3221

Table 2.13: *Linear rudder parameters compensated for δ_{max}*

Parameter	Value $[rad^{-1}]$
$k_{1L,lin}, k_{2L,lin}$	1.1999
$k_{1D,lin}, k_{2D,lin}$	0.3221

To calculate setpoints it is first assumed that the computed thrust T from the force allocation is perfect (this the case when there is no rudder induced drag force). The inverse equations for rudder angle is then

$$\delta_i = \begin{cases} L_i / \left(T_i k_{iL,lin} \right) & T_i \geq 0 \\ 0 & T_i < 0 \end{cases}.$$ (2.104)

The computed rudder angle δ is now used to compute an estimate of thrust loss from the rudder induced drag force as

$$D_i = \begin{cases} T_i k_{iD,lin} \delta_i & T_i \geq 0 \\ 0 & T_i < 0 \end{cases}.$$ (2.105)

The drag estimate is then used with computed thrust T, to calculate desired shaft speed n through the formula

$$n_i = \begin{cases} \sqrt{\left(T_i - D_i \right) / k_{iTp}} & T_i \geq 0 \\ \sqrt{\left(T_i - D_i \right) / k_{iTn}} & T_i < 0 \end{cases}.$$ (2.106)

k_{1Tp} and k_{1Tn} are thrust parameters as given in Section 2.5.1, Table 2.7.

Chapter 3

Force Feedback Control

In this chapter a force feedback control (FFC) system is suggested. The controller is based on standard PI control and is inspired by direct force control, specifically hybrid force/motion control as investigated in Section 1.5.4. The objective is to decrease deviation between output forces from actuators and desired force from the motion controller as implied in Section 2.5.

3.1 System Overview

In figure 3.1 the system as presented in Chapter 2 is given. In addition, three new blocks have been added - Force sensor module, force guidance system and force controller. These blocks, together constitutes the force feedback control system, and will be presented in the following sections. First we will clarify notation and concepts, and identify the control objective.
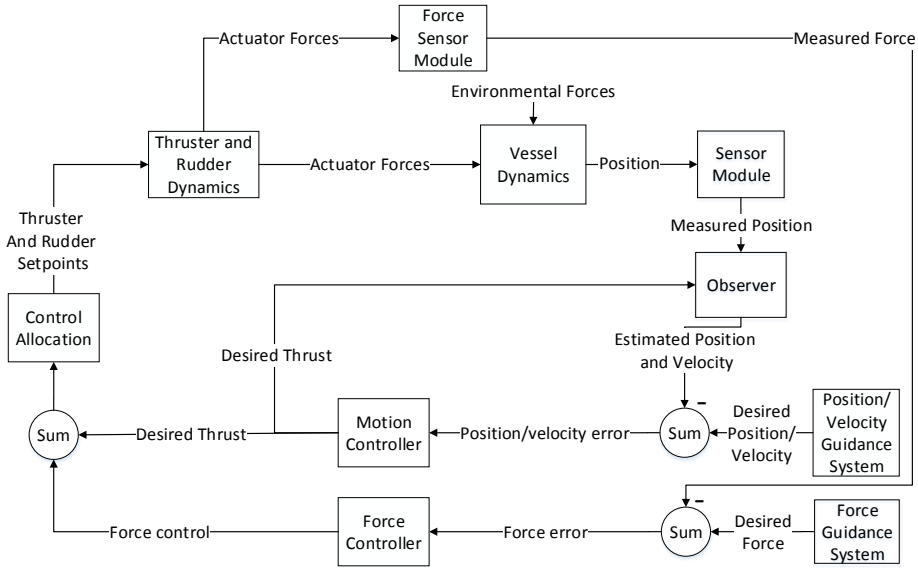
Figure 3.1: *Overview of DP system with force feedback control*

3.1.1   Notation and Concepts

As the amount of words and symbol grows with the expansion of the DP system so does the amount of symbols and concepts. In this subsection some clarifications are made with reference to expressions in Figure 3.1.

The output from the thruster and rudder dynamics are described as actuator forces. The input to the vessel dynamics are however normalized thrust $\tau = [F_x, \ F_y, \ M_z]^T$. When the expression output thrust or τ is used, this is thus equivalent to actuator forces. In the same manner measured force, force error and desired force is equivalent to measured thrust τ_m, thrust error τ_e, and desired thrust τ_d, respectively. This is further discussed in Section 3.2.2.

Output from the motion controller is denoted as desired thrust. It is later described as commanded thrust from motion controller and is symbolised with τ_η. This is done to distinguish it from the commanded thrust $\tau_c = \tau_\eta + \tau_F$. Here τ_F is commanded thrust from the force controller denoted as *Force control* in the figure.

3.1.2   Control Objective

In the robotics force control application, as presented in Section 1.5.4 force and motion control is perfectly separated. As a result pure motion control is applied in some DOFs, whilst force control is applied in others. This is fundamentally

different in DP application where the ambition is to control force and motion in the the three DOFs, surge, sway and yaw simultaneously.

The objective is based on the assumption that the motion controller is designed and tuned to more or less optimally track the desired position. Note that with perfect thrust allocation and no time delay or saturation limits, the desired thrust from the motion control τ_η would be equal to the output thrust τ from actuator forces. The goal with FFC is to add a thrust term τ_F to the commanded thrust, such that the output thrust τ is driven towards the perfect world scenario. To summarize commanded thrust is described as

$$\tau_c = \tau_\eta + \tau_F, \tag{3.1}$$

and the objective is to drive

$$\tau \to \tau_\eta \equiv \tau_d \tag{3.2}$$

within limited time. No proof of asymptotic or exponential stability is carried out, though performance is tested through simulation cases. Stability proofs should be conducted in future research.

3.2 Force Sensor Module

Force measurements are likely to be significantly exposed to measurement noise. In this thesis it is however assumed that it is of small significance. This is done to test the possible effect of force feedback at close to optimal conditions. In future research the effect of noise should be investigated, and a realistic noise model should be designed. This would naturally motivate to investigate noise filtering with e.g. a Kalman Filter. It is further assumed that modelling of thrust forces, T from propellers are perfect. Thruster force output may thus be used directly as input to the FFC. In the following subsection a simple model for implementation of measurement noise is proposed.

3.2.1 Measurement Noise

The force measurement noise implemented in this simulation model, is similar to that of the position and heading noise. Zero mean Gaussian noise is applied with variance as input parameter. The variance where set to 0.1 throughout the work with this thesis, which obviously are insignificant levels. One might as well add constant or slowly varying bias terms, though this is not done here. To accurately model noise in further work, studies of noise in real force measurements should be carried out.

3.2.2 Thrust Mapping

Note that the input to the force controller, has to be on the form

$$\tau_e = \tau_d - \tau_m = [F_{x,d} - F_{x,m}, \ F_{y,d} - F_{y,m}, \ M_{z,d} - M_{z,m}]^T \ ,$$

as the desired thrust τ_d is given in this form. In the previous equation, d and m represents desired and measured force/moment. Before measured forces, including rudder forces and thrust from rudders, are fed to the force controller, it thus need to be mapped to thrust in body frame. This is done as described in Section 2.5.2 with

$$\tau_i = \begin{bmatrix} T_i - D_i \\ L_i \end{bmatrix}. \tag{3.3}$$

and

$$M_z = F \times a,$$

where M_z is moment around the z axis, F is force in body frame and a is length between force and centre of gravity, perpendicular to the force direction. τ_i represents thrust for each device i.

3.3 Force Guidance System

The force guidance control system is in principle equal to that of the position and velocity guidance system. The desired forces is simply passed on to the controller. Note that the desired force, τ_η are however a dynamic signal, and tracking will therefore be more challenging.

3.4 Control Design

In Villani [2015] as discussed in Section 1.5.4 the PI FFC

$$f_\lambda = \lambda_d(t) + K_{P\lambda} [\lambda_d(t) - \lambda(t)] + K_{I\lambda} \int_0^t [\lambda_d(\tau) - \lambda(\tau)] \, d\tau \tag{3.4}$$

is proposed. Here f_λ denotes total force control input, $\lambda_d(t)$ desired force and $\lambda(t)$ measured force at time t. $K_{P\lambda}$ and $K_{I\lambda}$ are PDF proportional and integral matrix gains respectively. Compared to equation (3.1) we note that f_λ is equivalent to τ_c whilst λ_d is the counterpart in robotics to $\tau_\eta \equiv \tau_d$. To mirror the method from robotics, τ_F should be set to the remaining terms in (3.4). Force feedback control is thus suggested as a PI controller on the form

$$\tau_F(t) = K_{P\tau} [\tau_d(t) - \tau_m(t)] + K_{I\tau} \int_0^t [\tau_d(\sigma) - \tau_m(\sigma)] \, d\sigma \tag{3.5}$$

where $K_{P\tau}$ and $K_{I\tau}$ are PDF proportional and integral matrix gains. The FFC should be able to compensate for instant disturbance forces and constant or slowly varying force bias with its P and I feedback parts respectively. This control design seems to be an intuitively good choice. The total commanded force may finally be given as

$$\tau_c = \tau_\eta + K_{P\tau}\left[\tau_d\left(t\right) - \tau_m\left(t\right)\right] + K_{I\tau}\int_0^t \left[\tau_d\left(\sigma\right) - \tau_m\left(\sigma\right)\right]d\sigma \tag{3.6}$$

$$= \tau_\eta + K_{P\tau}\left[\tau_\eta\left(t\right) - \tau_m\left(t\right)\right] + K_{I\tau}\int_0^t \left[\tau_\eta\left(\sigma\right) - \tau_m\left(\sigma\right)\right]d\sigma. \tag{3.7}$$

Chapter 4

Results and Discussion

4.1 Tuning

Through the tuning process we seek to obtain optimal system performance, through tweaking of design parameters. In this section we present the method, design parameters and result of the tuning process.

4.1.1 Observer

The Kalman filter were tuned by initially setting the R matrix to a diagonal matrix of the measurement noise in the three degrees of freedom. $R = 10^{-2} \times diag[1\ 1\ 0.01]$. A good Q-matrix for station keeping were

$$Q = 10^{-6} \times diag[\mathbf{0}_3\ 100\ 600\ 0.1\ \mathbf{0}_3\ 10^3\ 10^3\ 10^3\ 1\ 1\ 0.001].$$

The wave filter frequencies were tuned to match the incident waves, with w_i around 0.6. The wave filter damping were set to 0.05.

4.1.2 Motion Controller

The error weighting matrix $\mathbf{Q}_{PD}$ and the control weighting matrix $\mathbf{R}_{PD}$ were chosen to optimize the performance in station keeping. The design parameters

were overshoot and time to steady state. The resulting matrices where

$$\mathbf{Q}_{PD} = \begin{bmatrix} 1000 & 0 & 0 & 0 \\ 0 & 400 & 0 & 0 \\ 0 & 0 & 50 & 0 \\ 0 & 0 & 0 & 50 \end{bmatrix}, \quad \mathbf{R}_{PD} = 10^{-2} \begin{bmatrix} 1.5 & 0 & 0 & 0 \\ 0 & 3 & 0 & 0 \\ 0 & 0 & 2 & 0 \\ 0 & 0 & 0 & 2 \end{bmatrix}.$$

For the integral gain the eigenvalue matrix where set to

$$\mathbf{\Lambda}_G = 10^{-2} \begin{bmatrix} -5 & 0 & 0 & 0 \\ 0 & -5 & 0 & 0 \\ 0 & 0 & -5 & 0 \\ 0 & 0 & 0 & -5 \end{bmatrix},$$

which ensured that the integral gains where 20 times lower than the proportional gain. The final PID gains were

$$\mathbf{G} = [\mathbf{G}_D \ \mathbf{G}_P]$$

$$\mathbf{G}_D = \begin{bmatrix} 430.87 & 0 & 0 & 0 \\ 0 & 218.66 & 0 & 0 \\ 0 & 0 & 121.93 & 0 \\ 0 & 0 & 0 & 103.94 \end{bmatrix}$$

$$\mathbf{G}_P = \begin{bmatrix} 258.20 & 0 & 0 & 0 \\ 0 & 115.47 & 0 & 0 \\ 0 & 0 & 50.00 & 0 \\ 0 & 0 & 0 & 50.00 \end{bmatrix}$$

$$\mathbf{G}_i = \begin{bmatrix} 12.91 & 0 & 0 & 0 \\ 0 & 5.77 & 0 & 0 \\ 0 & 0 & 2.50 & 0 \\ 0 & 0 & 0 & 2.50 \end{bmatrix}.$$

Saturation on the integrator were set to

$$[Int_x \ Int_y \ Int_\psi] = [10^5 \ 10^5 \ 10^5],$$

which effectively is infinite limit under the simulated environmental conditions. Windup were in any case not much of a problem, and saturation limits did in the end cause more problems than it solved.

4.1.3   Force Controller

The force controller gains where tuned by trial and error. As described in Chapter 3 the goal of the proportional control is to compensate for instant disturbance forces. If the proportional gain is tuned to high however, we risk to degrade performance

or even cause instabilities. The integral gain should compensate for constant or slowly varying force bias. As for proportional gain its magnitude has to be limited in order to avoid introducing noise or causing instabilities. The final gains as used in simulations were

$$K_p = \begin{bmatrix} 0.1 & 0 & 0 \\ 0 & 0.1 & 0 \\ 0 & 0 & 0.1 \end{bmatrix}$$

$$K_i = \begin{bmatrix} 0.01 & 0 & 0 \\ 0 & 0.01 & 0 \\ 0 & 0 & 0.01 \end{bmatrix}.$$

These gains corresponds to ten percentage of measured force and moment error being instantly compensated for by the proportional control in addition to one percentage of the accumulated error through the integral gain. For simulation cases without integral action, the integral gain were set to zero.

4.2 List of Cases

Through a thorough and logically built up case scheme, our scope is to verify each component of the model, and single out areas of improvement. In the following subsections we list and introduce each case.

4.2.1 Model Verification

In this first part we aim to test the model without advanced control allocation, thruster dynamics and feedback control of any kind. Through testing and mapping of the basic components, the aim is to ensure that the experimental setup will not effect DP simulations in any unexpected ways. In case 1 to 3 the effect of current and waves are tested, to validate the environmental models and their interaction with the vessel. As mentioned in Subsection 2.4.3 there is no wind in any of the cases. Incoming direction of current is 225 degrees or North East, where 0 represents South, 90 West, 180 North and 270 East at 0.2 m/s. Incident waves from North (180 degrees) with peak frequency $\omega_p = 0.6$, and significant waves $H_s = 2m$. This is the environmental configuration used in every case. Case 4 to 7 is designed to get an overview of the vessels response to force input. This is used as a basis for comparison for the force feedback cases. Forces are applied through the centre of gravity and thrusters are simply modelled as a first order time delay and thrust saturation.

1. Current
   - The vessel drifts freely with the current
   - No Waves

- No Thrust
2. Waves
    - The vessel drifts freely with the waves
    - No current
    - No thrust
3. Current and Waves
    - The vessel drifts freely with current and waves
    - No thrust
4. Surge force with simplified thrust scheme
    - Simplified thrust allocation and thruster/rudder dynamics
    - The vessel runs with thrust in surge
    - No thrust in sway or yaw
    - Environmental forces as in case 3
5. Sway force with simplified thrust scheme
    - Simplified thrust allocation and thruster dynamics
    - The vessel runs with thrust in sway
    - No thrust in surge or yaw
    - Environmental forces as in case 3
6. Yaw moment with simplified thrust scheme
    - Simplified thrust allocation and thruster dynamics
    - The vessel runs with thrust in sway
    - In reality this is obviously a combination of surge and sway thrust, but the resulting components in these directions are set to zero. The resulting thrust is "pure yaw".
    - Environmental forces as in case 3
7. Combined surge, sway and yaw with simplified thrust scheme
    - Simplified thrust allocation and thruster dynamics
    - Environmental forces as in case 3
    - Thrust forces in surge, sway and yaw direction

4.2.2 Force feedback verification

The following cases are designed to verify that the FFC drives output forces to the desired values. Every case is carried out with thrust allocation and dynamics as described in Section 2.2 and 2.9. The test scheme is otherwise a mirror of those in case 4 to 7. These are used as a basis for comparison.

1. Surge force with force feedback control
    - With thrust allocation and dynamics as described in Section 2.2 and 2.9
    - The vessel runs with thrust in surge
    - No thrust in sway or yaw
    - Environmental forces as in case 3
2. Sway force with force feedback control
    - With thrust allocation and dynamics as described in Section 2.2 and 2.9
    - The vessel runs with thrust in sway

- No thrust in surge or yaw
- Environmental forces as in case 3
3. Yaw moment with force feedback control
  - With thrust allocation and dynamics as described in Section 2.2 and 2.9
  - The vessel runs with thrust in sway
  - In reality this is obviously a combination of surge and sway thrust, but the resulting components in these directions are set to zero. The resulting thrust is "pure yaw".
  - Environmental forces as in case 3
4. Combined surge, sway and yaw input with force feedback control
  - With thrust allocation and dynamics as described in Section 2.2 and 2.9
  - Environmental forces as in case 3
  - Thrust forces is surge, sway and yaw direction

4.2.3   DP verification

In these final cases we aim to test and compare different variations of DP. From the simplest scheme without use of rudders to different variations of force feedback control. The objective is to asses the strengths of each design as well as discovering areas of improvements and further work. The experimental setup is as described in Chapter 2 and Chapter 3 with variations in force control and thrust allocation as described in each case.

1. Station keeping without force feedback control
   (a) Without rudders
   (b) With rudders
       - Initial condition at the origin in north-east-down frame, with zero yaw angle
       - Desired position at origin
2. Station keeping with force feedback control
   (a) DP with PI Force Feedback Control
   (b) DP with P Force Feedback Control
       - Initial condition at the origin in north-east-down frame, with zero yaw angle
       - Desired position at origin

4.3   Model Verification Cases

In this first part we aim to test the model without advanced control allocation, thruster dynamics, and feedback control of any kind. Through testing and mapping of the basic components, the aim is to ensure that the experimental setup will not effect DP simulations in any unexpected ways.

4.3.1 Case M1 - Current

The vessel drifts freely with current, without waves, thrust input or any kind of control system engaged. Incoming current direction is north east, at 0.2 m/s.

In Figure 4.1 we see the LF motion of the vessel in, north east Down (NED) frame. Motion is represented in the three unconstrained degrees of freedom (3DOF), north, east, and yaw. Measured, estimated and LF motion is outlined in Figure 4.2. The scope of this plot is to show consistency or possible deviation between estimated, measured and LF motion, which might indicate model errors. Figure 4.3 shows a north east representation of vessel position (estimated). This plot functions as an intuitive visual representation of position, though it does not give any indication to vessel heading.
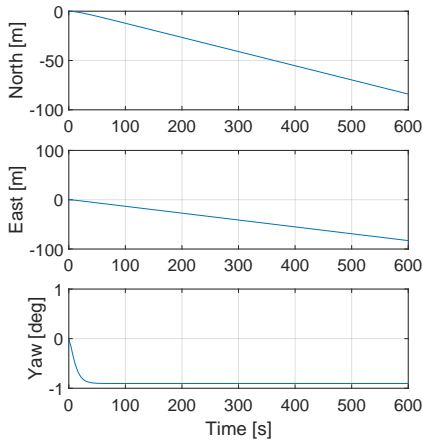
Figure 4.1: *LF position and heading of vessel in NED frame for case M1*
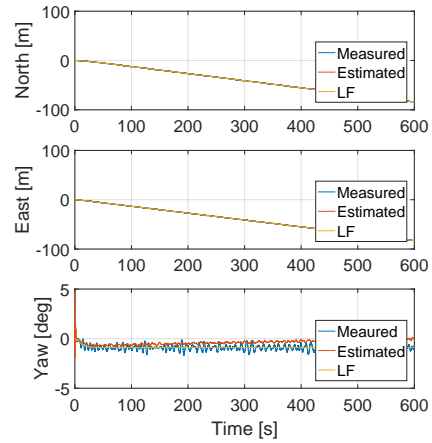
Figure 4.2: *Measured, estimated and LF position and heading of vessel in NED frame for case M1*
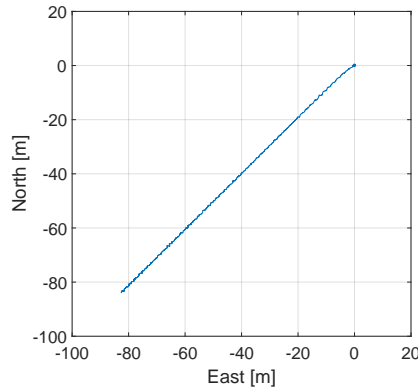
Figure 4.3: *Vehicle trajectory in north-east plane for case M1*

The results are as one should expect. The ship drifts towards the south west at a steady rate, whilst heading stays mainly constant, which is natural when there is steady current. The yaw estimates deviates slightly from LF and measurements, though this may be contributed to vessel speed, as the observer is designed for bollard pull conditions.

4.3.2   Case M2 - Waves

The vessel drifts freely with incident waves from north direction, modelled by the JONSWAP spectrum as described in Section 2.4.1. Peak frequency $\omega_p = 0.6$ and significant wave hight $H_s = 2m$. There are no other forces effecting the vessel, and no control scheme is applied.

As in case M1 Figure 4.4 shows LF motion, Figure 4.5 indicates consistency between estimates, measurements and LF motion, whilst the north east trajectory is plotted in Figure 4.6.
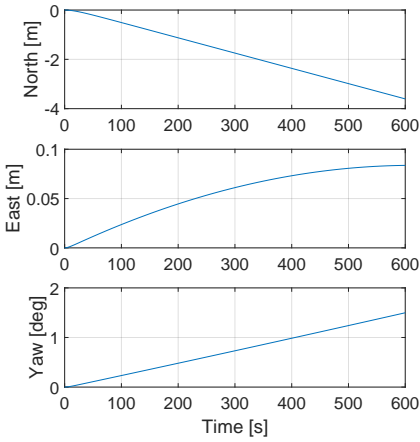
Figure 4.4: *LF position and heading of vessel in NED frame for case M2*
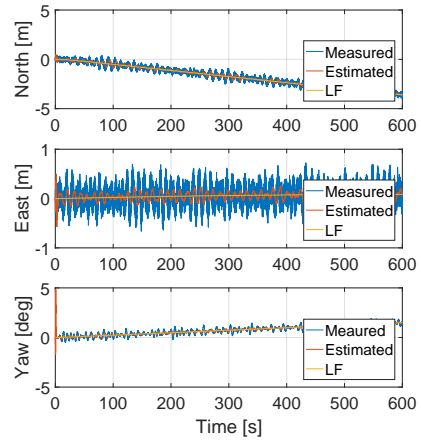
Figure 4.5: *Measured, estimated and LF position and heading of vessel in NED frame for case M2*
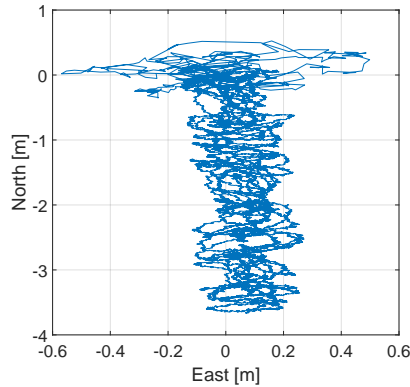
Figure 4.6: *Vehicle trajectory in north-east plane for case M2*

The vessel drifts southwards as expected with oscillatory motion from the WF component. The oscillatory motion inflicted by the waves is clear from position and heading measurements in Figure 4.5. Note that the observers implemented wave filter successfully mitigates the wave frequency motion.

4.3.3 Case M3 - Current and waves

Case M3 is a combination of case M1 and M2, with both current and waves as described in the previous sections. Waves from north with peak frequency $\omega_p = 0.6$ and significant wave hight $H_s = 2m$, and current from north east at velocity $v_c = 0.2m/s$. No DP system or any other force input except from environmental forces.

Figures are similar to previous cases, with LF motion in Figure 4.7, measured, estimated and LF motion in Figure 4.8 and north east trajectory in Figure 4.9.
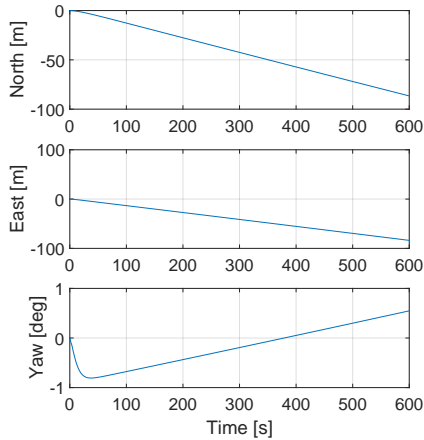
Figure 4.7: *LF position and heading of vessel in NED frame for case M3*
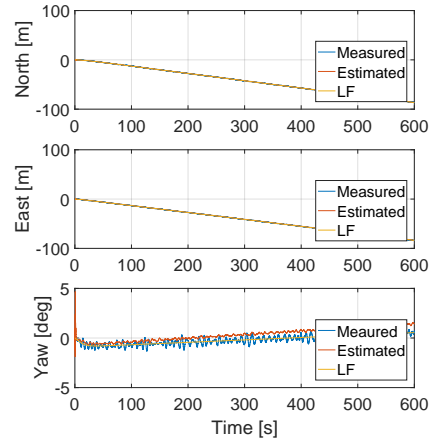
Figure 4.8: *Measured, estimated and LF position and heading of vessel in NED frame for case M3*
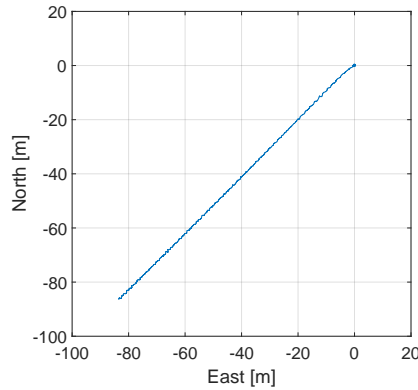
Figure 4.9: *Vehicle trajectory in north-east plane for case M3*

Note from fig 4.9 that the vessel is drifting slightly faster towards the south than east, as one would expect from the two previous cases and intuition.

4.3.4   Case M4 - Surge Force With Simplified Thrust Scheme

Case M4 investigates the vessel response under the influence of pure surge force and environmental forces as in case M3, i.e. current from north east and waves from north. Commanded thrust τ_c in sway and yaw direction is set to zero, whilst surge thrust is 50 kN. Force is applied through the centre of gravity (CG), and there is no advanced thrust allocation or control scheme. Thrusters are simply modelled as a first order time delay, with time constant $T = 5$.

For case M4 to M7 figures are similar. In Figure 4.10 LF motion in NED frame is presented, whilst Figure 4.11 shows output thrust. Surface trajectory in north east plane is visualised in Figure 4.12.
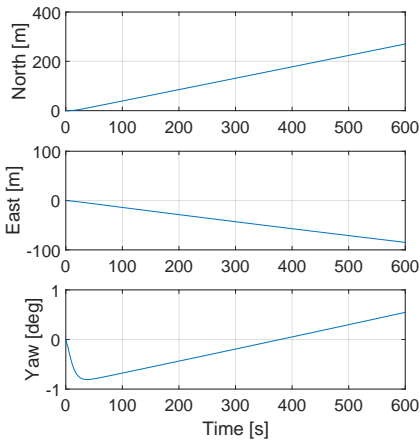
Figure 4.10: *LF position and heading in NED frame for case M4*
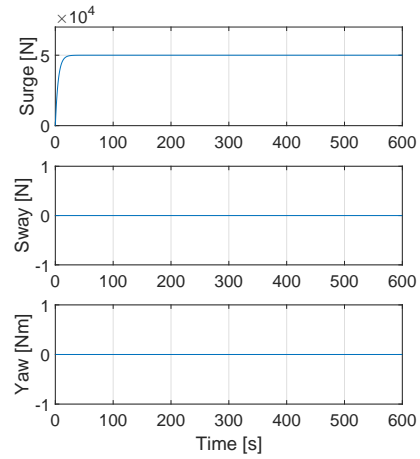
Figure 4.11: *Output thrust, τ in body frame for case M4*
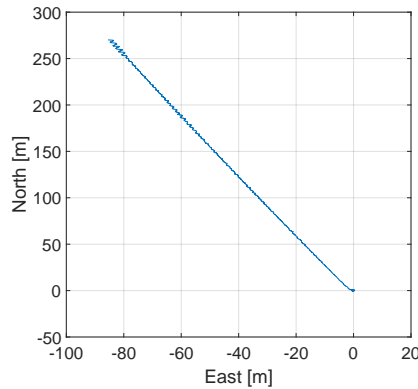
Figure 4.12: *Vehicle trajectory in north-east plane for case M4*

The vessel runs at steady rate towards north, whilst drifting westwards. When motion is compared to the north east trajectory in case M1 (Figure 4.3), it is clear that more or less all sideways drift can be contributed to the current. Note that the output thrust stabilizes at 50 000 N after a short time lag due to the first order delay.

4.3.5 Case M5 - Sway Force With Simplified Thrust Scheme

In case M5 The vessel is subjected to a force of 50 kN in sway. As in M4 thrust is applied through CG, and thrusters are modelled as a time delay. Environmental forces are as in case M3 i.e. current from north east and waves from north, whilst commanded force in surge and commanded moment in yaw is zero.

Figure 4.13 shows LF position and heading. Figure 4.14 presents output thrust and Figure 4.15 north east trajectory.
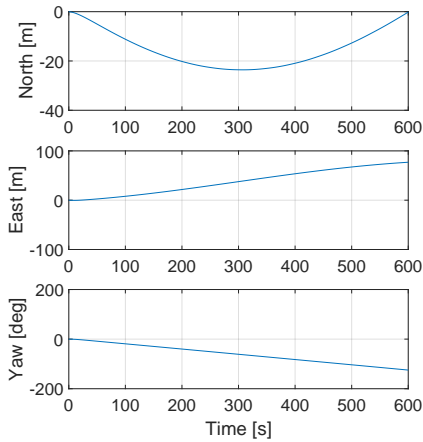
Figure 4.13: *LF position and heading in NED frame for case M5*
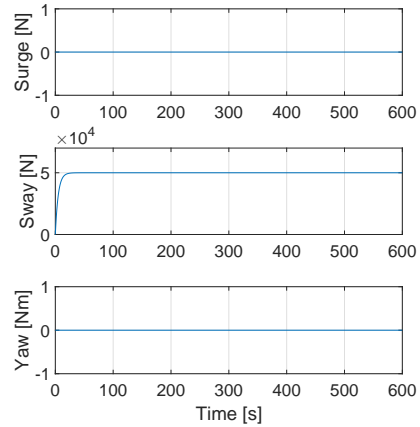
Figure 4.14: *Output thrust, τ in body frame for case M5*
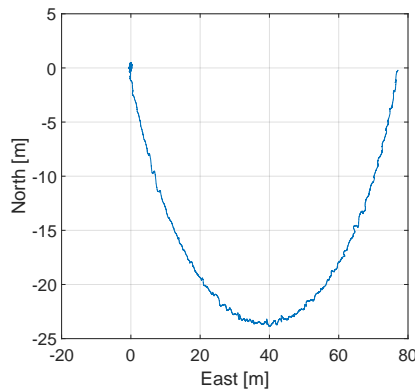
Figure 4.15: *Vehicle trajectory in north-east plane for case M5*

As in case M4, output thrust stabilizes at the commanded thrust after a short time delay. The motion is however more irregular. Probably due to Gunnerus being asymmetrical around the y-axis, a pure surge force through the centre of gravity results in a constant moment. I.e. motion in surge and yaw is not decoupled, resulting in curved motion as seen in fig 4.15.

4.3.6   Case M6 - Yaw Moment With Simplified Thrust Scheme

Case M6 has simplified thrust dynamics with pure moment of 50 kNm in yaw applied through the CG. Environmental forces as in previous cases with 0.2 m/s current from north east and incident waves from north. No DP control of any kind.

3DOF LF motion of vessel is given in Figure 4.16 whilst output thrust is plotted against time in Figure 4.17. In Figure 4.18 we present north east motion.
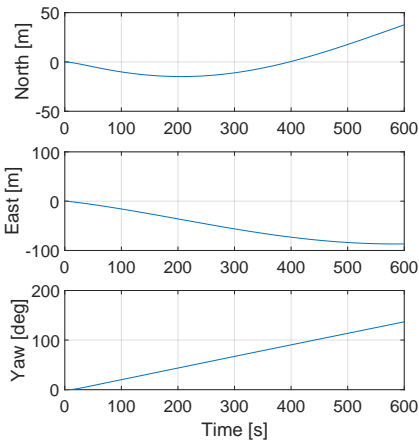
Figure 4.16: *LF position and heading in NED frame for case M6*
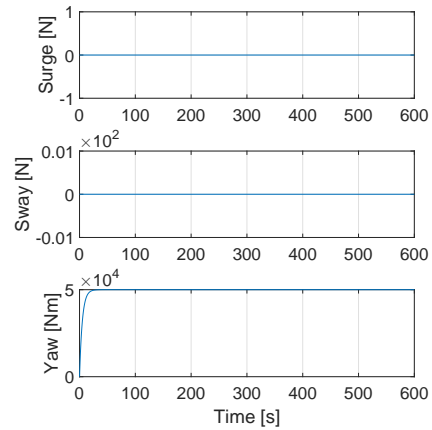
Figure 4.17: *Output thrust, τ in body frame for case M6*
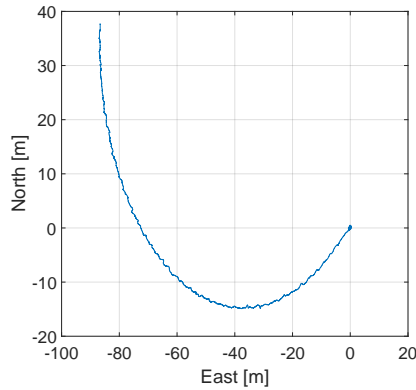
Figure 4.18: *Vehicle trajectory in north-east plane for case M6*

Once again there is circular motion due to coupled sway and yaw. Current and wave drift gives a resulting translation towards south west.

4.3.7   Case M7 - Combined Thrust Scheme

In the final case of the model verification series, we run a combined thrust simulation with 40 kN surge, 30 kN sway and -30 kNm yaw. As in case M4 to M6 there are no advanced thrust allocation and thrusters are simulated as a time delay. Current from North East at 0.2 m/s and waves from north as in previous cases.

Figure 4.19 shows LF motion, Figure 4.20 output force and Figure 4.21 north east trajectory.
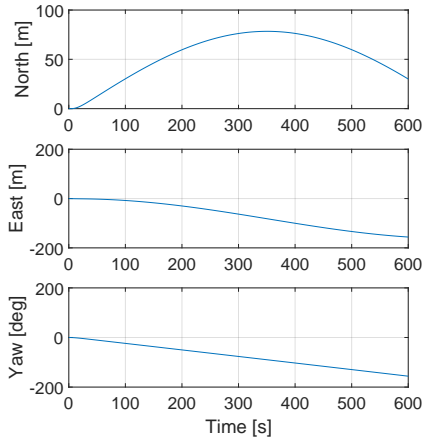
Figure 4.19: *LF position and heading in NED frame for case M7*
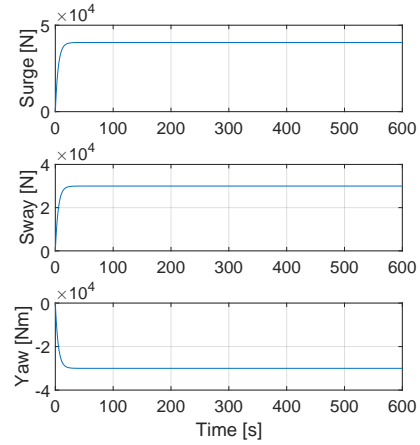
Figure 4.20: *Output thrust, τ in body frame for case M7*
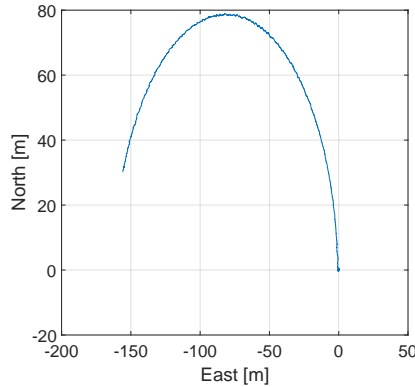
Figure 4.21: *Vehicle trajectory in North-East plane for case M7*

As previously $\tau \rightarrow \tau_c$ and the vehicle motion is as intuitively expected.

4.3.8   Concluding Remarks

From the model verification cases M1 to M7, we conclude that both environmental and thrust forces effects the vessel as one might intuitively predict. It is noted that surge and yaw motion is coupled, likely due to the vessel being asymmetrical around the y-axis (Faltinsen [1993]). The thruster time delay is as well notable.

We expect that these two observations, both directly linked with resulting force on the vessel, might have an effect on the force and moment feedback control system.

4.4   Force Feedback Control Cases

The following cases are designed to verify that the force feedback control drives output forces to the desired values.

4.4.1   Case F1 - Surge Force With Force Feedback Control

Case F1 investigates the vessel response under influence of pure surge force and environmental conditions as in case M3 i.e. current from north east and waves from north. Desired thrust in sway and yaw direction is set to zero, whilst surge thrust is 50 kN. Thrust allocation and dynamics are as described in Section 2.2 and 2.9, and no motion feedback is applied.

For case F1 to F4 figures are similar. In Figure 4.22 LF motion in NED frame is presented, whilst Figure 4.23 shows output thrust and the desired thrust value. Surface trajectory in north east plane is visualised in Figure 4.24. Figure 4.25 and 4.26 presents total commanded thrust and commanded thrust from force feedback loop respectively. Thrust output from each propeller is plotted in Figure 4.27 and measured rudder forces (L - Lift and D - Drag) are shown in Figure 4.28.
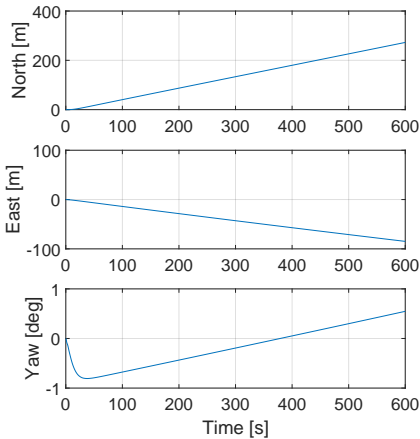
Figure 4.22: *LF position and heading in north east down frame for case F1*
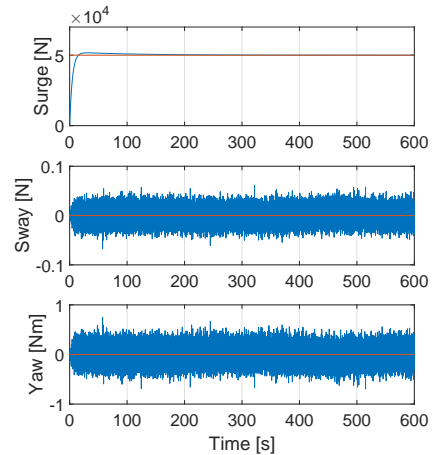
Figure 4.23: *Output (blue) and desired (red) thrust in body frame for case F1*
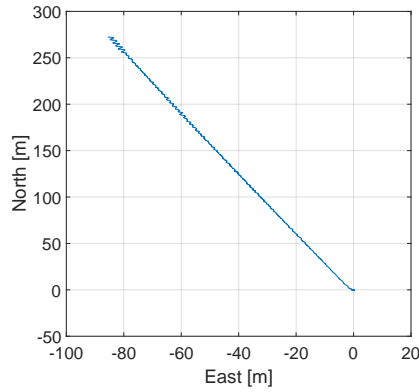
Figure 4.24: *Vehicle trajectory in north-east plane for case F1*
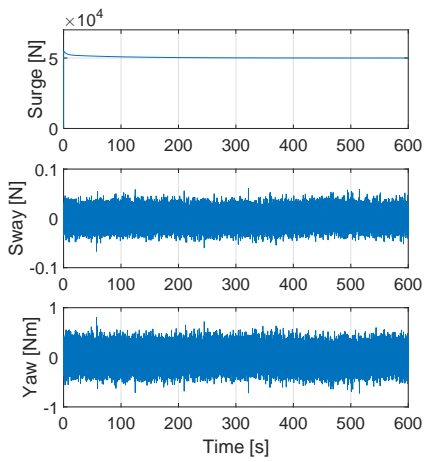
Figure 4.25: *Total commanded thrust, τ_c in body frame for case F1*
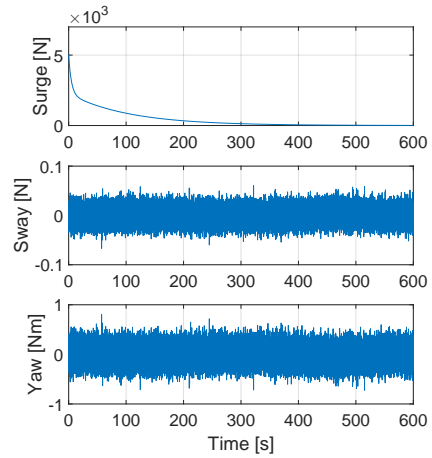
**Figure 4.26:** *Commanded thrust from force feedback control, τ_F in body frame for case F1*
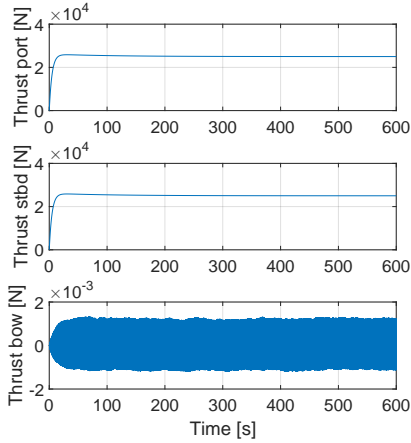
Figure 4.27: *Output forces from thrust devices for case F1*
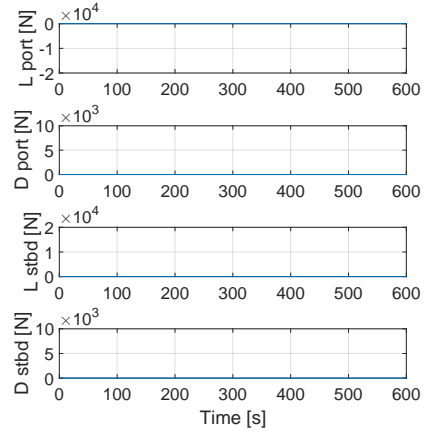
**Figure 4.28:** *Measured rudder forces (Lift - L and Drag - D) for case F1*

Compared with case M4 - surge force with simplified thrust scheme, we observe that the vessel motion is more or less identical. For surge motion no sideways force from rudders is necessary, and thus the force feedback term goes to zero over time. It is worth noting that the simulation initially has 5000 N in commanded surge from the force feedback controller, due to the first order time delay in thruster response. The effect is a small overshoot, though degrade in performance is minuscule. The thrust load is shared equally between port and starboard (stbd) thruster, as one should expect.

4.4.2   Case F2 - Sway Force With Force Feedback Control

In case F2 The vessel is subjected to a force of 50 kN in sway. Thrust allocation and dynamics is as described in Section 2.2 and 2.9, and no motion feedback is applied. Environmental forces are as in case M3, i.e. current from north east and waves from north, whilst desired force in surge and moment in yaw is zero.

Figure 4.29 shows LF position and heading. Figure 4.30 shows output thrust and Figure 4.31 north east trajectory. Further, commanded thrust, the sum of force feedback thrust and desired thrust, is plotted in Figure 4.32 whilst commanded thrust from the force feedback controller τ_F, is shown in Figure 4.33. Finally force output from thrusters and rudders are presented in Figure 4.34 and 4.35 respectively.
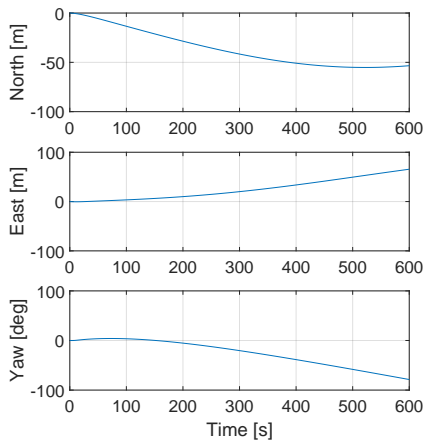
Figure 4.29: *LF position and heading in north east down frame for case F2*
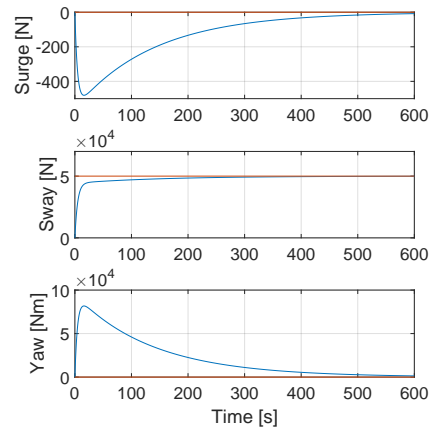
Figure 4.30: *Output (blue) and desired (red) thrust τ, in body frame for case F2*
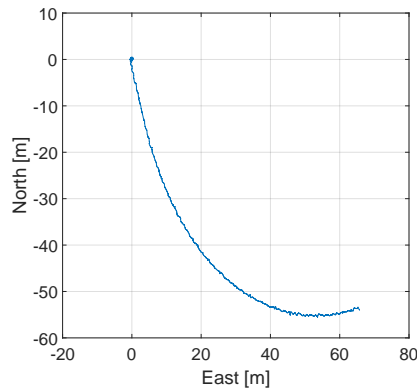
Figure 4.31: *Vehicle trajectory in north-east plane for case F2*
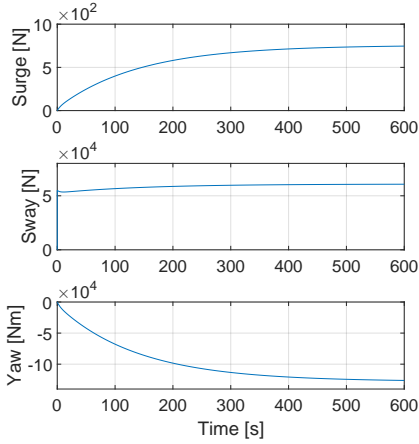
Figure 4.32: *Total commanded thrust, τ_c in body frame for case F2*
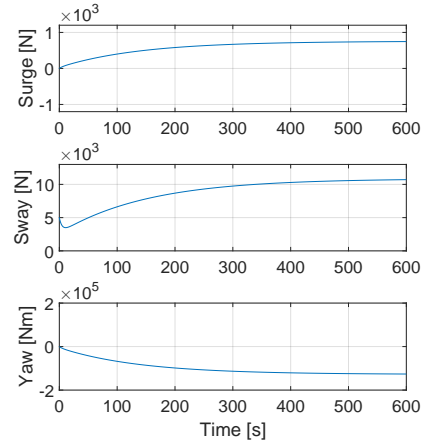
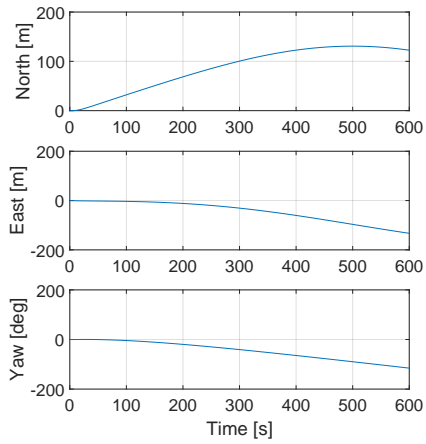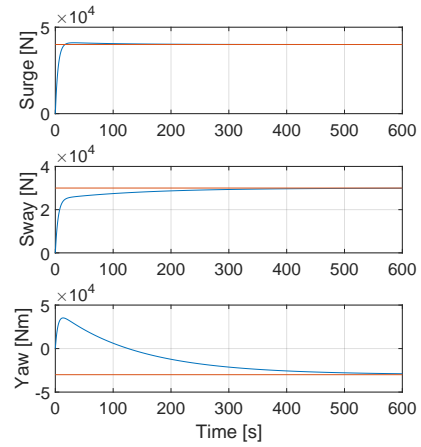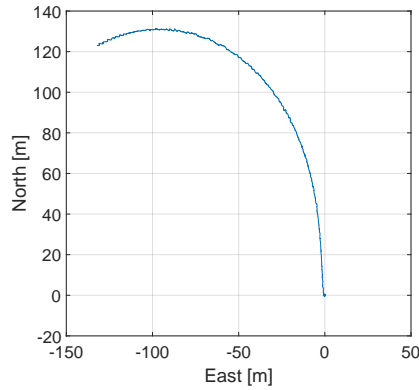**Figure 4.33:** *Commanded thrust from force feedback control, τ_F in body frame for case F2*
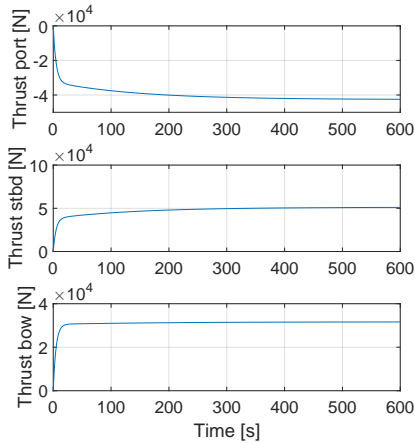
Figure 4.34: *Output forces from thrust devices for case F2*
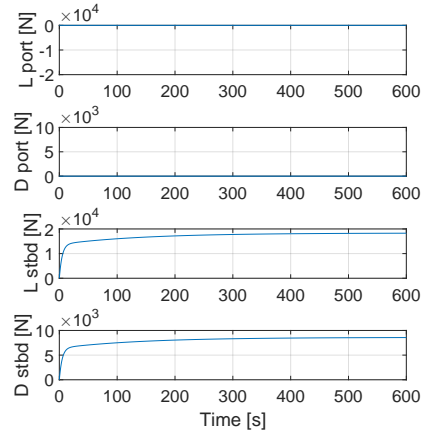
Figure 4.35: *Measured rudder forces for case F2*

The integral gain in the force feedback controller drives the output thrust to the desired thrust in around 600 seconds. Starboard rudder produces slightly less than 2 kN of the sideways thrust, whilst the bow thruster handles the remaining 3 kN. We observe that the difference in absolute value thrust between port side and starboard thruster is equal to rudder induced drag at steady state. Note that the north east trajectory is significantly different to that of case M5 (Figure 4.15). This is mostly due to the rather large positive output moment as seen in Figure 4.30.

4.4.3   Case F3 - Yaw Moment With Force Feedback Control

Case F3 has Thrust allocation and dynamics as described in Section 2.2 and 2.9. Pure moment of 50 kNm in yaw is applied through the CG and desired thrust forces are zero. Environmental forces are as in previous cases, with 0.2 m/s current from north east and incident waves from north. No motion feedback control.

3DOF LF motion of the vessel is given in fig 4.36 whilst output thrust is plotted against time in fig 4.37. In 4.18 we show north east motion. Figure 4.39 and 4.40 presents total and force feedback commanded thrust respectively and in Figure 4.41 presents thruster forces whilst Figure 4.42 shows rudder forces.
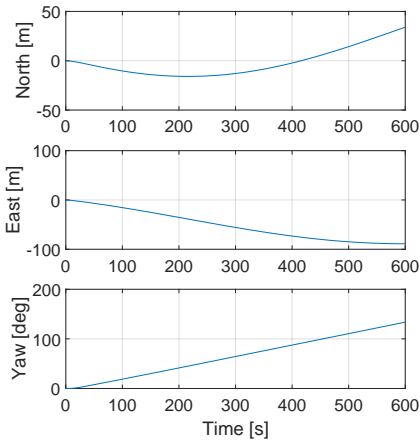
Figure 4.36: *LF position and heading in north east down frame for case F3*
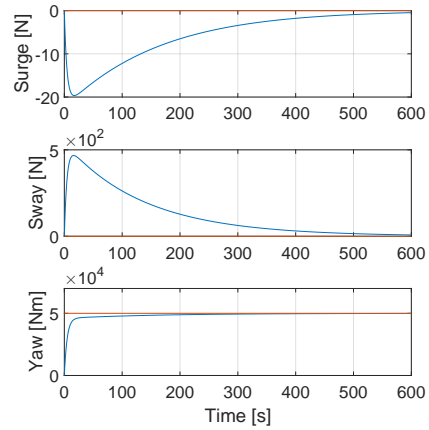
Figure 4.37: *Output (blue) and desired (red) thrust τ, in body frame for case F3*
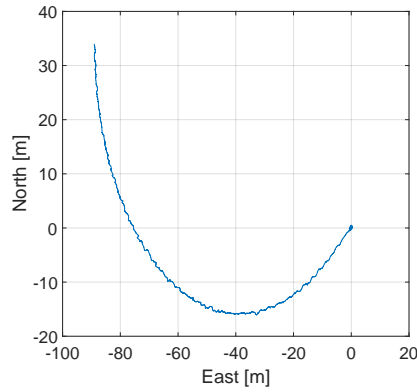
**Figure 4.38:** *Vehicle trajectory in North-East plane for case F3*
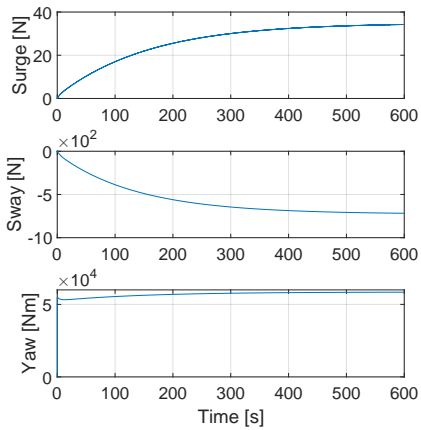
Figure 4.39: *Total commanded thrust, τ_c in body frame for case F3*
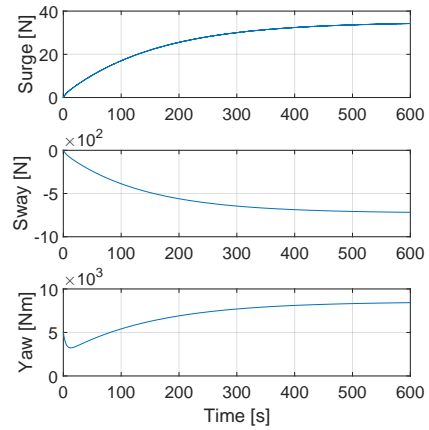
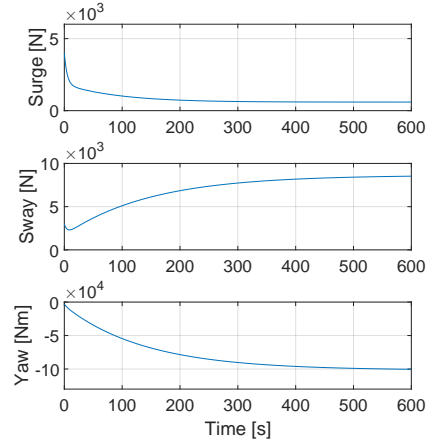**Figure 4.40:** *Commanded thrust from force feedback control, τ_F in body frame for case F3*
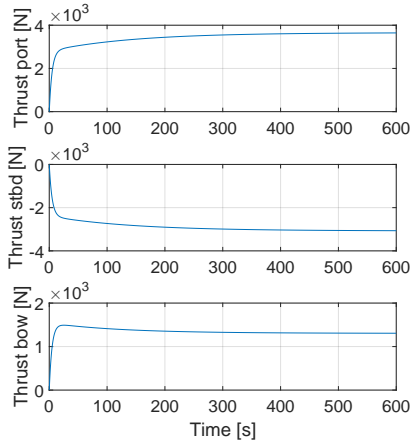
Figure 4.41: *Output forces from thrust devices for case F3*
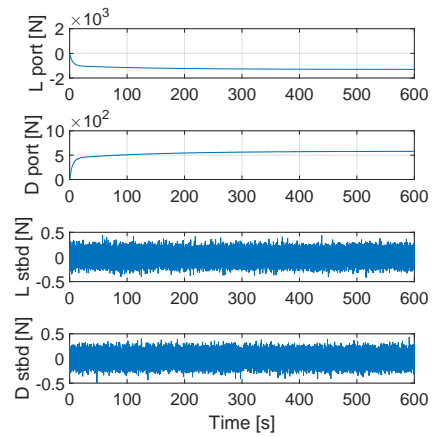
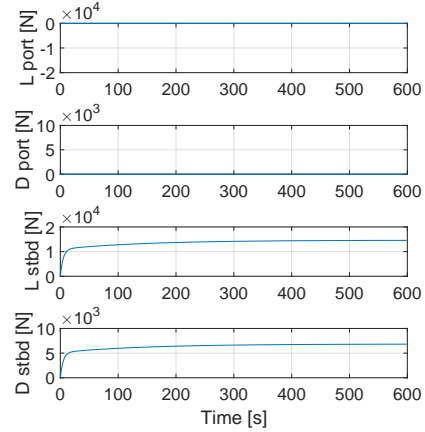**Figure 4.42:** *Measured rudder forces for case F3*

As in case F2 output thrust is driven to desired thrust in about 600 seconds. Performance is otherwise as expected compared to case M6 and previous force and moment feedback cases.

4.4.4 Case F4 - Combined Force Scheme With Force Feedback Control

In the final case of the force and moment feedback control verification series, we run a combined thrust simulation with desired thrust set to 40 kN surge, 30 kN sway and -30 kNm yaw. As in case F1 to F3 thrust allocation and dynamics are as described in Section 2.2 and 2.9, and no motion feedback is applied. Current from North East at 0.2 m/s and waves from north as in previous cases.

Figure 4.43 shows LF motion, Figure 4.44 output force and Figure 4.45 north east trajectory. Commanded thrust τ_c is presented in Figure 4.46, force feedback control forces in Figure 4.47, thruster forces in Figure 4.48 and rudder forces in Figure 4.49.

Figure 4.43: *LF position and heading in north east down frame for case F4*

Figure 4.44: *Output (blue) and desired (red) thrust τ, in body frame for case F4*

Figure 4.45: *Vehicle trajectory in North-East plane for case F4*
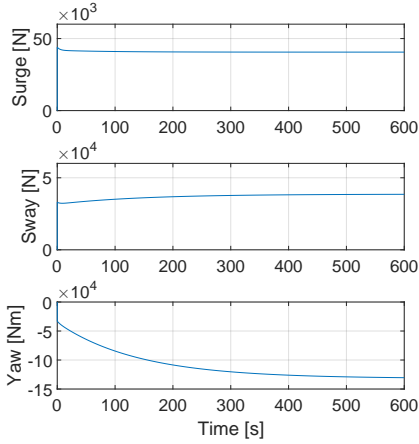
Figure 4.46: *Total commanded thrust, τ_c in body frame for case F4*

Figure 4.47: *Commanded thrust from force feedback control, τ_F in body frame for case F4*
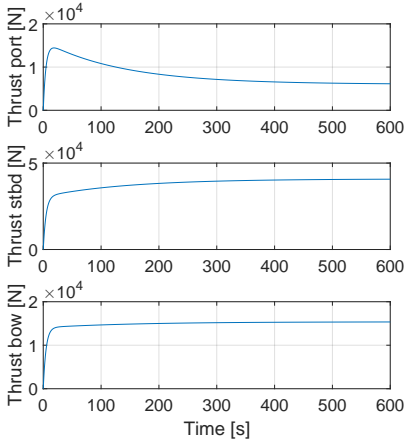
Figure 4.48: *Output forces from thrust devices for case F4*

Figure 4.49: *Measured rudder forces for case F4*

First and foremost we note that both forces and moment is drive to the desired values in around 600 seconds. North east trajectory is once again effected by output moment, though it is otherwise comparable to the trajectory in case M7. As in previous cases only the starboard rudder is utilized, as positive sway force is commanded.

4.4.5   Concluding Remarks

From the force feedback control verification cases we conclude that the FFC system performs at a satisfying level. In every case it drives both commanded force and moment towards the desired thrust within 600 seconds, and vessel motion is comparable to corresponding cases M4 to M7. Control allocation and thruster dynamics performs as expected, as thrust load is shared adequately between actuators. The first order time delay does not constitute any significant performance degrade. We are now ready to test the force control system in DP applications.

4.5   DP Cases

In these final cases we aim to test and compare different variations of DP. From the simplest scheme without use of rudders to different takes on force feedback. The goal is to asses the strengths of each design as well as to discover areas of improvements and further work.

4.5.1   Case DP1 - DP Without Force Feedback Control

Case DP1 compares DP performance with and without utilizing rudders. Force feedback control is turned off and environmental forces is as in case M3, i.e. current from north east and waves from north. Initial and desired position and heading at the origin, and the experimental setup is as described in Chapter 2 and 3. In case DP1a maximum rudder angle is set to zero degrees, and thus we effectively have no use of rudders. For DP2b maximum angle is set to the optimal 34 degrees. Otherwise the two cases are identical. At the end of the case, steady state output forces between simulations with varying maximum allowed rudder angle is compared.

Figures for case a) are shown in the the left hand column whilst whilst case b) is presented on the right hand side. This setup yields easy comparison between the two. In Figure 4.50 and 4.51 LF motion in NED frame is presented, Figure 4.52 and 4.53 shows position and heading error, and surface trajectory in north east plane is visualised in Figure 4.54 and 4.55. Figure 4.56 and 4.57 presents total output thrust whilst Figure 4.58 and 4.59 shows commanded thrust. Thrust output from each propeller is plotted in Figure 4.62 and 4.63 and measured rudder forces are displayed in Figure 4.64 and 4.65. In these figures L and D represents Lift and Drag force respectively. Finally the total amount of thrust force from port, starboard and bow thruster is displayed in Figure 4.66 and 4.67. This plot indicates the total power consumption of the corresponding control scheme. At the end steady state forces from each actuator is plotted versus maximum allowed rudder angle in Figure 4.68. Data for this plot are from DP simulations with max angle between 0 and 34 degrees with increment of 5.
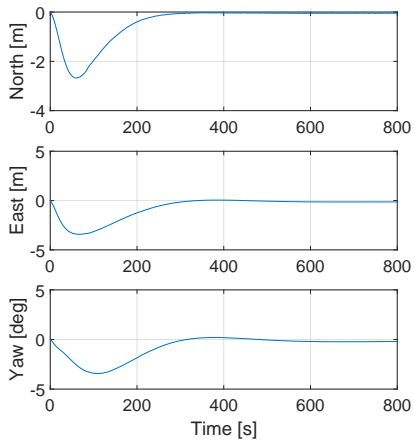
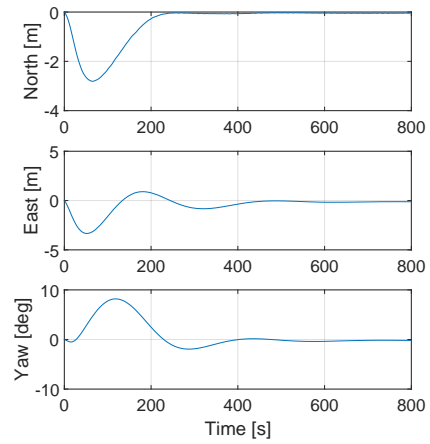**Figure 4.50:** *LF position and heading of vessel in NED frame for case DP1a*

Figure 4.51: *LF position and heading of vessel in NED frame for case DP1b*
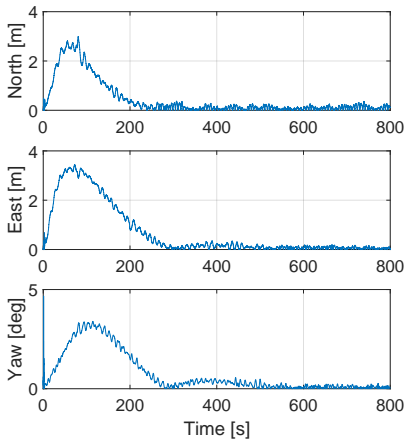

Figure 4.52: *Absolute value of estimated error in NED frame for case DP1a*
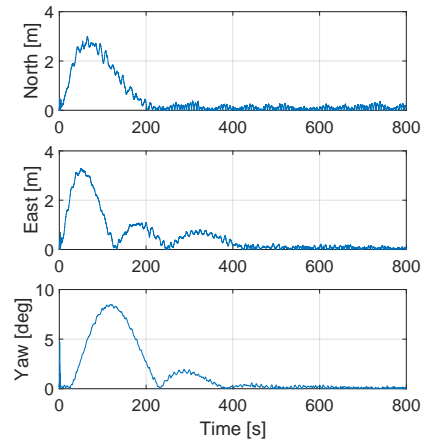

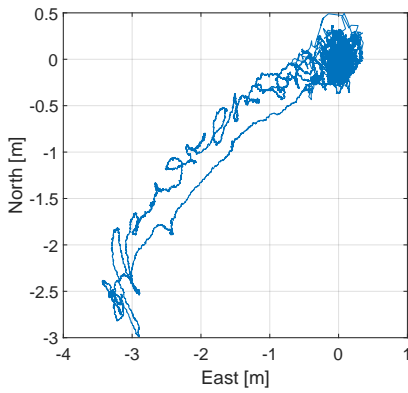**Figure 4.53:** *Absolute value of estimated error in NED frame for case DP1b*

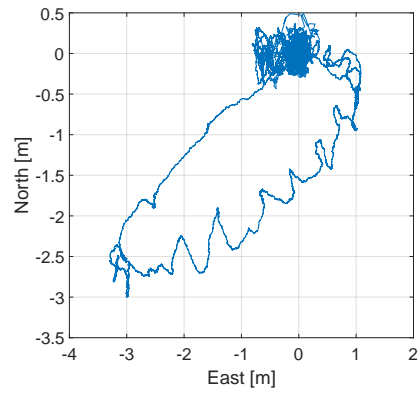**Figure 4.54:** *Vehicle trajectory based on position estimates in north east plane for case DP1a*

Figure 4.55: *Vehicle trajectory based on position estimates in North-East plane for case DP1b*
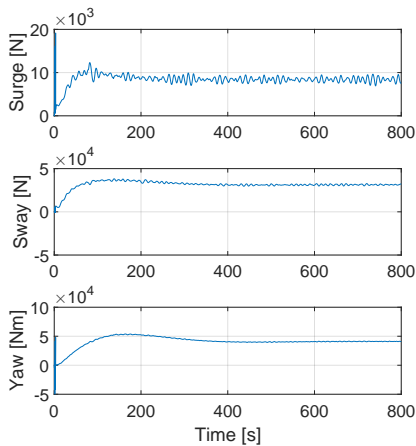
Figure 4.56: *Output thrust, τ in body frame for case DP1a*
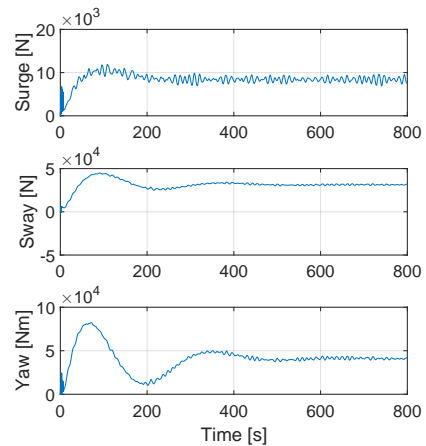
Figure 4.57: *Output thrust, τ in body frame for case DP1b*
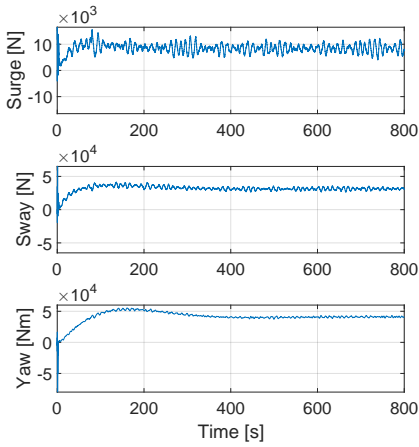
Figure 4.58: *Total commanded thrust, τ_c in body frame for case DP1a*
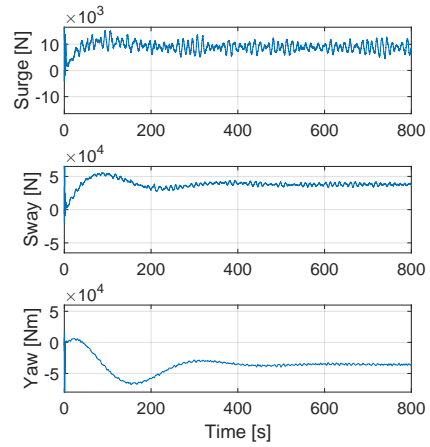
Figure 4.59: *Total commanded thrust, τ_c in body frame for case DP1b*
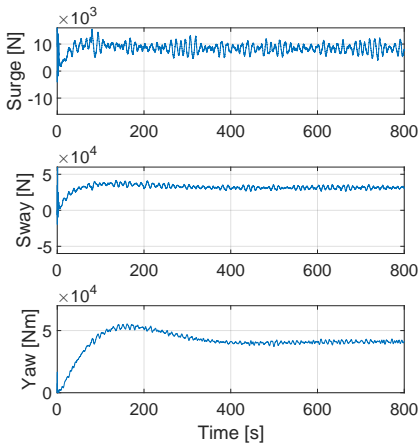
Figure 4.60: *Commanded thrust from position feedback control, τ_η in body frame for case DP1a*
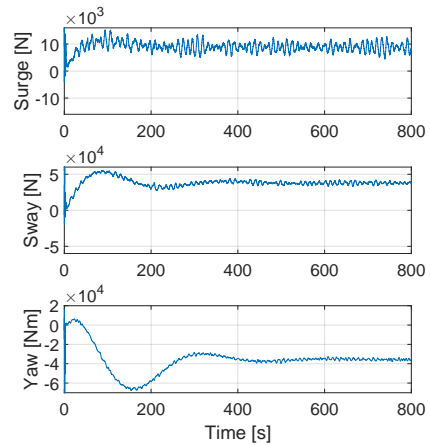

Figure 4.61: *Commanded thrust from position feedback control, τ_η in body frame for case DP1b*
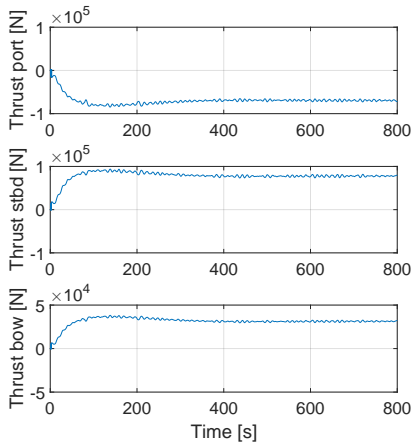
Figure 4.62: *Output forces from thrust devices for case DP1a*
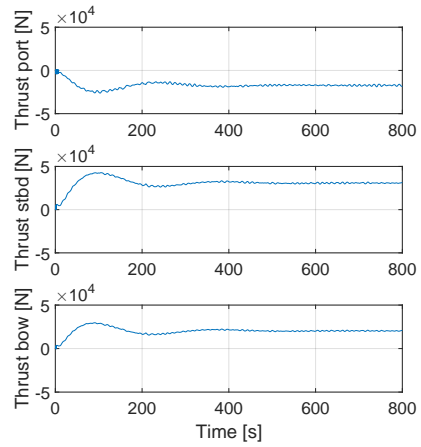

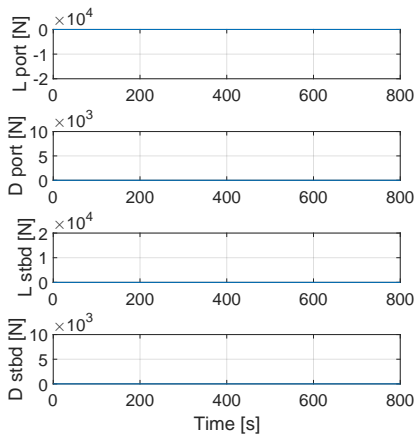**Figure 4.63:** *Output forces from thrust devices for case DP1b*

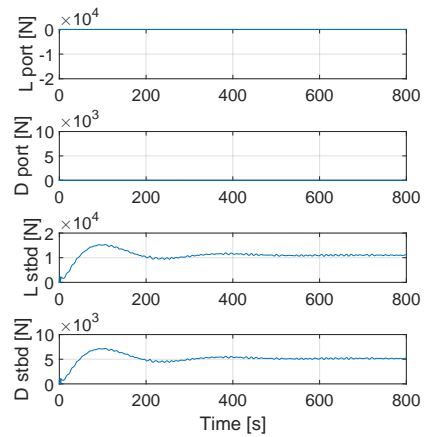**Figure 4.64:** *Measured rudder forces for case DP1a*

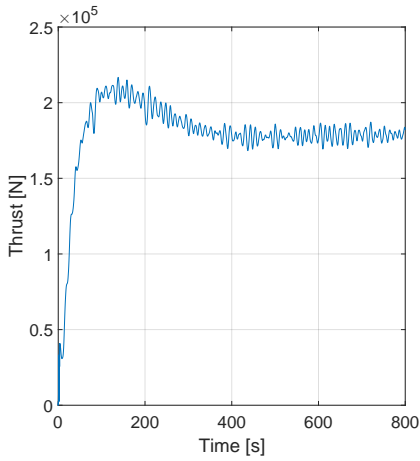**Figure 4.65:** *Measured rudder forces for case DP1b*

Figure 4.66: *Total thruster forces (absolute value) for case DP1a*
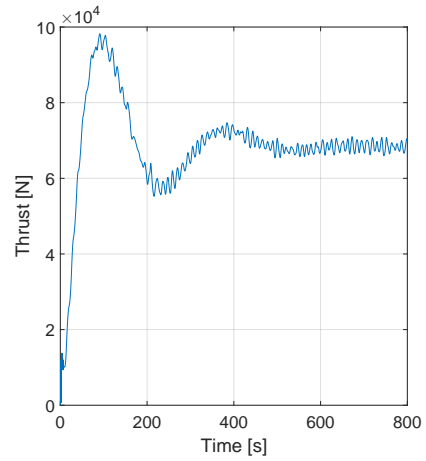

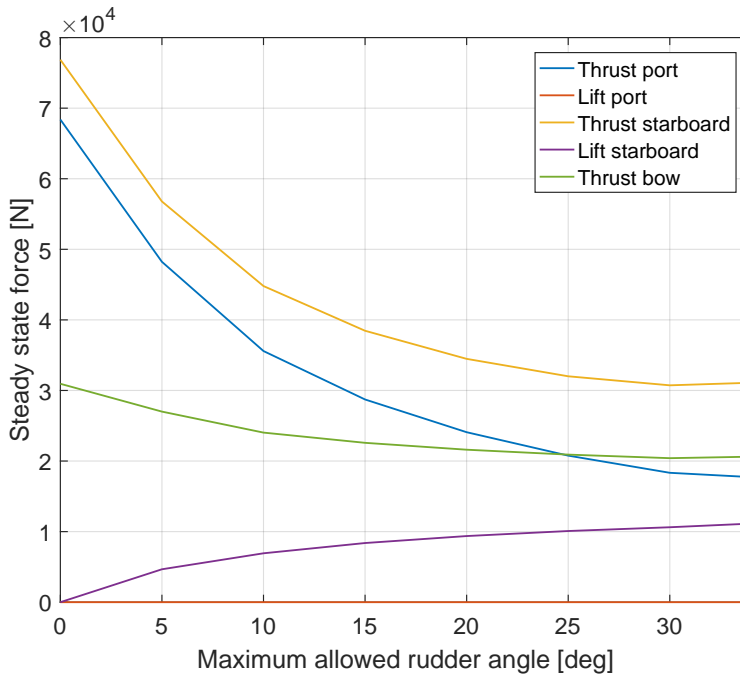**Figure 4.67:** *Total thruster forces (absolute value) for case DP1b*

Figure 4.68: *Absolute value of steady state force output from actuators at varying levels of maximum allowed rudder angle for case DP1*

First we note from Figure 4.52 and 4.53 that the position control is actually better without use of rudders. Especially heading control is significantly degraded. A probable cause is observed in Figure 4.56 and 4.57, where one may note that rudders contribute with a large and rapidly growing moment during the first 100 seconds. Do as well note that the commanded moment is in fact negative, to account for the deviation between the lift and drag model in the inverse mapping and thruster dynamics. (As described in Section 2.9 and 2.5).

Though position control is less precise with rudders, observe in Figure 4.66 and 4.67 that total thrust is significantly larger without use of rudders, and thus so is power consumption. This impression is further strengthened by Figure 4.68, where we note that thruster load decreases as max rudder angle increases. With larger rudder deflection more sideways force is produced by rudders at lower thrust cost. As rudder induced drag increases the gap between the port and starboard thruster grows. This is due to the fact that only the thruster producing positive force induces drag forces on the rudder.

4.5.2   Case DP2a - DP with Proportional-Integral Force Feedback Control

Case DP2a investigates DP performance with PI force feedback control. Experimental setup is as described in Chapter 2 and 3. Initial and desired position at the origin and environmental forces as in previous cases, i.e. 0.2 m/s current from north east and waves from north.

In Figure 4.69 LF motion in NED frame is presented, whilst Figure 4.70 compares measured, estimated and LF position and heading. Figure 4.71 and 4.72 displays position and heading error, and surface trajectory in north east plane respectively. Figure 4.73 presents output thrust, whilst total commanded thrust is shown in Figure 4.58. Total commanded thrust is as explained in Chapter 3 the sum of commanded thrust from motion and force feedback, which are plotted versus time in Figure 4.75 and 4.76 respectively. Thrust output from each propeller is plotted in Figure 4.77 and measured rudder forces, lift (L) and drag (D) are presented in Figure 4.78. Total thrust force from port, starboard and bow thruster is displayed in Figure 4.79, indicating the total power consumption.
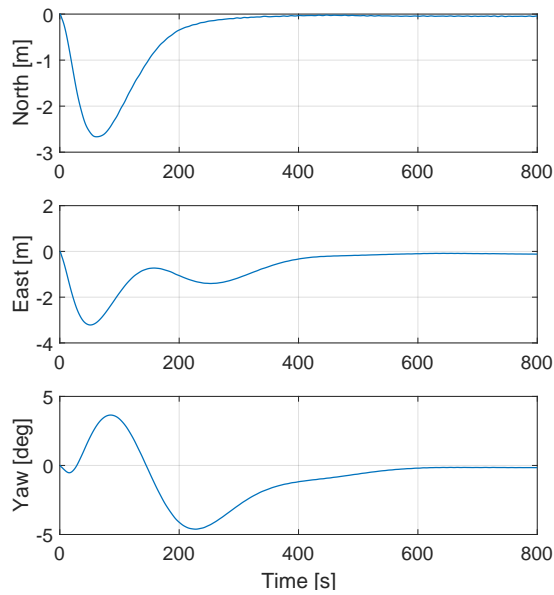
Figure 4.69: *LF position and heading of vessel in NED frame for case DP2a*

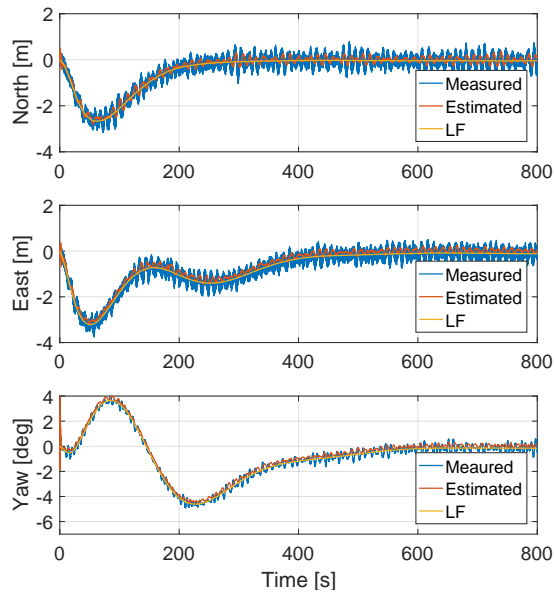*Figure 4.70:* *Measured, estimated and LF position and heading of vessel in NED frame for case DP2a*
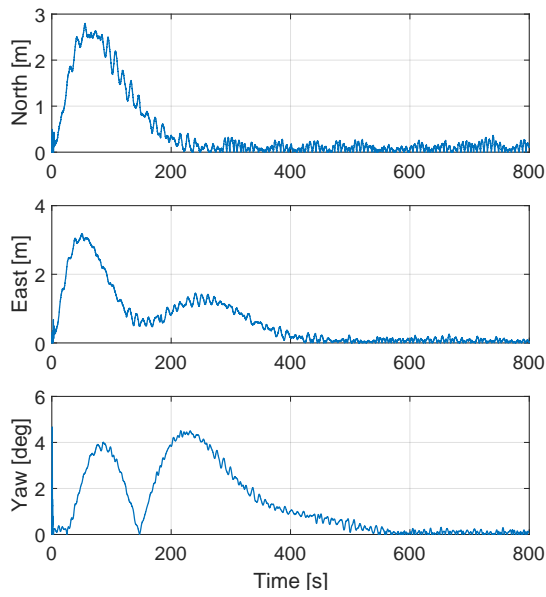
Figure 4.71: *Absolute value of error in NED frame for case DP2a*
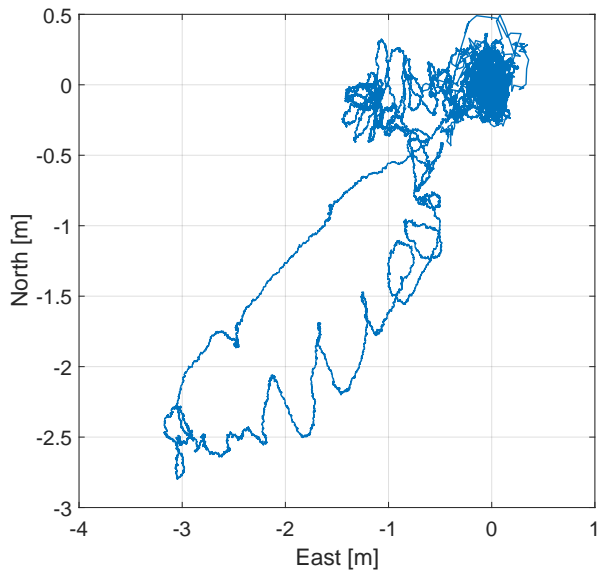
Figure 4.72: *Vehicle trajectory in north-east plane for case DP2a*
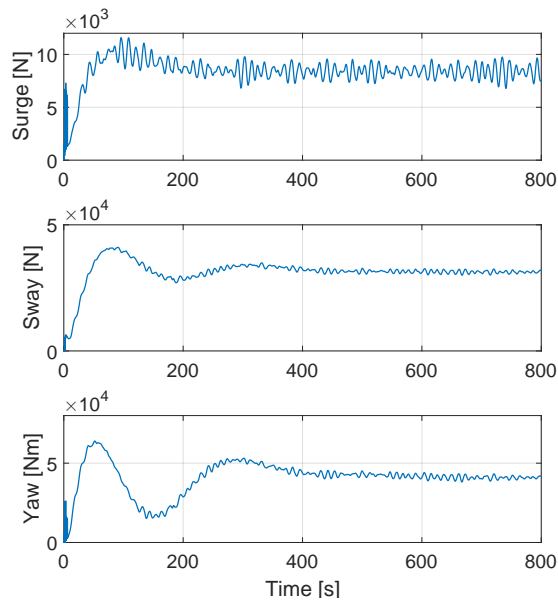
Figure 4.73: *Output thrust, τ in body frame for case DP2a*
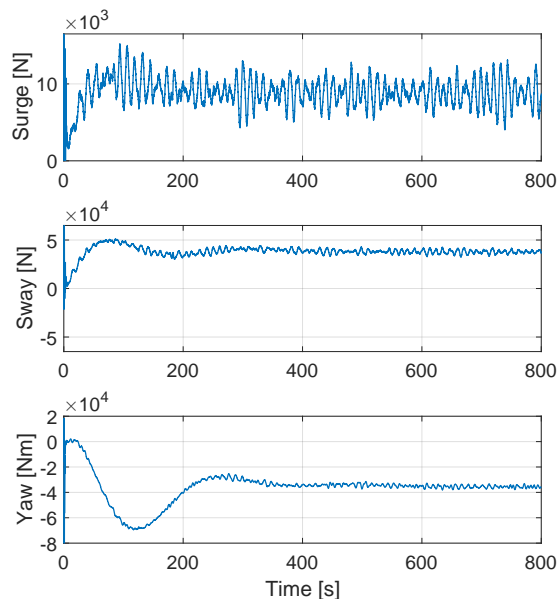
Figure 4.74:   *Total commanded thrust, τ_c in body frame for case DP2a*
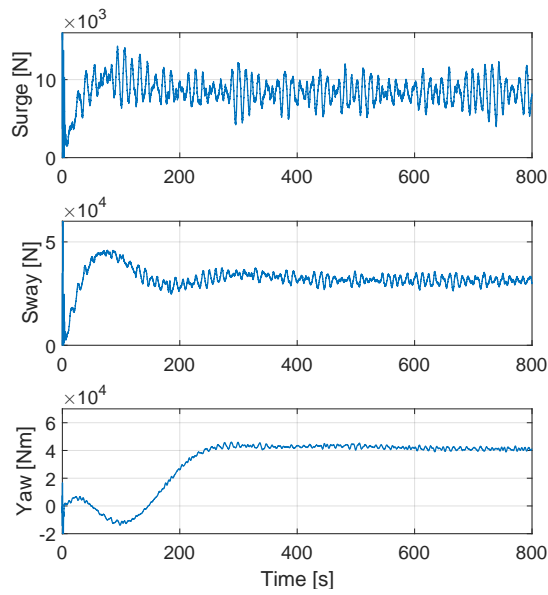
Figure 4.75: *Commanded thrust from position feedback control, τ_η in body frame for case DP2a*

Figure 4.76: *Commanded thrust from force feedback control, τ_F in body frame for case DP2a*

Figure 4.77: *Output forces from thrust devices for case DP2a*

Figure 4.78: *Measured rudder forces for case DP2a*
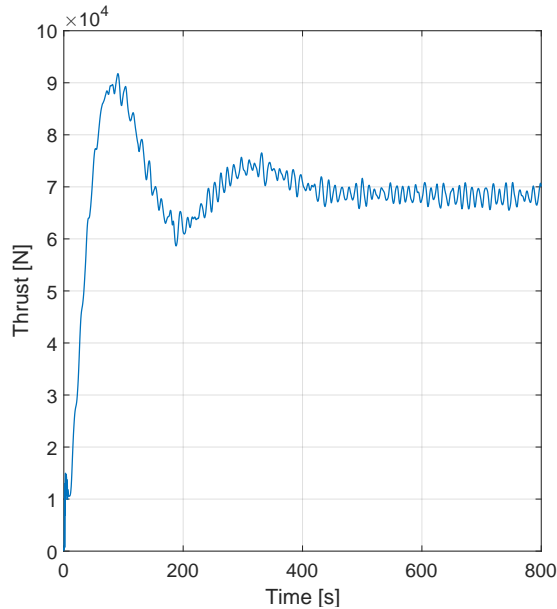
Figure 4.79: *Total thruster forces (absolute value) for case DP2a*

Most noticeable is the the difference in yaw motion compared to DP1b, without force feedback. Whether this is an improvement is difficult to asses without direct comparison, which is carried out 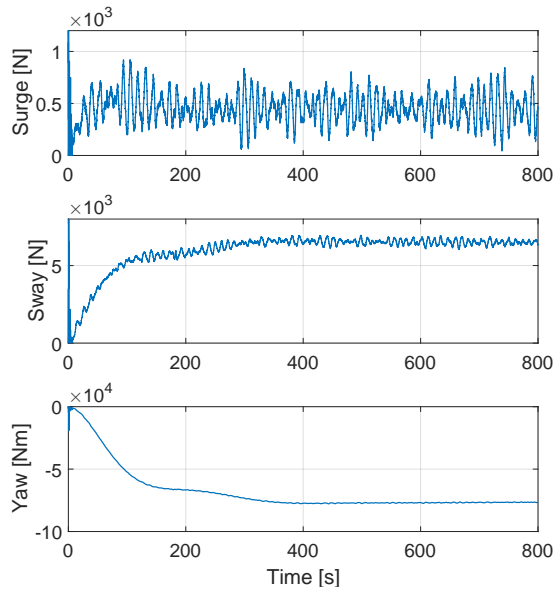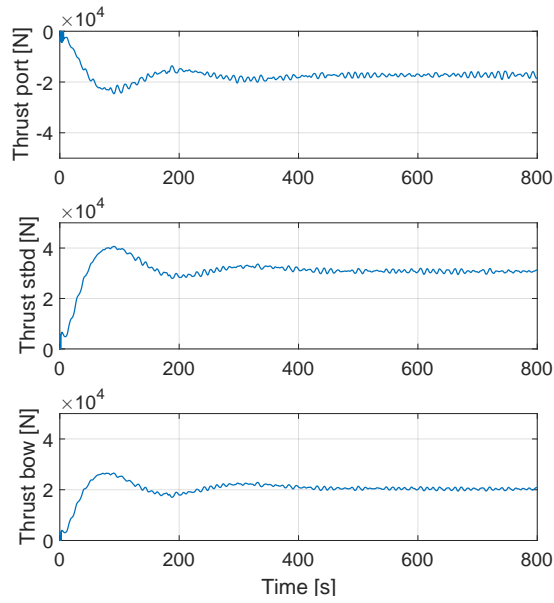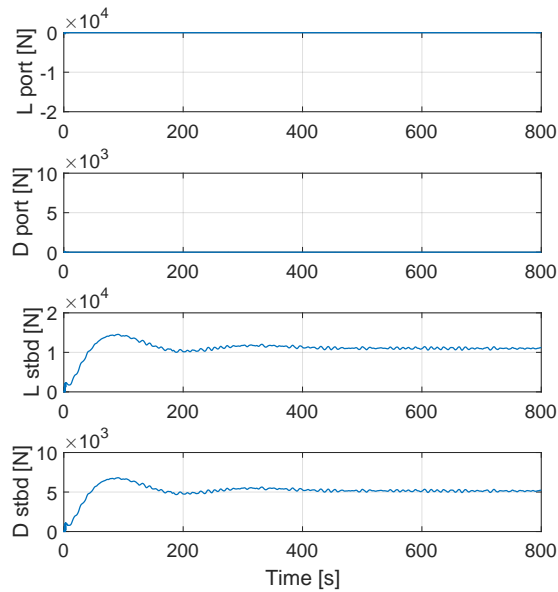in Section 4.5.4. We do however note that the power spike in "thrust consumption" as seen in Figure 4.79 is significantly lower compared to case DP1b, Figure 4.67. From the LF motion in Figure 4.69, it might seem as the sway and yaw controller is "fighting" each other. This effect is probably due to the coupling of sway and yaw motion as discussed in Section 4.3.5 and 4.3.6 where force in sway induces yaw moment and vice versa.

Filter action in the observer, yields estimates which are significantly less noisy and have less WF motion than measurements, as seen in Figure 4.70. There is however a small bias in sway and yaw compared to LF motion. This could have been removed with larger bias gains in the observer, though it is in no way crucial for testing of the force feedback controller. Faster bias correction does as well come at the cost of worse noise rejection.

4.5.3   Case DP2b - DP with Proportional Force Feedback Control

In this final case we investigate DP performance with proportional force feedback control, i.e. without integral gain. Experimental setup is otherwise as described in Chapter 2 and 3. Desired and initial position at origin and environmental forces is once again as in case M3. Current from north east and waves from north.

Figure 4.80 presents LF motion in NED frame, Figure 4.70 shows measured, estimated and LF position, Figure 4.71 error in position and heading, $\eta_d - \eta$, and 4.72 presents surface trajectory in north east plane. In Figure 4.73 output thrust is displayed and total commanded thrust is shown in Figure 4.58. Commanded forces from position and force feedback are plotted versus time in Figure 4.75 and 4.76 respectively. Thrust output from each propeller is plotted in Figure 4.77 and measured rudder forces, are presented in Figure 4.78. Total thrust force from port, starboard and bow thruster is displayed in Figure 4.79.
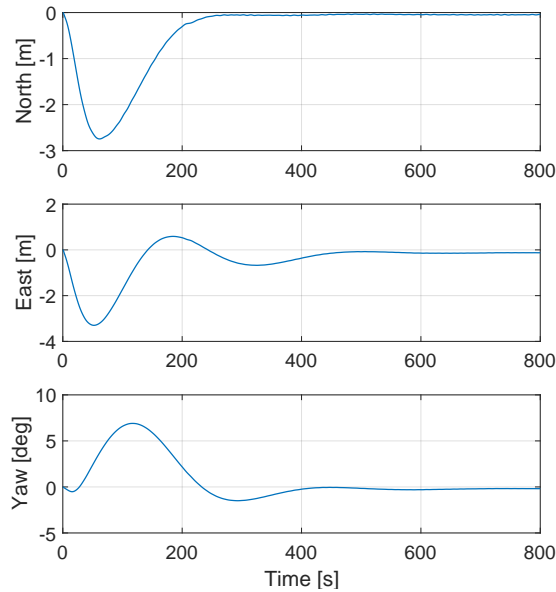
Figure 4.80: *LF position and heading of vessel in NED frame for case DP2b*
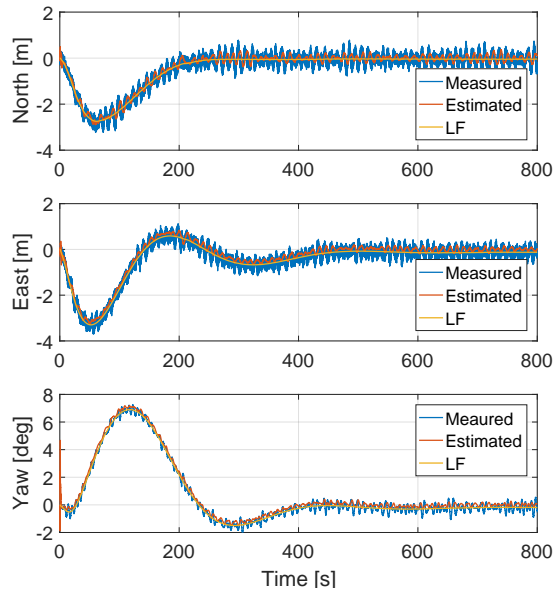
Figure 4.81: *Measured, estimated and LF position and heading of vessel in NED frame for case DP2b*
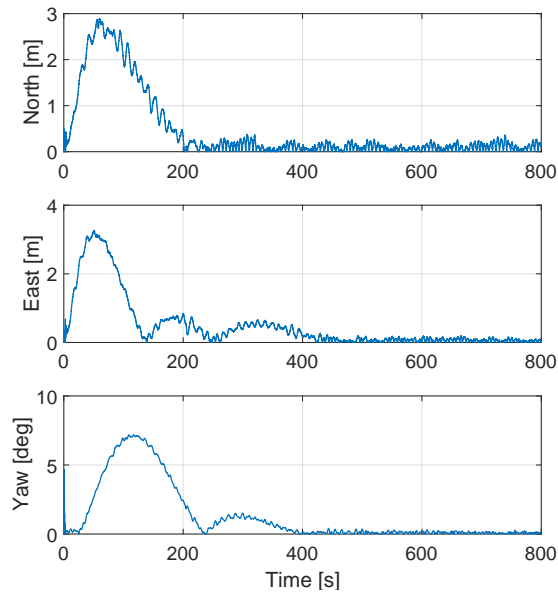
Figure 4.82: *Absolute value of error in NED frame for case DP2b*
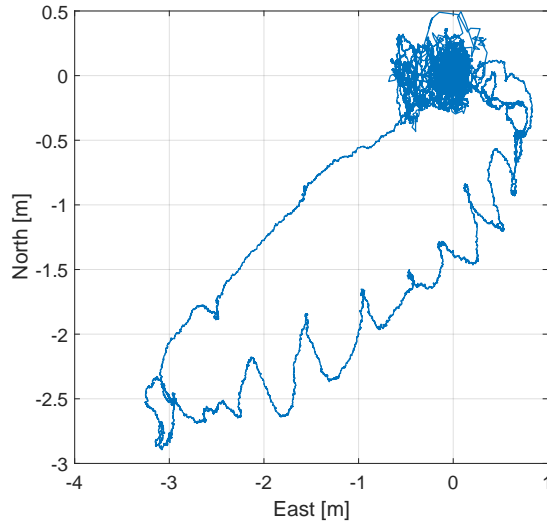
Figure 4.83: *Vehicle trajectory in north east plane for case DP2b*
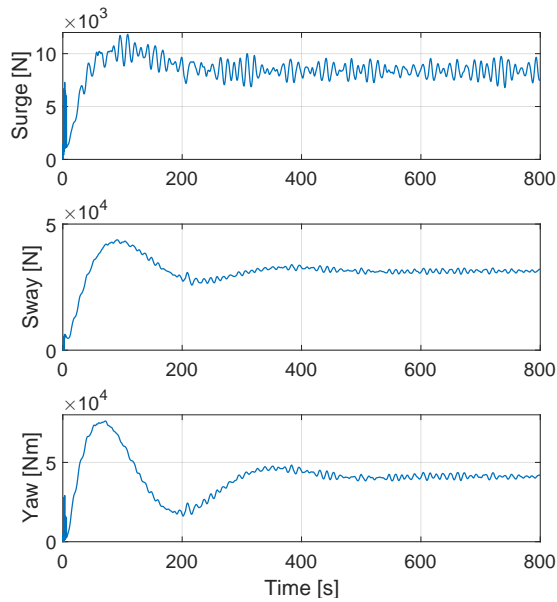
Figure 4.84: *Output thrust, τ in body frame for case DP2b*
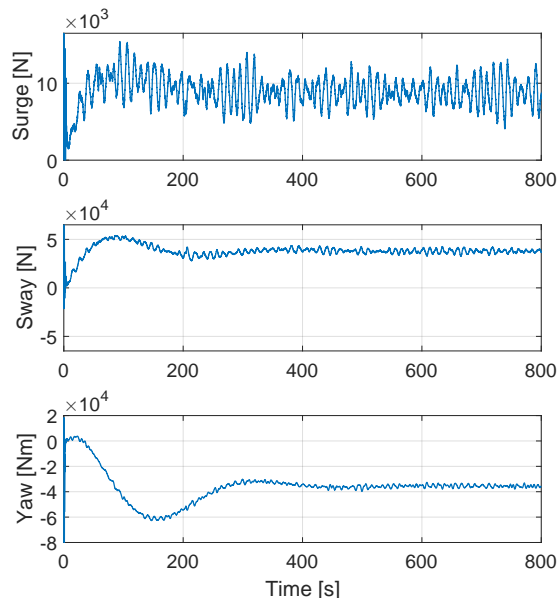
Figure 4.85:   *Total commanded thrust, τ_c in body frame for case DP2b*
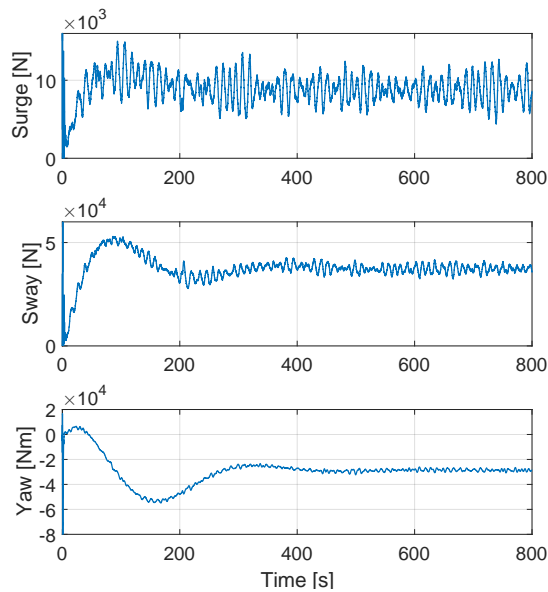
Figure 4.86: *Commanded thrust from position feedback control, τ_η in body frame for case DP2b*
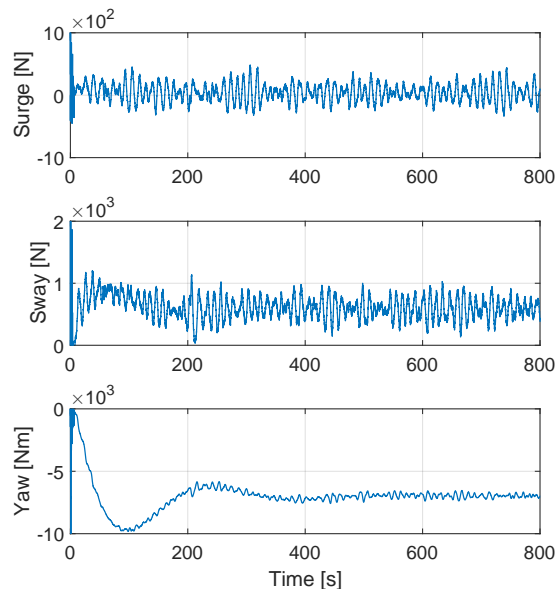
Figure 4.87: *Commanded thrust from force feedback control, τ_F in body frame for case DP2b*
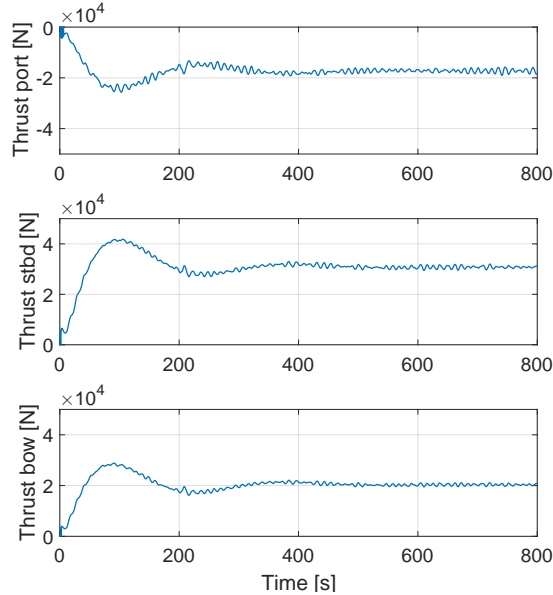
Figure 4.88: *Output forces from thrust devices for case DP2b*
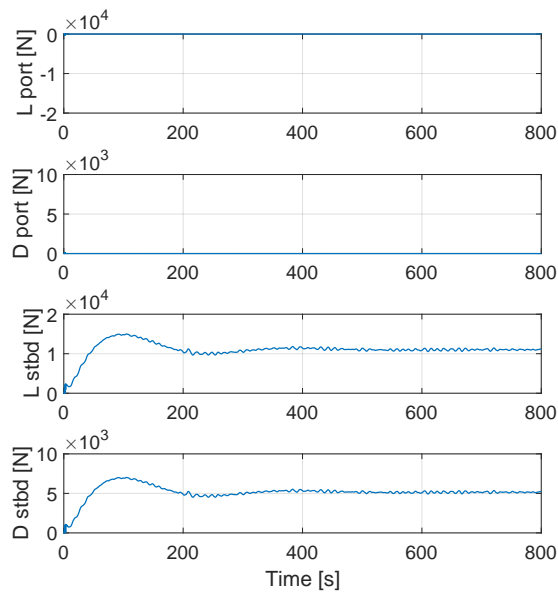
Figure 4.89: *Measured rudder forces for case DP2b*
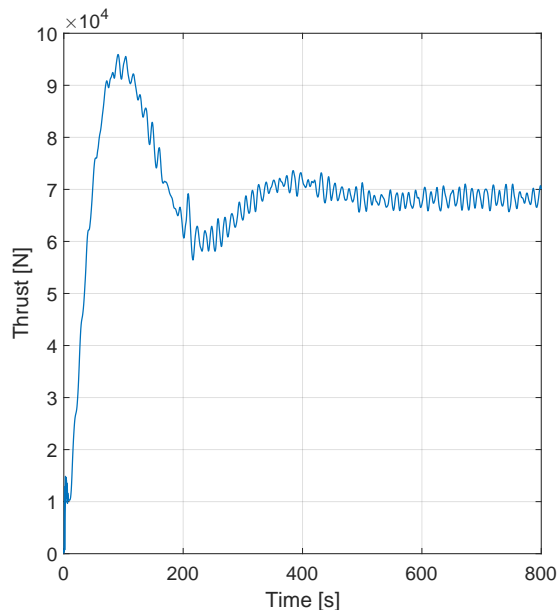
Figure 4.90: *Total thruster forces (absolute value) for case DP2b*

Without integral gain the vessel response is much like that in case DP1b. Dif-

ferences is otherwise difficult to spot without direct comparison, which is carried
out in the next subsection. We can however conclude that the accumulated force
output peak as seen in Figure 4.90 is smaller than without FFC, though slightly
larger than with PI FFC.

4.5.4   Comparison of DP Performance

In this subsection we compare the positioning performance of the different DP
schemes simulated in DP case 1 and 2. Case 1a) is without use of rudders and
FFC, 1b) is with use of rudders but without FFC, 2a) is DP with PI force feedback
and case 2b has FFC with only proportional gain.

In the three first plots case 1b) and 2a) and b) are compared i.e. DP with rudders,
whilst in the three last, full force feedback (PI) is compared with case DP1a -
DP without rudder forces. Figure 4.91, 4.92 and 4.93 shows north, east and yaw
motion respectively for the first comparison, whilst Figure 4.95, 4.96 and 4.97 does
the same for the second one. Figure 4.94 shows total force input for cases with
rudder utilization. In case DP1, Section 4.5.1 we have already concluded that
rudder use is clearly superior to no rudder use at power consumption.

Finally in Table 4.1 standard deviation from desired position is listed. The data in
this table is based on motion estimates over 600 seconds of simulation. This limit
were chosen, as all states are roughly at steady state from here on out.
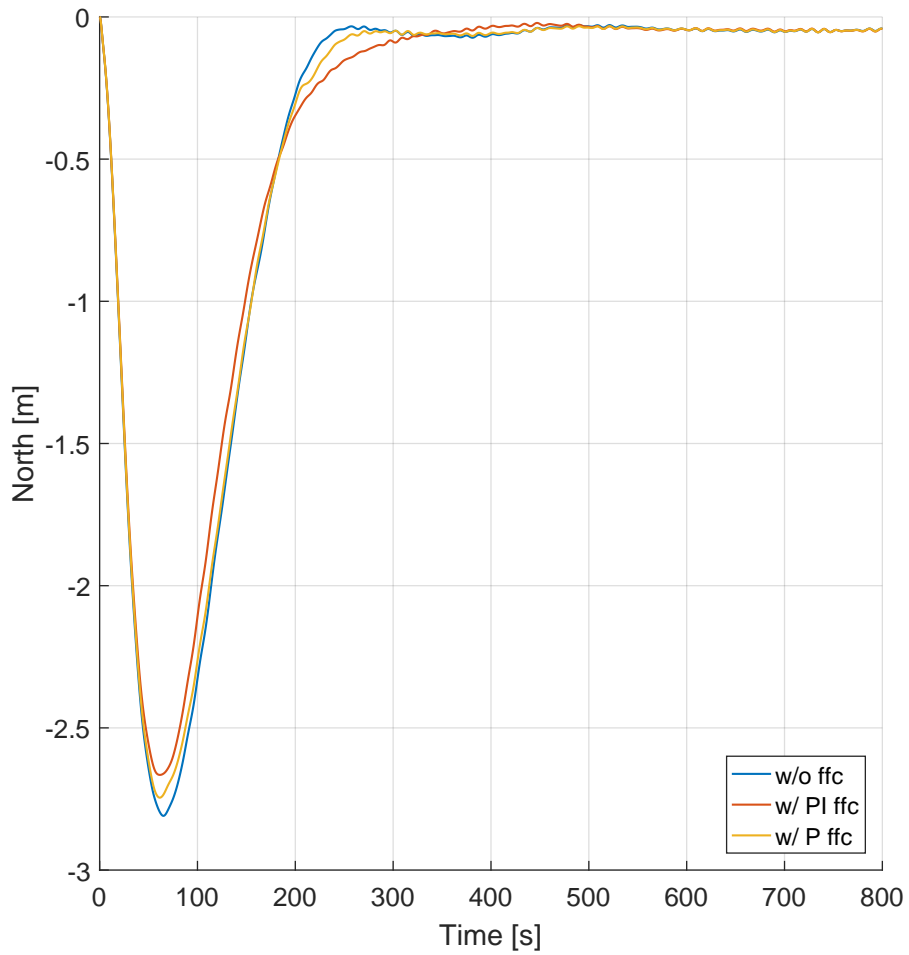
Figure 4.91: *Performance comparison - North position of vessel in DP case 1b, 2a and 2b*
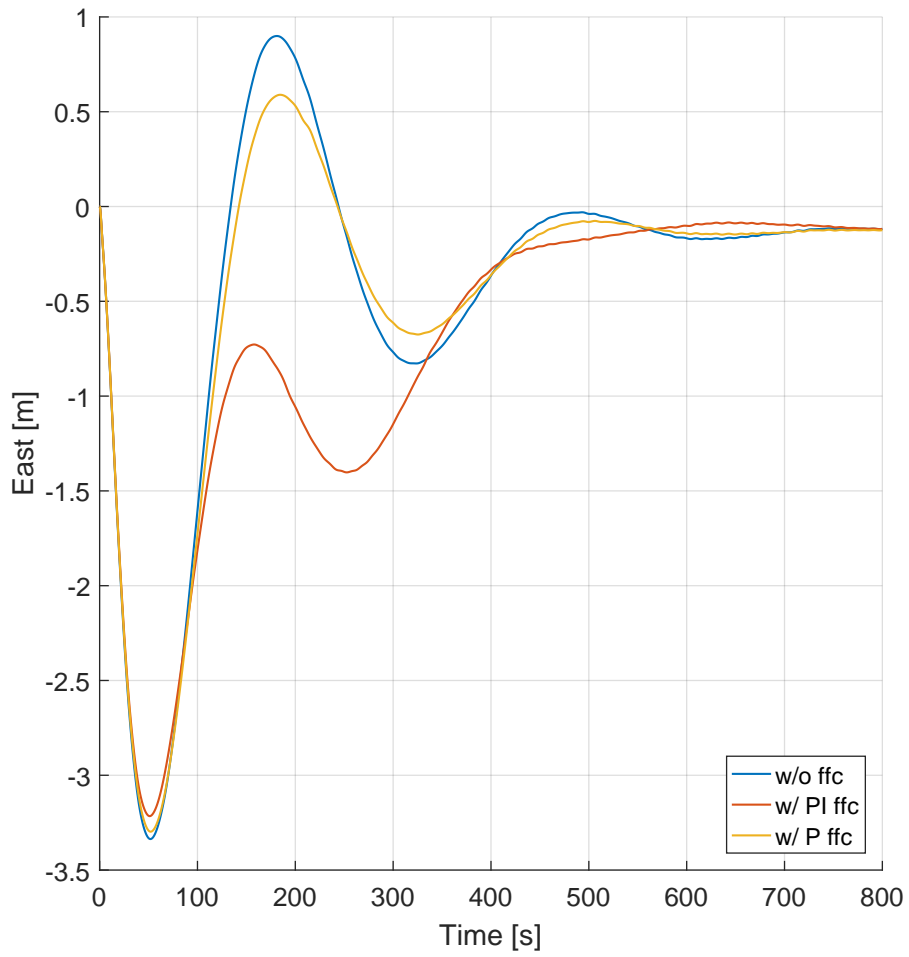
Figure 4.92: *Performance comparison - East position of vessel in DP case 1b, 2a and 2b*
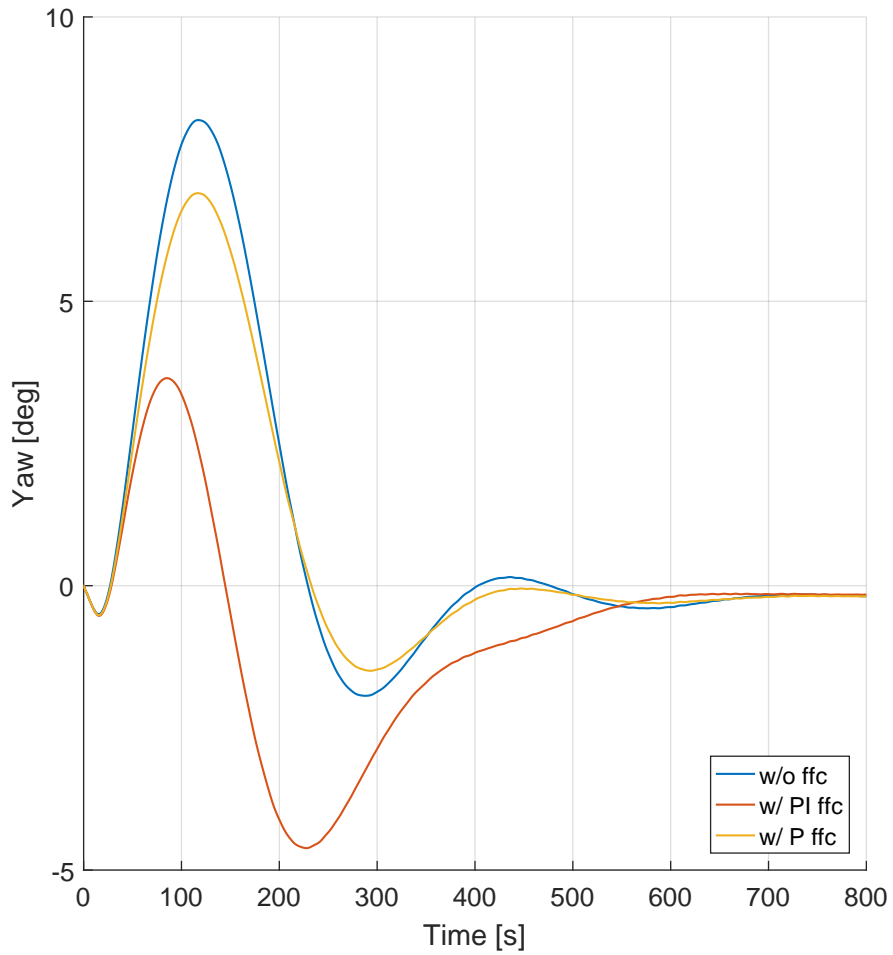
Figure 4.93: *Performance comparison - Heading of vessel in DP case 1b, 2a and 2b*
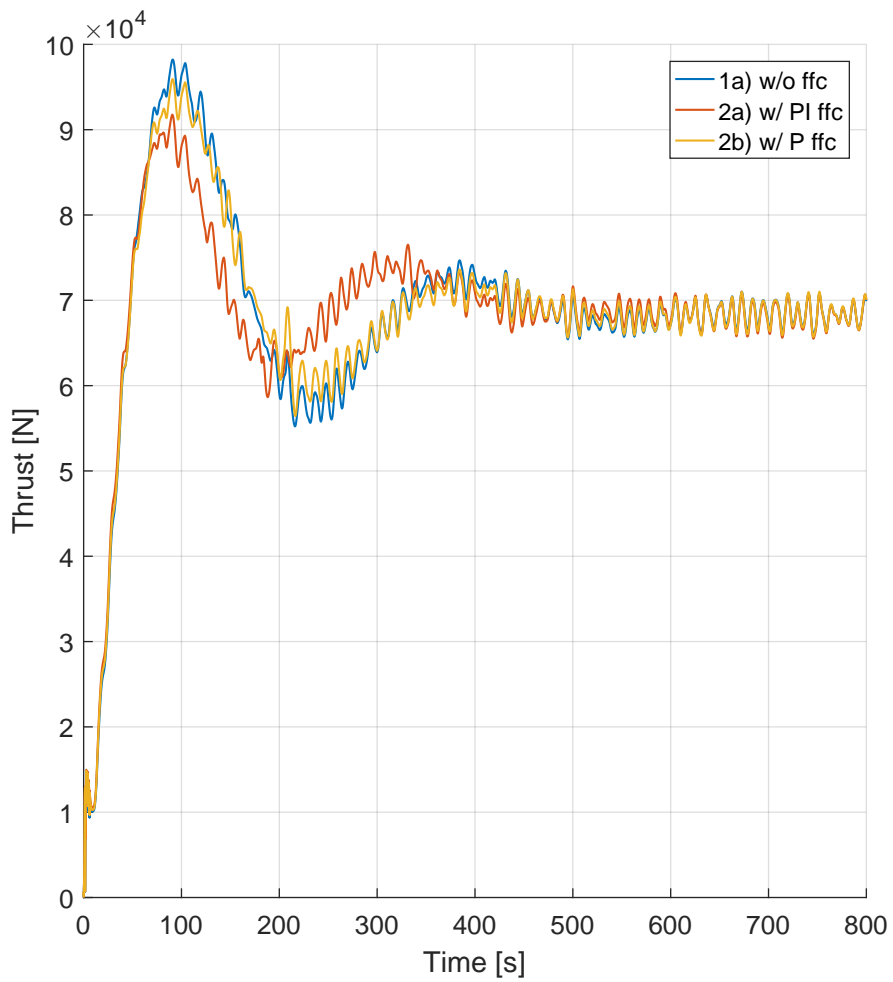
Figure 4.94: *Performance comparison - Total output force in DP case 1b, 2a and 2b*
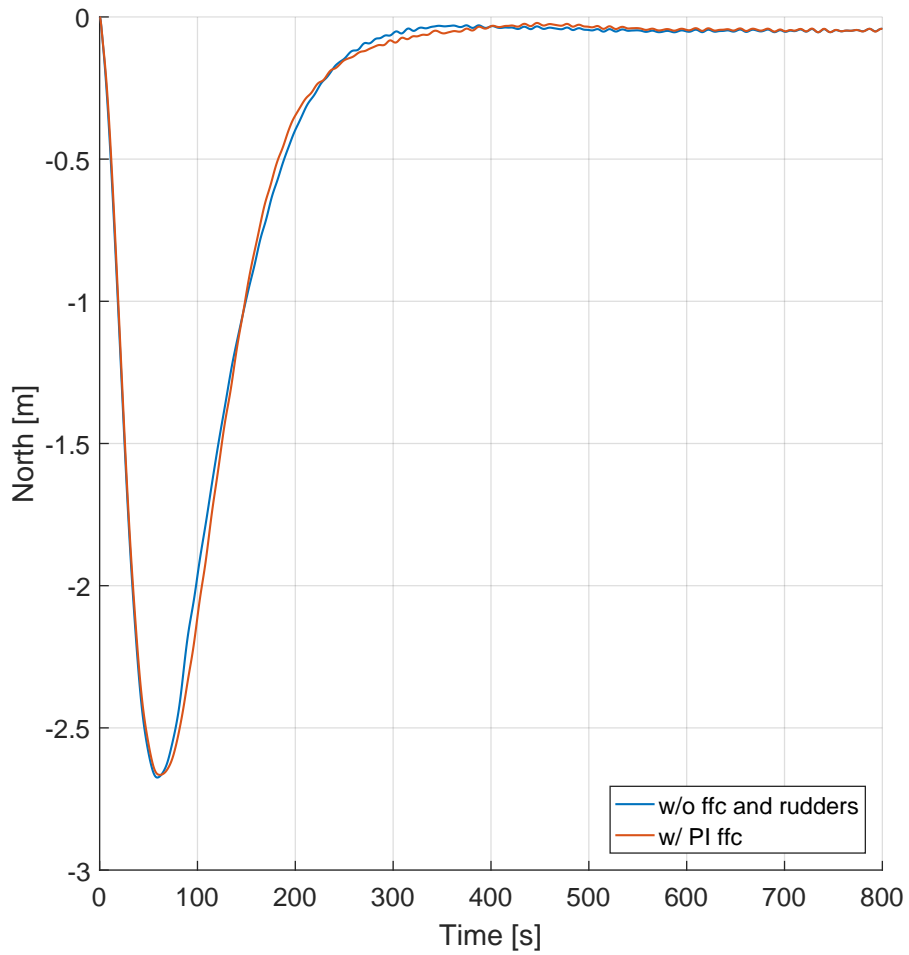
Figure 4.95: *Performance comparison - North position of vessel in DP case 1a without rudders and FFC and 2a with rudders and FFC*
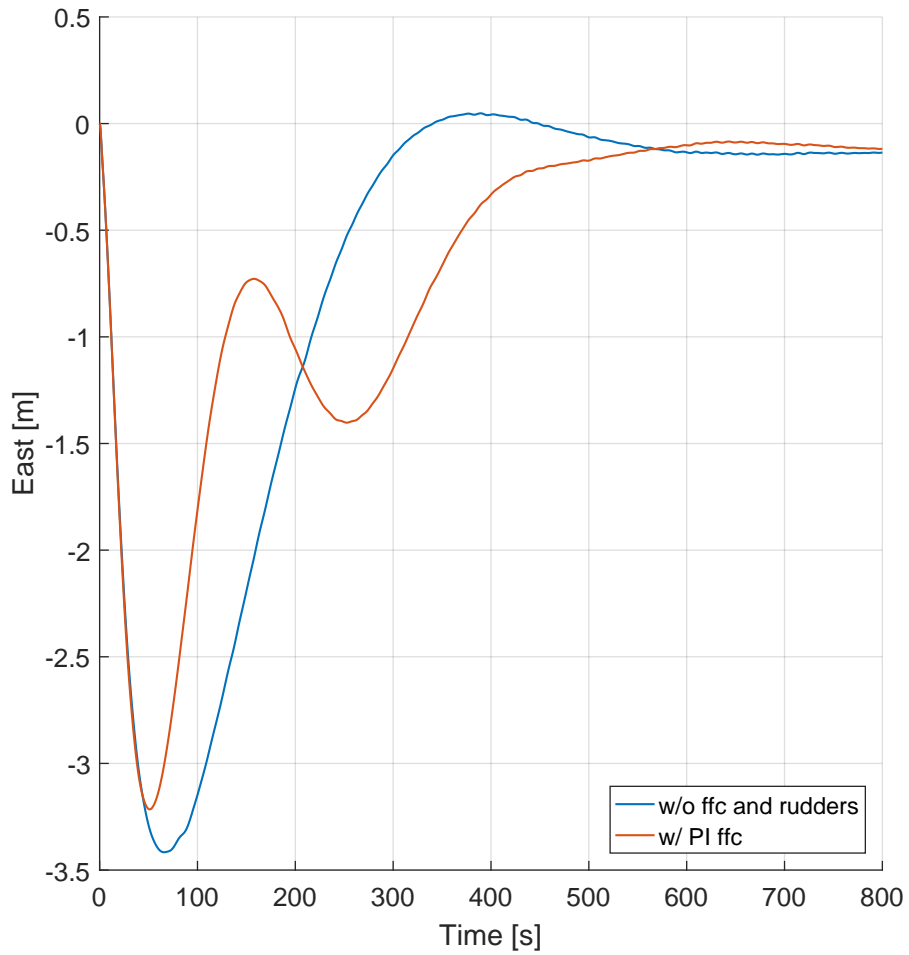
Figure 4.96: *Performance comparison - East position of vessel in DP case 1a without rudders and FFC and 2a with rudders and FFC*
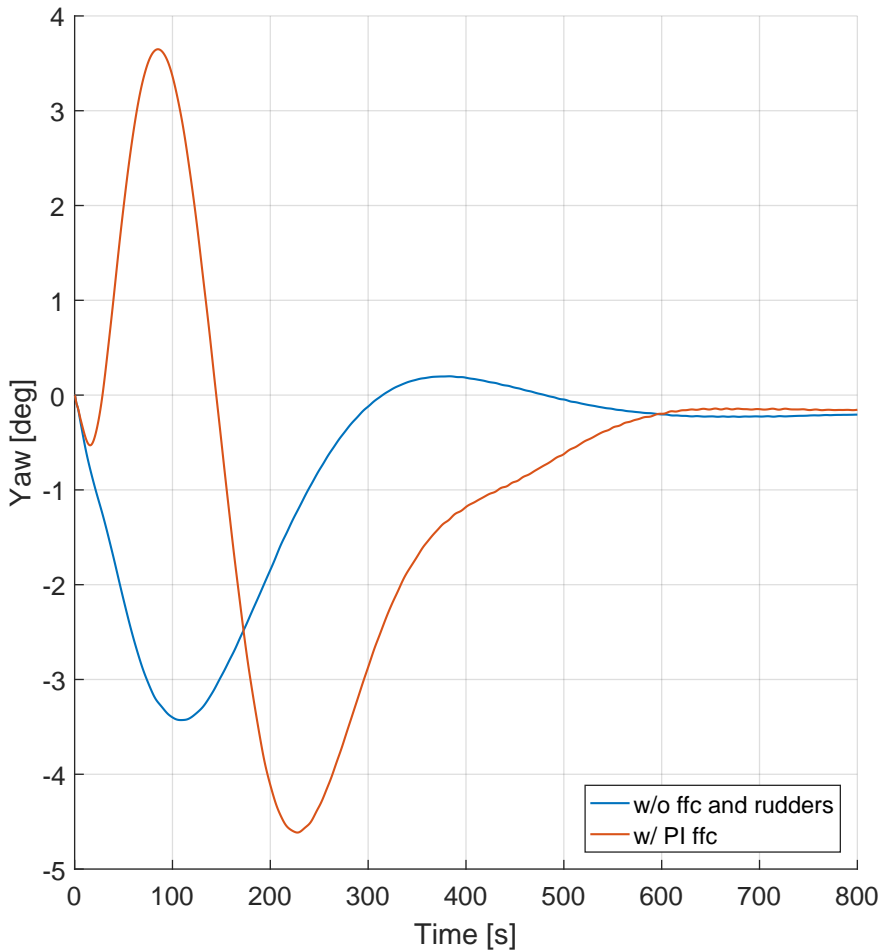
Figure 4.97: *Performance comparison - Heading of vessel in DP case 1a without rudders and FFC and 2a with rudders and FFC*

Table 4.1: *Standard deviation in position and heading estimates*

	1a (w/o rudder)	1b (w/o FFC)	2a (PI FFC)	2b (P FFC)
North	0.963	1.034	0.967	1.021
East	1.433	1.088	1.166	1.054
Yaw	1.451	3.380	2.266	2.870

Starting with the first comparison between cases with use of rudders, note that PI FFC does have slightly smaller position deviation compared to proporional FFC and no FFC. It is as well slightly more "careful" when approaching the desired

position and heading, and thus has less overshoot and oscillation. In yaw, PI FFC performs significantly better compared to the two others as the extrema is quite a bit lower. In general both proportional force feedback and proportional-integral force feedback performs superiorly to no FFC. They have less overshoot and also less oscillatory motion. Steady state LF motion is slightly off zero in every case and DOF. This is not due to the control scheme but rather to the small steady state bias in position and heading estimates, and thus it is off no concern in these tests. From Table 4.1 we observe that in terms of standard deviation both PI and P FFC outperforms no force feedback. PI in sway is slightly larger though it makes up for this with significantly less standard deviation in yaw. Note that the scheme with no use of rudders outperfoms the others in terms of yaw motion, though it is as expected equal to PI FFC in surge and significantly worse in sway. As a final remark we note from Figure 4.94 that the integral of total force over time is close to equal for each case.

When investigating the second comparison case it appears as if the force feedback integral gain drives vessel motion towards a path more similar to the scheme without rudders. It especially counteracts the large positive moment generated by the deviation between thruster model and inverse kinematics as discussed in case DP1. This is precisely the performance one might expect according to theory. Case 1a) has a smoother path towards the origin for sway and yaw, and significantly less maximum deviation in yaw, though DP with PI FFC does actually have slightly smaller deviation in sway.

4.5.5   Concluding Remarks

Through the DP verification cases we have observed that utilizing rudders is clearly superior to not using them regarding power consumption. Motion control is however degraded, though force feedback control with proportional and integral gain is able to partly recover performance. Yaw is still slightly worse, though surge is more or less identical and sway control is arguably better. The control allocation scheme distributes force in what seems to be a sensible way and performance regarding thrust output is predictably increasing with larger allowed rudder angle. With the chosen gains, the steady state at desired position and heading is attained after roughly 600 seconds in each case.

For cases utilizing rudders integral of force over time is approximately equal with and without force feedback control, and thus we can not argue that the proposed FFC scheme is less power consuming compared to no FFC.

4.6   Final Discussion

In case M1 to M7 it is verified that the environmental model and thrust input interacts well with the vessel model, and coupling in sway and yaw motion and

the first order time delay were identified as possible challenges for force feedback control. Case F1 to F4 verified that the force feedback control system performs up to expectations when desired forces is set to constant values in each degree of freedom. The time delay did not represent much of a challenge, though it is not certain that this would be the case in model of full scale tests with a real vessel. Through DP performance testing in case DP1 and DP2 it is demonstrated how utilizing rudders, drastically decreases power consumption, and finally we observed how force feedback control increase positioning performance in station keeping.

Although some questions were answered, further investigations need to be carried out. We saw that force feedback performed well in case F1 to F4, and these cases have much in common with path following. Investigating force feedback in autopilot could thus be interesting, and could possibly be hugely beneficial.

In the simulations carried out through this project, the amount of force measurement noise were negligible. How would force feedback perform with large amount of white or maybe coloured noise? Or maybe under time varying environmental conditions? Rudder forces are known to vary with changing conditions e.g. incoming velocity. This could possibly have a massive effect on force control performance. Also environmental conditions where chosen to avoid thrust saturation. Saturation would have caused large problems, as the applied control allocation scheme has no system for redistribution of thrust between actuators. This should be addressed in further work.

Finally model and full scale testing on real vessels is necessary to further verify the results in this thesis.

Conclusion and Further Work

5.1 Conclusion

Through this master thesis a vessel model with DP system including advanced thrust allocation have been implemented. The control allocation is cable of effectively utilizing rudders for low speed control purposes. A force feedback control system loosely based on theory from robotics has been designed and implemented, and through simulations it is demonstrated that this system is both power saving compared to not using rudders and has enhanced position tracking compared to DP without force feedback.

In the introduction of this thesis we raised the question; "Can the rudder be a viable option for well boats in exposed aquaculture?" To answer this it is necessary to look at a few deciding factors. First, how is the operational profile of a well boat? There can be no doubt that it will mainly operate in transit, though a substantial amount of time might be kept in DP operations. How then will the rudder perform in these conditions? In transit it is generally agreed upon the fact that it is the most fuel efficient system, and rudder force feedback might also improve transit performance significantly. In DP operations it is know that more flexible systems such as the azimuth thruster is more effective and reliable. We do however believe, as indicated in this thesis, that there is room for improvement. The rudder will probably never be able to compete in pure DP performance, though through utilizing every aspect of it, one may create a system which both complies with safety standards and is relatively energy efficient. Aft thrusters is necessary in most cases, though with effective use of rudders one might keep it at one instead of two. This would obviously save money both in procurement, installation and maybe in maintenance as well.

Overall we conclude that it is absolutely possible that rudders are a part of the

propulsion and manoeuvring arrangement which is most cost effective for well boats, and that systems such as force feedback control, could improve performance significantly.

5.2   Further Work

Before any definite conclusion can be drawn there are several areas of further work which should be addressed.

On the basic level of force feedback we have already touched upon some possible areas of improvement and further research. It is necessary to know how force measurement noise effects the system, and design of noise filters should be investigated. A standard Kalman filter could be a possible solution. More advanced control schemes should as well be tested and stability proofs for the proposed FFC need to be carried out.

To account for time varying rudder dynamics, methods for monitoring and online model identification should be developed. Hybrid systems as presented in Hespanha [2001] might be the right tool, in order to perform online parameter estimation based on measurements of rudder forces, current velocity, etc.

Effective control allocation should be further investigated, and especially systems for redistribution of force is necessary in cases where thrust saturation limits are reached. To comply with standards of safety and performance, control allocation for different actuator setups is necessary. Twin rudders with one bow thruster and one or two aft thrusters could be a feasible arrangement.

To optimize transit, both force feedback and online model adjustments might be utilized for improved autopilot performance. If the system could have precise rudder models at every moment in time, the autopilot would surely be both more effective and precise. For autopilots it is necessary to use both rudders simultaneously, which imposes yet another requirement and area of further work on control allocation.

Furthermore, to obtain a clear picture of total expenses through a well boats life, total life cycle cost comparisons between different thrust devices and arrangements should be carried out. It should be in every ship owners interest to know which configuration is most cost effective. Last though not least, model and full scale tests of vessels with advanced use of rudders has to be carried out. We can only get an indication of performance through simulations - The real world is after all not quite as predictable.

Bibliography

Astrom, K. J. [1995], 'Pid controllers: theory, design and tuning', *Instrument society of America* .

DNV [2000], 'Ships newbuildings - hull and equipment - part 3 chapter 3 - hull equipment and appendages'.

Faltinsen, O. [1993], *Sea loads on ships and offshore structures*, Vol. 1, Cambridge university press.

Fossen, T. [2011], *Handbook of Marine Craft Hydrodynamics and Motion Control*, John Wiley & Sons.

Fossen, T. I. and Perez, T. [2004], 'Marine Systems Simulator (MSS', `http://www. marinecontrol.org`.

Hespanha, J. P. [2001], 'Tutorial on supervisory control'.

Hogan, N. [1984], Impedance control: An approach to manipulation, *in* 'American Control Conference, 1984', IEEE, pp. 304–313.

Jin, S., Cardellach, E. and Xie, F. [2014], *GNSS remote sensing*, Springer.

Johansen, T. A., Fuglseth, T. P., Tøndel, P. and Fossen, T. I. [2008], 'Optimal constrained control allocation in marine surface vessels with rudders', *Control Engineering Practice* **16**(4), 457 – 464. Special Section on Manoeuvering and Control of Marine Craft.
URL: *http://www.sciencedirect.com/science/article/pii/S0967066107000329*

Lindegaard, K. P. [2003], Acceleration Feedback in Dynamic Positioning, PhD thesis, Norwegian University of Science and Technology.

Lindegaard, K. P. and Fossen, T. I. [2003], 'Fuel-efficient rudder and propeller control allocation for marine craft: experiments with a model ship', *IEEE Transactions on Control Systems Technology* **11**(6), 850–862.

NTNU [2017*a*], 'Research vessel r/v gunnerus'.
URL: *https://www.ntnu.edu/oceans/gunnerus*

NTNU [2017*b*], 'Research vessel r/v gunnerus specifications'.
URL: *https://www.ntnu.edu/oceans/gunnerus/spesifications*

Raibert, M. H. and Craig, J. J. [1981], 'Hybrid position/force control of manipulators', *Journal of Dynamic Systems, Measurement, and Control* **102**(127), 126–133.

Siciliano, B. and Villani, L. [2012], *Robot force control*, Vol. 540, Springer Science & Business Media.

SINTEF [2017], 'Introduction to shipx/veres'.
    URL: *https://www.sintef.no/en/software/shipx/*

Sørensen, A. J. [2011], 'A survey of dynamic positioning control systems', *Annual reviews in control* **35**(1), 123–136.

Sørensen, A. J. [2013], *TMR4240 Marine Control Systems. Propultion and Motion Control of Ships and Ocean Structures*, Akademika forlag.

Steen, S. [2007], *Kompendium TMR 4247 Marin Teknikk 3 - Hydrodynamikk - Motstand og propulsjon - Propell- og foilteori*, Institutt for Marin Teknikk.

Villani, L. [2015], Force control in robotics, *in* J. Baillieul and S. Tariq, eds, 'Encyclopedia of Systems and Control', Springer, London.

Yang, X. and Marjanovic, O. [2011], 'Lqg control with extended kalman filter for power systems with unknown time-delays', *IFAC Proceedings Volumes* **44**(1), 3708–3713.

Appendices

Appendix A

Documents of Interest

In this appendix two documents of interest is presented. Appendix A.1 is the problem description for this thesis, whilst A.2 contains additional data for R/V Gunnerus. Note that the vessel has been reconfigured since this documentation were published in 2006, and the vessel does for example not have rudders installed currently.

A.1 Problem Description

Master thesis project 2017

Johan M. Haugland

Supervisor: Ingrid Schjølberg

Department of Marine Technology, NTNU

DP Solutions with Rudder Force Feedback for

Exposed Aquaculture

Aquaculture and especially exposed aquaculture is a business heading into a period of large growth and rapid change. Considerable amounts of resources are and will be put into research to insure safe and sustainable operations at exposed locations and for the business in general. A key factor here is precise maneuverability of vessels operating at fish farms, both to avoid collision and in insuring minimal disturbance on the fish environment.

As the business grows, so does the vessels. This will impose even higher demands on their maneuverability. One way to meet this demand might be DP systems, but to insure the necessary maneuverability we should aim to develop the solutions of today even further. By measuring drag and lift forces on the rudder and using these directly in the feedback loop, we might reach this goal. More research is however needed. In this thesis, we therefor aim to provide more knowledge on the application of rudder force measurements in DP solutions and how this might be utilized in aquaculture.

Scope of work

1. Identify a test case and ship model with relevance for exposed aquaculture
2. Investigate rudder models and adapt to profiles of rudder force measurements
3. Implement and test control allocation with use of rudder in simulator
4. Implement and test force feedback in simulator
5. Testing and verification of solutions for rudder force feedback in DP
6. Write thesis

It is expected that some of the work will be performed at the Becker-lab in Hamburg.

Timeline

Scope of work	
Test case and ship model identification	February
Testing and study of rudder models	February/March
Implementation of feedback loop solutions	March/April
Strategy development	April
Testing and verification of full scale solutions – either in simulation or on a real ship	May
Write thesis	May/June
	Deadline June 11

A.2   Documentation for R/V Gunnerus

RV GUNNERUS - LNVZ
Multipurpose research vessel for Norwegian University of Science and Technology (NTNU)

Name	R/V GUNNERUS
Owner	Norwegian University of Science and Technology (NTNU)
	Faculty of Natural Sciences and Technology
Designed by	Polarkonsult AS, Norway
Built by	Larsnes Mekaniske Verksted, Norway
Delivery year	2006
Port of Registry	Trondheim, Norway
Classification Society	Norwegian Maritime Directorate

Main dimensions

Length over all	(Loa)	31.25 m
Length between pp	(Lpp)	28.90 m
Length in waterline	(Lwl)	29.90 m
Breadth middle	(Bm)	9.60 m
Breadth extreme	(B)	9.90 m
Depth mld. Main deck	(Dm)	4.20 m
Draught, mld	(dm)	2.70 m
Mast height / antenna		14.85 / 19.70 m
Dead weight		107 t

Class, Service Area

Range	Coastal areas out to 20 nautical miles from the coast (Liten Kystfart) Designed and built according to European trade.
Class Notation	DNV + 1A1 + Ice C + E0 + R2 Cargo ship

Deck equipment, scientific equipment and lab facilities

Trawl winches	2 x Mjosund 6 t, (wire D=14 mm, L=1000 m).
Net drum	Mjosund 5 m^3, D=2000mm, d=320mm
Main deck crane	Palfinger 14 m / 35 tm
CTD crane	HIAB/Mjosund, 5 m / 3.3 tm,
	Water sampler wire 5 mm/750m
	CTD wire 6,5 mm/750 m.
Stern mounted A-frame	6 t, hydraulic.
Hydraulic diving platform	500 Kg, 1,5m x 0,8m.
Hydraulic aggregate	Mjosund 110 kW
Capstan	Mjosund 8t/220bar, D=410, d=320, L=300
Anchor winch	Mjosund 2 drums, 20 m/min, 2 x 12,5m ø 22mm K2 chain/
	210m ø22mm. wire
Compressed air	Atlas copco compressor
Workdeck	75 m^2
Wet lab	13.9 m^2
Dry lab	11.8 m^2
Computer lab	11.2 m^2
Container attachment:	5, 10, 15 & 20 feet alongside or 20 feet abeam.
CTD	Saiv
CTD	Sealogger 25, Seabird electronics inc.

Watersampler system   Carousel water sampler, 12 x 2,5l bottles. Seabird electronics inc
Workboat   Polarcirkel 560 Work, Yamaha 80hp

Capacities

Crews cabins / berths	6 / 11
Daytime personnel capacity	25 incl. crew
Deadweight	107 t
Deck load	45 t
Fuel oil	44 m^3
Fresh water	11 m^3
Water ballast	62 m^3
Cargo hold	42 m^3
Galley	4,5 m^2
Mess, conference and dayroom	32 m^2 With 46" LCD monitor.

Machinery: Diesel electric propulsion

Main electric propulsion	1000 kW (Siemens 2 x 500 kW)
Main generators	3 x Nogva-Scania 450 kW
Bow tunnel thruster	1 x Brunvoll 200 kW
Speed at 100% MCR	12,6 kn
Cruising speed	9,4 kn
Gear	2 x Finnøy
Rudder	2 x Rolls-Royce, Ulstein Hinze Rudder FB-H 1200
Steering gear	2 x Rolls-Royce, Tenfjord SR562-FCPX2

*The diesel electric system has been specially designed for low hydroacoustic noise levels.
Diesel generators are mounted on a common double elastic frame and one of the generators
are mounted in a noise dampening hood for special low noise mode.*

Navigation, communications and electronic equipment

Dynamic Positioning system	Kongsberg SDP-11 / cPos
DP - Reference systems	GPS
	Kongsberg Seatex DPS 232
	HPR, Kongsberg transponders.
	Kongsberg Seatex RADius
Heading, Attitude and Positioning Sensor	Kongsberg Seapath 300
Acoustic positioning system	Kongsberg HiPAP 500
Motion reference unit (MRU)	Kongsberg Seatex
Autopilot	Simrad AP50
Compass, magnet	Nautisk service NS 150-A
Compass, gyro	Simrad GC80 / 85
Bearing repeater	Simrad DR76
Differential positioning sensor	Kongsberg DPS 232
Heading, attitude and positioning sensor	Kongsberg Seatex Seapath 300
GPS	Furuno Navigator GP-90
Radar	Furuno FAR 28x7 /FAR 21x7
Log	Furuno Doppler speed log DS-80
Echo sounder	Furuno FCV-1200L. 38, 50, 200 kHz – 2000m
Echo sounder, multibeam	Kongsberg EM 3002s
Catch monitoring system	Simrad PI54

Chartplotter 1	Telchart (AIS)
Chartplotter 2	Olex (Installed AIS, HT, SB, ITI, MBES)
Chartplotter 3	Olex LT (Office version)
AIS	Furuno FA-150
Navtex	JMC NT900
GMDSS console	
VHF fixed radio	Sailor
VHF handheld radios	Jotron
UHF handheld radios	Icom
Satellite phone	Sailor
Internet in sea	ICE & Telenor mobilt bredbånd
Internet at pier Trondheim	Wireless broadband NTNU.

Safety

MOB boat, inflateable craft	Narwhal 6 persons SOLAS aproved, Propulsion Mariner 20 Hp
Rescue boat davit	Ned Deck Marine
Life rafts	2 x 25 men each
Survival suits	25 Stearns model ISS-590i
Life jackets	Seamaster – 1983, SOLAS Approved
Work vests	25 Regatta
EPIRB	Jotron
SART	Jotron
Aircraft beacon	Jotron
Fire alarm system	Minerva Marine T1008
Fixed system	Engine room, CO_2
Fire suit	Draeger
Search light	Tranberg
SAR	SECurus prototype, Apto maritime (Under construction)
Day and night vision	SECurus prototype, Apto maritime (Under construction)
Oil spill monitoring	SECurus prototype, Apto maritime (Under construction)

Details are believed to be correct but not guaranteed